
**SELECTIVE RECORDING AND
STIMULATION OF NEURONS IN THE
MOUSE HIPPOCAMPUS AND CORTEX:
TWO-PHOTON IMAGING, UNCAGING,
AND BEHAVIOUR**

Thesis submitted for the degree of
Doctor of Philosophy
at the University of Leicester

by

JULIETA ERNESTINA CAMPI

Centre for Systems Neuroscience

University of Leicester



October 5, 2016

Abstract

SELECTIVE RECORDING AND STIMULATION OF NEURONS IN THE MOUSE HIPPOCAMPUS AND CORTEX: TWO-PHOTON IMAGING, UNCAGING, AND BEHAVIOUR

JULIETA ERNESTINA CAMPI

Two-photon imaging is becoming one of the most widely used technique in Neuroscience. Combined with selective neuronal stimulation (or inhibition) techniques, it offers an infinite variety of experiments aimed to better understand the brain at different scales. However, the optimal conditions for applying each of these techniques are not usually the same, and even though there are ways of overcoming this limitation, these solutions require expensive resources. This PhD thesis aimed to optimise the combination of two-photon imaging and two-photon uncaging by finding an excitation wavelength suitable for both processes, which is the main limitation when the two methods are used together. This method was designed in order to be suitable for both in vitro and in vivo experiments. First, in vitro experiments were performed in order to maximise the quality of brain slices. Secondly, the physicochemical characteristics of the protein used for Calcium imaging, GCaMP6s, were studied with the objective of finding a range of excitation wavelengths suitable for doing imaging but, at the same time, closer to the optimal uncaging wavelength. Two-photon uncaging of Glutamate was achieved using light at 850 nm, a wavelength that also permitted monitoring the neuronal response to the stimulation. It is expected that this technique will soon be applied in vivo with the objective of developing an animal model for concept representation in the hippocampus. This project consists of training mice in a virtual reality set-up that allows testing them in a two-forced choice paradigm. In the case of finding neurons firing selectively to one of these objects, independently of low-level features, the uncaging technique will be useful for manipulating the normal activity of those neurons and study how this manipulation affects the animal's behaviour.

Acknowledgements

I would like to thank my supervisor Rodrigo Quian Quiroga, for giving me the opportunity to work in such a great environment, and for trusting me with such a challenging project.

To my co-supervisor, Ian Forsythe, for teaching me so much about imaging, electrophysiology, and pharmacology, and for always being willing to help me.

To Roberto Etchenique for providing us with the RuBiGlutamate and for his technical advice and results interpretation.

To Conny Kopp-Scheinflug, Joern Steinert, and Emanuele Schiavon for showing me how to prepare slices and helping me with the experiments. Also, to the rest of the people from Ian's lab, with whom I was so lucky to share so many days in the lab (and coffee breaks).

To Manuel Molano-Mazón, Pinar Boyraz, and Emanuele Schiavon, for being part of the everyday life in the CRF. To Dr. Todor Gerdjikov for his invaluable help and advice with experiments, training and equipment.

To Vincenzo Marra, for helping me with the setting up of the imaging experiments and for his advice.

To Julia Humphreys, Sue Atkinson, and Alex Archibald, for always being so helpful and friendly with me.

To the rest of my colleagues at the Centre for Systems Neuroscience for creating a perfect friendly environment: Matias, Manuel, Alex, Joaquin, Hernan, Emanuela, Hugo, Fanis, Alessandro, Carlos, Fernando, Luis, Natalia, Vtor, Sandra, Lisandro, Maryam, and Zaira.

To my Leicester friends, because this experience would not have been the same without them: Mati, Ceci, León, Hernan, Lisandro, Katia, Vitor, Vero, Manu and Nati.

To my parents Nora and Roberto, for putting aside their feelings to support this adventure. To my sisters Mercedes and Mariana, my brother in law Fede, and my nephews, for making me want to go back home. To my second family: Fernando, Hildegart, Cami, Javi, Ale, Heberto, and Noemí, for the visits, the trips around Europe and for welcoming me to their family with so much love.

To Joaco, for being my support, my strength, my happiness.

©Julieta Ernestina Campi, 2016

This thesis is copyright material and no quotation from it may be published without proper acknowledgement.

List of Publications

Journal

- **Campi J.**, and Quian Quiroga R. (2015). “Neuronal Encoding of Memory in the Human and Mouse Hippocampus”. *European Journal of Neurodegenerative Diseases* Vol3. No 2 pp 91-99.

Poster presentation

- Schiavon E., Molano-Mazón M., **Campi J.**, Boyraz Jentsch P., Forsythe I. and Quian Quiroga R. “Decision Making in a Virtual Reality Environment for Mice” *Neuroscience and Behaviour Day, University of Leicester, 2015* Leicester, United Kingdom.

Contents

Abstract	i
Acknowledgements	iii
List of Publications	iv
1 Introduction	1
1.1 The Hippocampus	1
1.1.1 Anatomy and organisation	2
1.1.2 Hippocampus and memory	4
1.1.3 Place cells	5
1.1.4 Concept cells	6
1.2 Neocortex	8
1.3 Neurophysiology recordings	9
1.3.1 Electrophysiology	9
1.3.2 Optical imaging	10
1.4 Stimulation of neural activity	16
1.4.1 Electrical Stimulation	16
1.4.2 Pharmacological Stimulation	17
1.4.3 Optogenetics	17
1.4.4 Caged compounds	18
1.5 Aims and organisation of the thesis	23
2 <i>In vitro</i> electrophysiology	25
2.1 Introduction	25
2.2 Methods	25
2.2.1 Animals	26
2.2.2 Slices	26
2.2.3 Extracellular recordings and stimulation	27
2.2.4 Data Analysis	29
2.3 Results	30
2.3.1 Extracellular recordings and stimulation	30
2.4 Conclusions	34

3	<i>In vitro</i> two-photon imaging and Glutamate uncaging	38
3.1	Introduction	38
3.2	Methods	39
3.2.1	Animals	39
3.2.2	Intracranial virus injection	39
3.2.3	Slices	41
3.2.4	Microscope	42
3.2.5	Electrical stimulation	43
3.2.6	Drug delivery	43
3.2.7	GCaMP6s characterisation	44
3.2.8	Glutamate Stimulation	45
3.2.9	RuBi-Glutamate uncaging with light at 850 nm	46
3.2.10	Data Analysis	47
3.3	Results	50
3.3.1	Virus injection	50
3.3.2	GCaMP6s characterisation	53
3.3.3	Glutamate stimulation	57
3.3.4	Glutamate uncaging with light at 850 nm	57
3.4	Conclusions	63
4	Development of an animal model for concept representation in the hippocampus	66
4.1	Introduction	66
4.2	Methods	67
4.2.1	Animals	68
4.2.2	Head-plate implantation	68
4.2.3	Virtual Reality Set-up	69
4.2.4	Training paradigm	71
4.2.5	Data Analysis	73
4.3	Results	74
4.3.1	VR set-up and animals' habituation to the set-up	74
4.3.2	Performance	74
4.4	Conclusions	76

<i>CONTENTS</i>	vii
5 General Conclusions	78
5.1 <i>In vitro</i> electrophysiology	79
5.2 <i>In vitro</i> two-photon imaging and uncaging	80
5.3 In search of an animal model for studying concept representation .	83
5.3.1 Current state of the project	85
List of Abbreviations	86
Bibliography	89

List of Tables

1.1 Comparison of RuBi and MNI compounds	20
2.1 Composition of the different artificial cerebro-spinal fluid used for <i>in vitro</i> experiments	27

List of Figures

1.1	Neural circuit of the Hippocampus	4
1.2	Spike sorting from an extracellular electrode	11
1.3	Dendrites and cell bodies from CA1 and Dentate gyrus	12
1.4	Comparison between 1P and 2P excitation	14
1.5	Structure of [Ru(bpy) ₂ (PMe ₃)(GluH ₂)] (RuBiGlutamate)	19
1.6	Jablonski diagram for a typical inorganic caged compound photorelease	22
2.1	Responses to electrical stimulation in hippocampal slices	31
2.2	Pharmacological modulation of electrically-evoked EPSPs.	33
2.3	Gamma Oscillations induced by Kainate	34
2.4	Power spectrum and single cell phase-locking to the LFP	35
3.1	Coordinates for intracranial injections	41
3.2	Schematic representation of the beam path for two-photon excitation	43
3.3	Two-photon imaging set-up	44
3.4	Experimental design for uncaging	46
3.5	Differences in Expression with serotypes AAV5 and AAV9	52
3.6	Cortical and hippocampal cells expressing GCaMP6s	53
3.7	Target area and area of expression	54
3.8	Normalised Fluorescence for different wavelengths	55
3.9	Activity measured after stimulation	56
3.10	Comparison of three different excitation wavelengths against 920 nm	58
3.11	Effect of glutamate (+sulforhodamine 101) in granule cells	59
3.12	Response to glutamate	59
3.13	Onset time and amplitude of response to glutamate	60
3.14	Response to stimulation with RuBiGlutamate	61
3.15	Onset time and amplitude of response to RuBiGlutamate uncaging.	63
4.1	Virtual Reality Set-Up	70

LIST OF FIGURES

x

4.2	Decision process from the beginning to the end of the trial. . . .	72
4.3	Daily mean performance and p-value	75
4.4	Weekly performance of an animal	77
5.1	Weekly performance of an animal and <i>in vivo</i> 2P imaging	87

Chapter 1

Introduction

Undoubtedly, one of the biggest mysteries for the human being is how the brain works. The first mention of the brain of which we have a record is from the 17th Century BC. In an ancient papyrus, the word “brain” can be found among the description of symptoms and diagnosis of head injuries. Great advances have been made since then, and yet studying the brain and understanding how it works remains a challenge that many scientists are willing to accept.

1.1 The Hippocampus

Many of the greatest physiologists and anatomists of the XIX and XX centuries were captivated by the unique structural organisation of the hippocampus. Among the greatest contributors to our current knowledge of the hippocampus we can count: Camillo Golgi, with his cell staining technique and drawings; Karl Schaffer, with his study of axons connecting cells from different areas; Santiago Ramón y Cajal, who, based on his principle of dynamic polarisation, predicted the direction of impulse flow through this area; and Rafael Lorente de Nó, who defined different areas in the hippocampus and named them CA1 to CA4 (from cornu ammonis), based on the dendritic trees and connections among the cells in each area.

1.1.1 Anatomy and organisation

The hippocampus proper is divided in 3 areas: CA3, CA2¹, and CA1². The hippocampal formation includes the dentate gyrus, the subiculum, presubiculum, parasubiculum, and entorhinal cortex. The dentate gyrus, the proper hippocampus and the subiculum have the principal cells organised in a single layer, while the layers above and underneath it are either less-cellular or acellular.

This organisation of the cells in a single layer, in contrast with the columnar organisation in the cortex (see Section 1.2), is a very distinctive characteristic of the hippocampus. The direction of the afferent fibres is also quite peculiar, since they run in a horizontal direction and orthogonal to the apical dendritic axis, while in the cortex the afferent fibres are radially oriented.

The dentate gyrus and the proper hippocampus are organised in layers, each of them with different components, such as cell bodies, dendrites, axons, interneurons, etc.

The dentate gyrus has three layers (Amaral et al., 2007): the granule cell layer, the molecular layer, and the polymorphic layer (also known as the hilus). The granule layer is the middle one, and contains the granule cells, which are the principal cells in the dentate gyrus. Above the granule layer is the molecular layer that has no cells but contains the dendrites of the granule cells and the basket cells (a type of interneuron). This layer receives the input from the Entorhinal Cortex through the perforant path. Below the granule cell layer is the polymorphic layer, containing a large amount of interneurons –most of which are inhibitory (Freund and Buzsáki, 1996)– and the axons of the granule cells, known as mossy fibres.

The hippocampus is divided into several layers. The alveus, the closest layer to the cortex, receives some of the afferent fibres from the Entorhinal cortex (Deller et al., 1996) and the axons from the principal cells. The stratum oriens contains the basal dendrites of the cells in the pyramidal layer and

¹CA2 has been a matter of debate during several years. It seems to be a region of transition between CA3 and CA1, having large pyramidal cells as CA3 but no mossy cell innervation, like CA1. However, accumulating evidence would indicate that CA2 is a separate region with distinctive features and specific functions (Hitti and Siegelbaum, 2014; Caruana et al., 2012; Jones and McHugh, 2011)

²CA4, more commonly referred to as hilus, is not considered to be part of the proper hippocampus.

some interneurons. It also receives afferents from the Septum (Andersen et al., 2007). The pyramidal layer contains the principal cells. Pyramidal neurons are more tightly packed in CA1 than in CA2 and CA3. The next layer, in CA3 but not in CA1 nor CA2, is the stratum lucidum, which contains the mossy fibres coming from the dentate gyrus. Underneath the pyramidal layer in CA1 and CA2 and the stratum lucidum in CA3 is the stratum radiatum, where the axons of cells connecting CA3 with other cells in CA3 and with cells in CA1 (Schaffer collaterals) can be found. This layer also contains many interneurons and the portion close to CA1 has some neurons called stratum radiatum “giant cells” that express a form of long term potentiation (Gulyas et al., 1998). Finally, the last layer (the closest one to the hippocampal fissure) is the stratum lacunosum-moleculare. Most of the axons from the entorhinal cortex reach this layer together with afferents from other regions (Deller et al., 1996). Interneurons can be found in this layer as well (Lacaille and Schwartzkroin, 1988).

Another characteristic property about the hippocampal formation is its unidirectionality (Amaral et al., 2007): the fact that an area projects to another does not necessarily mean that this area will project back to the first one.

Most of the sensory inputs that reach the hippocampus do it through the entorhinal cortex via the adjacent perirhinal and postrhinal cortices (McCormick and Shepherd, 2004). Entorhinal cells, mostly from layer II but also from layers V and VI³, project to the dentate gyrus and CA3 through the perforant path. Also, through the temporoammonic pathway, neurons from layer III in the entorhinal cortex project to pyramidal cells in CA1. The granule cells in the dentate gyrus project to the CA3 region via the Mossy fibres. Pyramidal cells in CA3 either project to CA1 through the Schaffer collaterals or interconnect with other pyramidal cells within the same area (recurrent connections). Finally, CA1 cells project to both the subiculum and entorhinal cortex (the subiculum also projects to the entorhinal cortex), which in turn, projects back to the cortical areas that originally projected to it, closing the loop (Figure 1.1)⁴.

³As other cortical areas, the entorhinal cortex has a laminar organisation, having four cellular (II, III, V, and VI) and two acellular layers (I and IV).

⁴The basic circuit of the hippocampal formation is even more complex than the one described here. For the sake of simplicity, only the most important circuits have been described.

This way the information coming from cortical areas and passed, through the entorhinal cortex, to the rest of the hippocampal formation reaches back the cortex, which is believed to be essential for the storage of long-term memories.

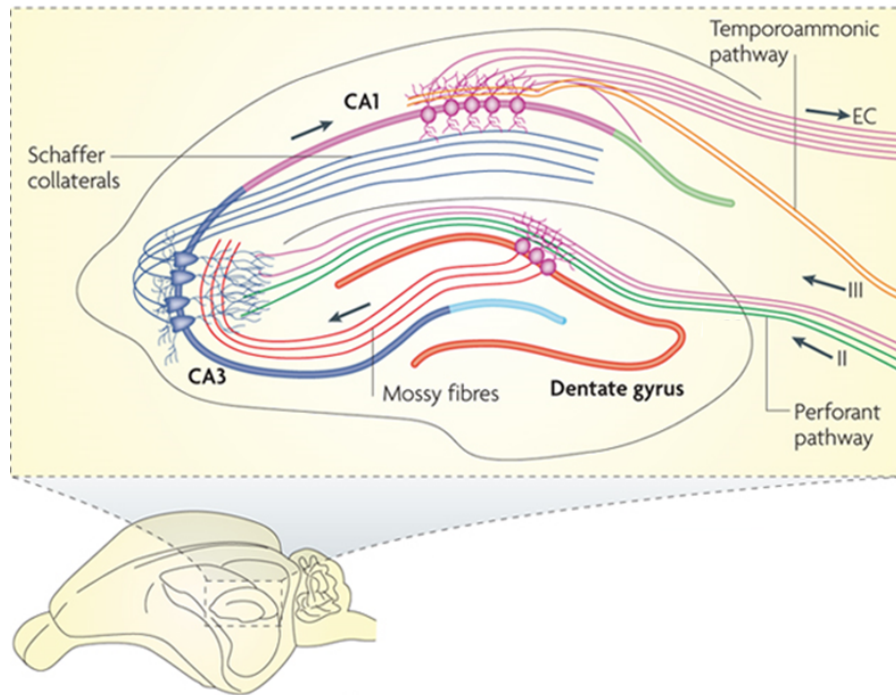


Figure 1.1: **Neural circuit of the Hippocampus.** Neurons from layer II (and to a lesser degree, from layers V and VI) in the entorhinal cortex (EC) project to the dentate gyrus and CA3 through the perforant pathway (PP). Granule cells from the dentate gyrus project to the pyramidal cells in CA3 through mossy fibres. CA3 pyramidal neurons connect with CA1 pyramidal neurons through Schaffer collaterals and with other pyramidal neurons from CA3 (recurrent connections). CA1 pyramidal neurons project to the subiculum and to neurons in the EC and, in turn, receive innervation from neurons of EC layer III through the temporoammonic pathway (TA). Adapted from Deng et al. (2010).

1.1.2 Hippocampus and memory

The interest generated by the anatomy and the physiology of the hippocampus was nothing compared to the interest generated by a discovery made in the 1950s. A patient known as H.M.⁵ underwent an experimental surgery in the

⁵His name was Henry Molaison, but during his life he was known as H.M. to protect his identity. His full name was only disclosed after his death, in 2008.

search of some relief from his incapacitating epilepsy. After the failure of several less radical treatments, the neurosurgeon William Scoville bilaterally resected the anterior two-thirds of his hippocampus and hippocampal gyrus, together with the uncus and the amygdala (Scoville and Milner, 1957). After surgery, his recovery was normal and the seizures were much more manageable than before; however, an unexpected effect of the surgery was noticed immediately after: a severe anterograde amnesia (Corkin, 2002). H.M. had no problem with remembering people, names or events from before the surgery, but failed to store any new piece of information (e.g. the doctors had to introduce themselves every day). Even though his procedural memory was intact, he seemed to have a severe case of anterograde amnesia in terms of declarative memory. This patient, together with other studies (Scoville and Milner, 1957; Penfield and Milner, 1958; Zola-Morgan et al., 1986; Rempel-Clower et al., 1996; Reed and Squire, 1998; Manns et al., 2003; Bayley et al., 2006), provided the first clues about the involvement of the Medial Temporal Lobe (MTL)⁶, and the hippocampus in particular, in transferring short-term memory (a memory that lasts a short period of time) into a long-term memory (something we remember for hours, days or even years).

1.1.3 Place cells

In the 1970s there was another striking discovery involving the hippocampus. Recording from rats with electrodes implanted in CA1, O'Keefe and Dostrovsky (1971) found cells in CA1 that increased their firing every time the animal was in a specific location (i.e. the "place field"). The conclusion from this and later work was that these pyramidal cells in the hippocampus conformed a spatial map that relies on an abstract concept such as place (O'Keefe, 1979). The most important characteristics of these hippocampal cells can be summarised as follows: (1) they are very selective in their firing, since they only fire when the animal is crossing the place field (Wilson and McNaughton, 1993); (2) the same cells can have place fields in more than one environment, representing the space in different places (O'keefe and Conway, 1978); (3) they are independent

⁶The Medial Temporal Lobe is formed by the hippocampal region (including the CA fields, the dentate gyrus, and the subicular complex), the amygdala, and the entorhinal, perirhinal and parahippocampal cortices (Squire, 2004).

of direct visual input: the absence of light or the removal of some visual cues does not change their firing pattern, as long as the location is clear (Quirk et al., 1990; Save et al., 1998); (4) place cells have a non-topographic organisation (O'Keefe, 1979; Redish et al., 2001).

Based on the cognitive map theory (Tolman, 1948), O'keefe and Nadel (1978) proposed that these cells are part of a neural system that forms a map of the environment, with each of the cells representing only one part of that environment.

1.1.4 Concept cells

Neurons in the human MTL were found to respond (i.e. increase their firing rate with respect to baseline) to a specific person, animal or landscape (Quiroga et al., 2005). For example, a neuron in the left posterior hippocampus of a patient⁷ increased its firing rate every time a picture of the actress Jennifer Aniston was presented, while when the patient was looking at a picture of any other person, animal or place the neuron remained either silent or with a low firing rate. Regardless of the visual or any other low-level features of the stimuli, the neuron fired every time the patient was shown a picture of Jennifer Aniston. This characteristic is called invariance, and is one of the most salient features of the concept cells. Other neurons fired to the written name of the stimulus eliciting the response (preferred stimulus) and even to the spoken name pronounced by a computer synthesised voice (Quiroga et al., 2009). It was also seen that some neurons responded to associated stimuli (e.g. two characters from the movie Star Wars: Yoda and Luke Skywalker). Furthermore, an experiment showed that it was possible to create an association of two unrelated concepts: two stimuli (a place and a person), one previously eliciting a response and a neutral one, were put together and after a few trials the neuron started firing to the non-preferred or neutral stimulus as well as to the originally preferred stimulus (Ison et al., 2015). This kind of associations are believed to be crucial for the formation of episodic memories (Howard et al., 2005; Quiroga, 2012).

Taking all this information together, we can argue that these neurons fire

⁷These recordings are taken from epileptic patients that have intracranial electrodes implanted for clinical reasons.

to concepts and not to specific visual or sensory features. The facts that a cell might (1) respond with a high degree of invariance to a specific stimulus (Quiroga et al., 2005), (2) respond not only to pictures but also to cartoons and to the written and spoken name of the stimulus (Quiroga et al., 2009), (3) respond to two or more associated stimuli (Quiroga and Kreiman, 2010; Quiroga et al., 2009; Quiroga, 2012), and (4) rapidly encode new associations (Ison et al., 2015) indicate that, in the MTL, there is a thorough interpretation of the stimulus, deep enough to associate it to other individuals or objects.

Given the fact that concept cells are located in areas that are known to be involved in memory formation, it has been argued that concept cells constitute a solid base for memory – i.e. the conceptual representation that allows the rapid formation of new associations (Quiroga, 2012). In everyday life, we are exposed to a massive amount of information that we cannot remember, because there is a limit to the amount of information we can store. This way, we tend to remember what is relevant to us and forget details that are not so important. It is not surprising then that concept cells were found to respond to persons, objects or places that were familiar or somehow important to the patients (Viskontas et al., 2009). Furthermore, creating a network of associations between different concepts could make it easier to store and retrieve information (Viskontas et al., 2009; Quiroga, 2012). If we consider that cells responding to the same stimulus form a cell assembly, and that there is some overlapping between two assemblies encoding two different concepts, then we can understand how one stimulus can rapidly evoke the memory of the other one (e.g. seeing a picture of Yoda can trigger the memory of Luke Skywalker). If there are two concepts that are in principle unrelated to each other, but for some reason we form a new association between the two of them, then that association could be explained by Hebbian plasticity: new connections are made (or old connections are strengthened) between cells that form part of the two different cell assemblies. This way, the activation of one assembly can, from now on, trigger the activation of the other.

1.2 Neocortex

The cerebral cortex is the most superficial layer of the brain. Its functional organisation and heterogeneity among different areas has also attracted the attention of many scientists.

Different areas of the cortex process basic sensory stimuli or determine behaviour and other high level processes, and they are delimited according to functionality: the visual cortex processes visual information (Hubel and Wiesel, 1962), the auditory cortex, auditory information (Heffner and Heffner, 1986), somatosensory cortex processes sensory information (Purves et al., 2004), as well as barrel cortex (Petersen, 2007), and olfactory cortex, olfactory information (Squire et al., 2012). The motor cortex controls motility through connections with the muscles (Squire et al., 2012). Other parts of the cortex, such as the prefrontal cortex, are associated with higher level processing, like decision making, social behaviour, and personality (ODoherty, 2004; DeYoung et al., 2010; Bechara et al., 2000; Damasio et al., 1994).

Like the hippocampus, the neocortex⁸ shows a laminar organisation; however, the anatomical organisation of the two regions differ in many aspects. Three to six layers can be identified in the cortex, each of which has characteristic functional and anatomical features as well as different input sources and output targets. The cells in the different layers make connections either in the vertical axis (across layers) or in the horizontal axis (lateral connections). Lorente de Nó (1922) was one of the first and main contributors to the description of this layered structure. The main characteristic of these layers can be summarised as follows:

Layer I contains the apical dendrites of pyramidal neurons and some axons, together with some glial cells. Layer II contains small pyramidal neurons and some stellate neurons. Layer III contains pyramidal neurons and non-pyramidal neurons with their axons. Layer IV contains a few kinds of pyramidal and stellate neurons and receives projections from the thalamus and intrahemispheric cortico-cortical afferents. Layer V has large pyramidal neurons whose axons leave the cortex and reach other subcortical areas. Layer VI has a few small

⁸The neocortex is supposed to be the most recent part of the cortex (in evolutionary terms), distinguished by the time of its emergence in evolution from the archicortex (hippocampus) and paleocortex (olfactory bulb and olfactory cortex).

pyramidal neurons and several small spindle-like pyramidal neurons that send projections to the thalamus.

Perpendicular to the layers, from the surface to the white matter, there are groups of cells that have similar functional properties (Mountcastle, 1997). Experiments with electrophysiology in the cat's and monkey's somatosensory cortex showed that when the electrode was perpendicular to the surface of the brain all the cells located at different depths (perpendicular to the layers) had the same receptive field –area of the body which after tactile stimulation elicits a response in the cortical cells– (Mountcastle et al., 1957; Powell and Mountcastle, 1959). This first idea of a columnar organisation of the cortex was later found to be also true for the visual cortex (Hubel and Wiesel, 1962, 1963) where all the cells in a column have the same receptive field –bars with specific orientations– (Ohki et al., 2005).

1.3 Neurophysiology recordings

There are plenty of techniques for studying the brain that can be divided into two broad groups: the ones that measure the normal activity of the brain without affecting it, such as optical imaging and electrophysiology, and the ones that alter its normal functioning to study the effect of these alterations, such as lesions and ablations, and optogenetics.

1.3.1 Electrophysiology

The cells in the brain communicate with each other through electro-chemical activity (Buzsáki et al., 2012).

Electrophysiology, one of the most popular techniques to measure the activity of the brain, takes advantage of the electrical properties of the neurons. Furthermore, it offers a wide variety of techniques, each suitable for different problems or questions: intracellular –voltage (Huxley, 1996) and current clamp– and extracellular recordings. This technique can be used for *in vitro* and *in vivo* experiments, with a high signal-to-noise ratio (SNR). It also offers very high temporal resolution. It permits the study of either one neuron (or even a single ion channel) or a whole population of cells (Harvey et al., 2009). For

intracellular recordings the electrode is normally a glass micro-pipette filled with a solution that mimics the intracellular fluid. The electrode penetrates the cell (or contacts the membrane) and records voltage or current changes across the membrane. Even though intracellular recordings provide precise information of the firing patterns of a neuron and its subthreshold activity, it can become challenging when trying to record from awake and behaving animals, since the movements from the brain, the respiration, and the body jeopardises the stability of the recording (i.e. a minimum change in the position of the micropipette will bring as a consequence the loss of the signal). Although there are some advances in the area (Long and Lee, 2012), extracellular recordings are still of preference at the time of designing an experiment to study the neural correlates of a specific behaviour.

For extracellular recordings, the electrode is placed near the cells (not necessarily in contact with them) and records the activity of several neurons that are close to the electrode tip. From these recordings, the activity of single neurons can be identified and isolated with a method called spike sorting (Quiroga et al., 2004). This allows the acquisition of information of several neurons at the same time, but also to study the behaviour of a single neuron (Figure 1.2).

Extracellular recordings have been a crucial ally to study neuronal correlates of behaviour or responses to different stimuli and also an invaluable tool for assessing the effect of specific modifications to the normal activity of the brain (see: Section 1.4).

1.3.2 Optical imaging

Optical imaging involves the use of light to visualise neurons and their activity patterns. The main advantages, compared to electrophysiology, are that the recorded cells can be perfectly identified –we can know cellular type and location of these cells–, and that neurons that are not active can also be seen. Although sometimes we can identify the cellular type with electrophysiology by the firing frequency or the shapes of the spikes (Ison et al., 2011), it requires a thorough data analysis and previous knowledge. Imaging also provides great spatial resolution over a wide range of scales: going from dendritic spines (Chen et al., 2011; Popovic et al., 2015) to a big neuronal population (Dombeck et al., 2010;

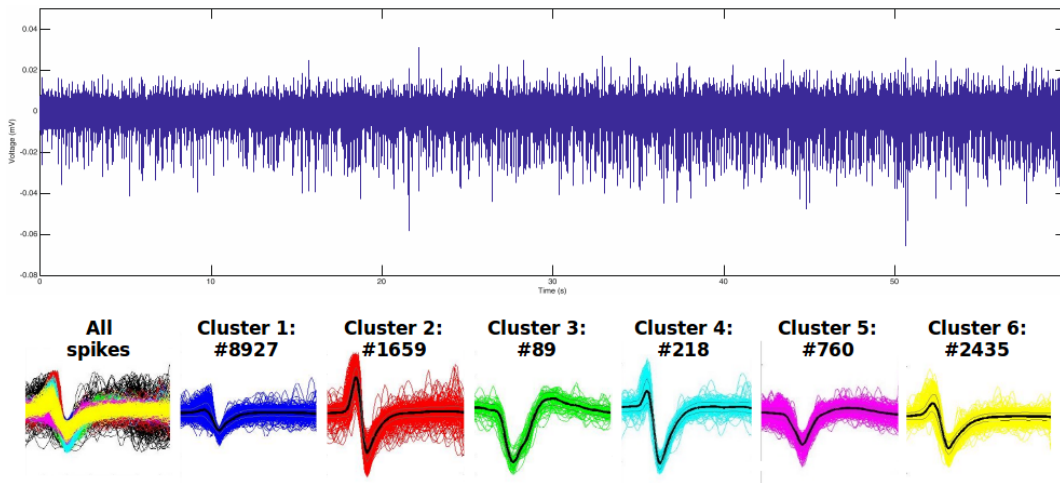


Figure 1.2: **Spike sorting from an extracellular electrode.** Top: Signal recorded from an extracellular electrode from a mouse hippocampal slice. The signal was high-pass filtered (300-3000 Hz) for spike visualisation. Bottom: Spikes detected after spike sorting with Wave_clus. First, all the spikes detected are shown together (All spikes) with the colour of the cluster to which they were assigned. In this example, 6 different clusters were detected, 5 of which probably correspond to single units (clusters 2-6) and the remaining one to multi-unit activity. More than 14,000 spikes were detected and classified. These spikes correspond to a one-minute long recording from a mouse hippocampal slice. The activity was induced with Kainate (200 nM).

Huber et al., 2012) (Figure 1.3).

Another great advantage is that the use of light is relatively less invasive than the use of electrodes, in terms of the damage produced to the cells. The insertion of electrodes is more harmful for the neurons than light passing through the tissue (Scanziani and Häusser, 2009).

Optical imaging has broadly two major components: light and fluorescence. In order for the cells of interest to emit fluorescent light, they need a reporter, which can be in the form of a chemical fluorescent molecule (Paredes et al., 2008; Grienberger and Konnerth, 2012) or a fluorescent protein (Heim et al., 1995; Nakai et al., 2001; Chen et al., 2013). Once the cells are able to emit fluorescence through these indicators, light is necessary to excite them. In the simplest case, when a fluorophore absorbs energy (in the form of light) an electron can be promoted from the ground singlet state (S_0) to the first (or in some cases second) excited singlet state (S_1 or S_2). The relaxation back to S_0 is normally both non-radiative (i.e. the energy is dissipated as vibrations)

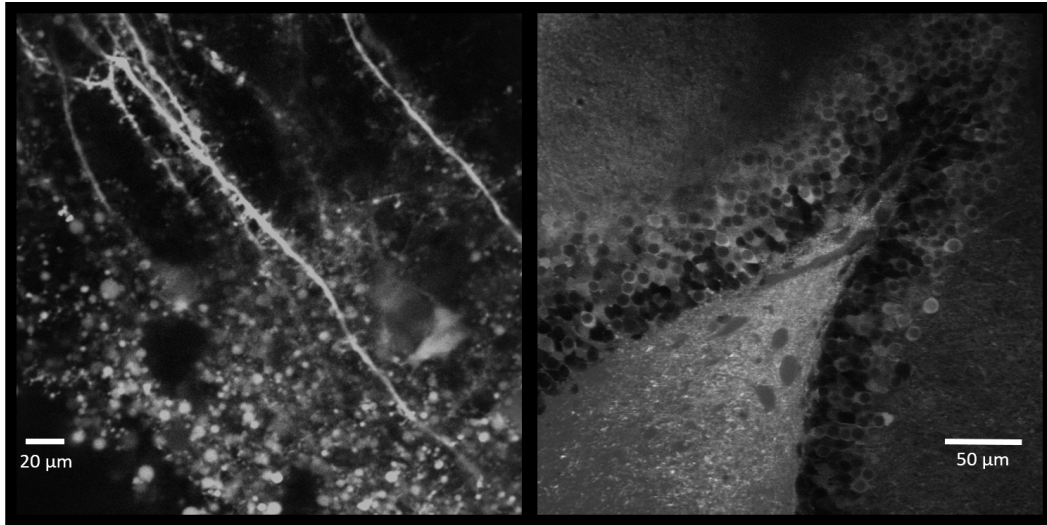


Figure 1.3: **Dendrites and cell bodies from CA1 and Dentate gyrus.** Dendritic spines from CA1 pyramidal cells (left) and granule cells from the dentate gyrus (right) expressing GCaMP6s and imaged with a two-photon microscope, after electrical stimulation (left) or excitation with Glutamate (right). Mouse brain slices (350 μm thick, depth: 50 μm -left- and 150 μm -right- from the surface of the slice). Both pictures were taken with the two-photon microscope in the laboratory.

and radiative (i.e. emission of light). This light emission is what is known as fluorescence (Lakowicz, 2013). Because part of the energy absorbed is dissipated in a non-radiative way, the fluorescence emitted always has a longer wavelength (i.e. less energy) than the absorbed light.

In spite of great advances in the field, imaging neurons in an intact brain remains a major challenge due to limitations that have not been yet overcome. Wide-field fluorescence microscopy is strongly limited by light scattering, which makes it a suitable technique for imaging cell cultures or thin slices, but it becomes less useful when imaging at greater depths. Confocal microscopy partly overcomes the effects of light scattering with the use of a pinhole, which rejects out-of-focus fluorescence. This way, the pinhole increases the optical resolution of this technique, compared to wide-field microscopy, but at the cost of losing part of the signal, which implicates increased excitation light power and photodamage. Wide-field and confocal microscopy use excitation light within the range of visible light, and it is based on the absorption of one photon (1P) of light by the fluorophore. In contrast, two-photon (2P) excitation, uses

near-infrared (NIR) light. The main advantage of 2P over 1P microscopy is the possibility of deep imaging within tissue with high resolution (Denk et al., 1990). NIR suffers from much less absorption from biological tissue than visible light. Visible light is absorbed by different endogenous chromophores, such as water, proteins, melanin, etc. The photons that are absorbed by these chromophores will no longer be able to excite the fluorophores, and therefore are lost for imaging purposes. Also, visible light is more scattered than NIR light. As the light penetrates deeper and deeper in the tissue, the probability of the photons hitting scattering particles or being absorbed by endogenous chromophores increases, and therefore there will be less light reaching the focus.

2P imaging is based on the virtually simultaneous –less than 10^{-5} s– (Helmchen and Denk, 2005) absorption of two NIR photons, whose combined energy is sufficient to produce the excitation that ends up in emission of light (So et al., 2000). Because of the fact that the probability of two photons of NIR light being absorbed almost simultaneously is very low, it only happens where there is a high photon density, and this only occurs within a small volume of tissue around the focal point of about $0.1 \mu\text{m}^3$ (focal volume). This localisation of the excitation is of extreme importance for imaging thick samples, because given that there is no excitation outside the focal volume, there is no out-of-focus emission (Figure 1.4).

To increase the probability of the 2P absorption to take place, high intensities of light are needed. However, light at high intensity might be damaging for the living tissue. This can be avoided by using a pulsed laser source and by focusing the laser beam through a high numerical aperture objective. The fact that the pulses are very short (80 fs) means that most of the time there is no light being shone onto the sample. This way, the pulses can be of very high intensities (around 150,000W) but the average intensity of the light reaching the tissue is around 1W, along the total time of irradiation.

Titanium-Sapphire (Ti:sapphire) lasers have these characteristics, which is why they are ideal for 2P imaging. These are tuneable lasers with light within the range of $\sim 700\text{-}1100$ nm that generate ultrashort pulses of light, with frequencies of 80-150 MHz (Denk, 1994).

Summarising, 2P microscopy has four major advantages over 1P imaging (Svoboda and Yasuda, 2006):

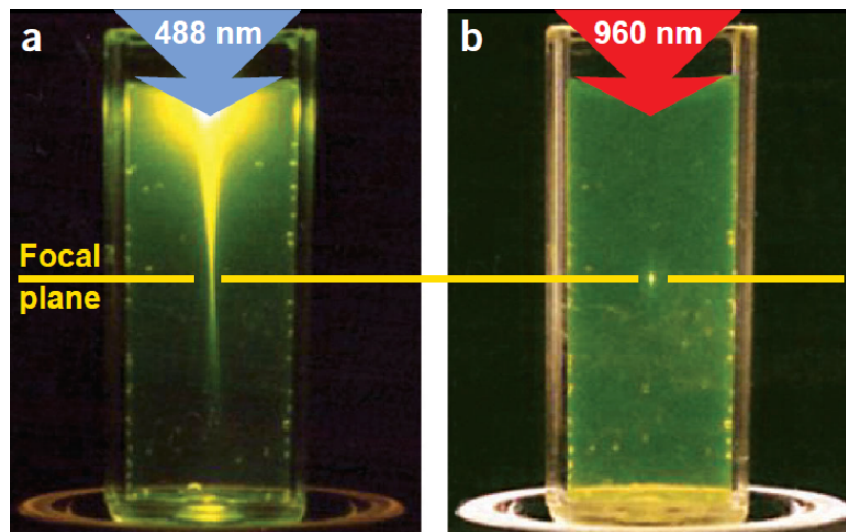


Figure 1.4: **Comparison between 1P and 2P excitation.** Left: 1P excitation (488 nm) of fluorescein. Right: 2P excitation (960 nm) of the same fluorophore. The phenomenon of localisation can be observed in this picture. While the excitation with 1P can be observed in a large volume, when the fluorophore is excited with 2P there is only a small volume emitting light. From Zipfel et al., 2003.

1. 2P microscopy uses deep red and NIR light, which makes the penetration of light through the tissue more efficient than with visible wavelengths. This is because the light is not only less scattered but also it is less frequently absorbed by endogenous chromophores.
2. Scattered photons are too few to produce detectable fluorescence.
3. Because the excitation is highly localised, all the emitted photons, scattered and non-scattered (ballistic), can be detected and contribute to the useful signal.
4. The wide gap between excitation and emission wavelength permits the rejection of excitation light by the detectors, which would only contribute to the background noise.

Calcium Indicators

As stated before, fluorophores are needed to visualise neurons, but more importantly, they can be good indicators of a neuron's activity. The most

common ones are the Calcium indicators, but there are also voltage sensitive dyes (Peterka et al., 2010).

Calcium is a very important second messenger involved in a wide variety of responses in the cells (Berridge et al., 2000). Specifically, in neurons, when action potentials (AP) are fired, the change in the membrane potential opens Ca^{2+} channels that will allow the influx of this cation into the cell (Bean, 2007). A raise in the concentration of intracellular Ca^{2+} ($[\text{Ca}^{2+}]_i$) in the presynapsis mediates the exocytosis of vesicles with neurotransmitters that will be released into the synaptic cleft, having an effect on the postsynaptic cell (Neher and Sakaba, 2008).

Calcium indicators take advantage of the direct relationship between Calcium and AP firing: given that increases in the $[\text{Ca}^{2+}]_i$ are tightly coupled to AP firing, fluorescence changes of indicators are good estimators of the neuron's activity (Yuste et al., 2011).

Most of the calcium indicators are synthetic molecules or proteins that have the property of binding Calcium. When they bind free Calcium they suffer conformational changes that lead to an increase in the fluorescence emission.

Proteins (also known as Genetically Encoded Calcium Indicators GECIs-) have a more sophisticated mechanism to estimate the $[\text{Ca}^{2+}]_i$. The proteins belonging to the GCaMP family, the most commonly used type of GECI, are formed by circularly permuted Green Fluorescent Protein (cpGFP) or Enhanced Green Fluorescent Protein (EGFP), the calcium binding protein calmodulin, and calmodulin-binding peptide (M13) (Miyawaki et al., 1997; Mao et al., 2008). In the presence of Calcium, the interaction between calmodulin and M13 induce conformational changes in the fluorescent protein that lead to an increase in the fluorescence emitted (Mank and Griesbeck, 2008).

Both types of indicators, the synthetic and the GECIs, have advantages and disadvantages. While the synthetic indicators have a higher SNR, loading them can be challenging as not only they can accumulate in intracellular compartments but also are sometimes sequestered into vacuoles by the cell (Di Virgilio et al., 1988). This is a serious impediment for performing long-lasting *in vivo* experiments (Looger and Griesbeck, 2012). The GECIs, despite being less sensitive and having slower kinetics, last for much longer periods of time and also can be expressed in a specific cellular type, or even subcellular locations

(Hasan et al., 2004). These are the main reasons why a protein from the GCaMP family was chosen to carry out this project. The potential to apply some of the results obtained in this thesis *in vivo* is very high, given that some limitations are overcome.

1.4 Stimulation of neural activity

As mentioned before, manipulating the normal brain activity is a useful tool to understand its functioning. Four ways of manipulating the brain will be described in this section: electrical stimulation, pharmacological stimulation, optogenetics, and uncaging.

1.4.1 Electrical Stimulation

As stated in Section 1.3.1, neurons communicate through electrical signals. Thus, a simple way of stimulating them is by injecting current into the neurons to change their membrane potential. This can be easily achieved using a stimulation electrode and a stimulator –or stimulus generator–.

Important results have been obtained from studies using electrical stimulation, *in vitro* and *in vivo*. An example of this is the discovery of Long-Term Potentiation, a phenomenon observed in the hippocampus after repetitive stimulation of the perforant path (Bliss and Lømo, 1973). More recently, APs firing of place cells were paired with electrical stimulation of the medial forebrain bundle, which is known to induce reward (Hernandez et al., 2006). After this pairing, mice spent more time in the place field of the neurons whose APs had been paired with the stimulation, creating this way a false memory of something that never took place (de Lavilléon et al., 2015).

Electrical stimulation can also be useful to decipher simple neuronal circuits. When stimulating one area or neuron and recording from a different one, an idea of how the two areas or cells are connected between each other can be obtained.

1.4.2 Pharmacological Stimulation

Another classic way of stimulating brain cells is by the use of a wide variety of ions, such as K^+ and Na^+ , and drugs, such as neurotransmitters, toxins, and receptors' agonists and antagonists. There are inhibitory and excitatory neurotransmitters, being GABA (γ -aminobutyric acid) and glutamate the most important in the mammalian brain, respectively. The effect of these neurotransmitters can be mimicked by agonists and antagonists of their receptors. Some GABA receptors agonists are muscimol (for GABA_A receptor) and baclofen (for GABA_B receptor) while drugs such as bicuculline and phaclofen antagonize the subtypes A and B of these receptors, respectively (Johnston, 1994). Having the glutamate so many different subtypes of receptors, it is difficult to name agonists and antagonists for each of them, but some of the most well-known are kainic acid, NMDA, and AMPA, all of which gave their name to the subtypes of receptors they activate (Dingledine et al., 1999). Among the many antagonists, kynurenic acid, ketamine (a drug used for anaesthesia), and 6,7-dinitroquinoxaline-2,3-dione (DNQX) can be mentioned (Marosi et al., 2010; Jin et al., 2013; Honore et al., 1988).

The pharmacology of the neurotransmitter receptors in the mammalian brain is highly complex and pharmacological stimulation (or inhibition of activity) has been and still is broadly used to understand different processes and phenomena related to the brain (Collingridge et al., 1988; Cunningham et al., 2003; Gipson and Yeckel, 2007; Kim et al., 2012).

1.4.3 Optogenetics

One of the most exciting recent developments in Neuroscience is the introduction of Optogenetics (Lima and Miesenböck, 2005).

This technique uses light to excite or inhibit neuronal activity (Deisseroth, 2011). It is based on a series of proteins called opsins, which are gated ion channels sensitive to light. These opsins can either produce optogenetic excitation (Channelrhodopsin) or inhibition (Halorhodopsin), depending on the ion they are specific for. These proteins are usually activated by light of different wavelengths, which allows their simultaneous use with no interference. Currently, Channelrhodopsin2 (ChR2) (Nagel et al., 2002) is the most widely

used opsin for optogenetics (Cardin et al., 2009; Kohara et al., 2014; Kohl et al., 2011; Sato et al., 2014). When ChR2 is exposed to light of the appropriate wavelength, part of the protein suffers a conformational change which in the end makes the cation channel open, allowing mainly Na^+ ions influx (Nagel et al., 2002). Normally, to stimulate with light *in vivo*, animals are implanted with an optic fibre that delivers light, although for stimulating superficial cells, light can be delivered through the thinned skull (Cardin et al., 2010).

Liu and colleagues managed to create a false memory in mice (Liu et al., 2012) using optogenetics and other genetic manipulations. In order to do this, they genetically marked neurons in the dentate gyrus that were active during the encoding of a context, inducing the expression of ChR2 only in those cells. Following this, they artificially reactivated these neurons with light during fear conditioning in a different context. They found that animals showed a fear response whenever they were exposed to the first environment, unrelated to the fear conditioning. Interesting findings about memory formation and manipulation, using the same technique, followed this work (Liu et al., 2013; Ramirez et al., 2013; Redondo et al., 2014).

1.4.4 Caged compounds

In the 1970s, Kaplan et al. (1978) started to develop a new tool for biological experiments that currently continues to be improving. The possibility of having precise spatio-temporal control of the application of an excitatory or inhibitory molecule is a useful tool for biological experiments. Caged compounds provide the possibility of selectively activate or inhibit single cells (or even parts of a cell). They consist of two main parts: a photolabile protective group and a biologically active molecule (Figure 1.5). While the two parts remain together, the biologically active molecule has no effect on cells; however, when the bond between the two parts is broken, the molecule recovers its biological activity. The way of breaking this bond is by delivering energy, which can be in the form of light.

The caged compound can be applied to the biological preparation (cell culture, slices or even the whole animal), in principle, with no effect at all. The experimenter can control exactly when and where to release the molecule of interest by pointing a laser on the region of interest, that can go from several cell

bodies to a single dendritic spine (Matsuzaki et al., 2004; Kwon and Sabatini, 2011).

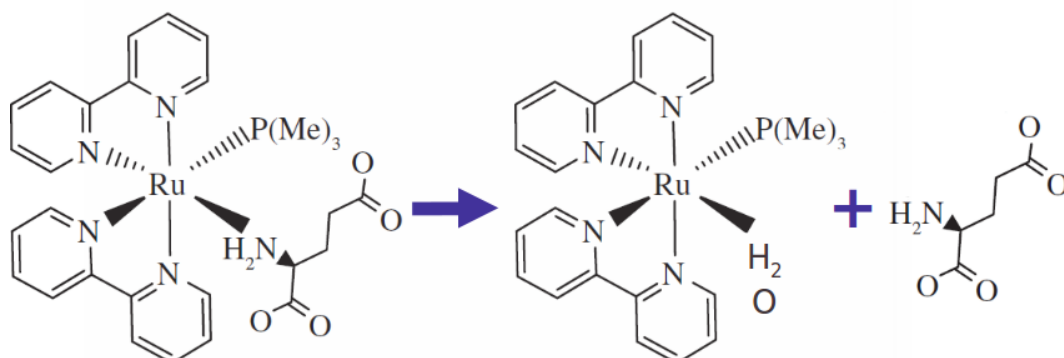


Figure 1.5: **Structure of [Ru(bpy)₂(PMe₃)(GluH₂)] (RuBiGlutamate).** The inorganic cage consists of a centre of Ruthenium coordinated with a trimethylphosphine, and two bipyridine (in cis configuration). The remaining coordinating site is occupied by the glutamate. Light absorption produces the release of the glutamate, which recovers its biological activity when it is free. Its site is occupied by a molecule of water (if in aqueous solution). Adapted from Zayat et al. (2013).

Nowadays, there are different types of caged compounds, all of them differing in the physicochemical properties of the protective group. These differences translate into different uncaging strategies. Some of the existing compounds, especially the older ones, need UV light to break. UV light is not optimal for experiments with living tissue, mainly because of two reasons: it causes photodamage to the cells (i.e. mutations in DNA) and it is highly scattered, which reduces the spatial resolution. For this reason, different protective groups were developed in order to improve their compatibility with living tissue (Wieboldt et al., 1994; Canepari et al., 2001; Zayat et al., 2007; Trigo et al., 2009; Salierno et al., 2010).

Ideally, caged compounds must be soluble in water (or polar solvents) and resistant to hydrolysis when not activated by light. There should not exist any interaction between the cells in the living tissue and the compound, as long as there is no photolysis. Also, the photolysis should occur with a high quantum efficiency, and at long wavelengths, to make it less harmful for the cells (Givens et al., 1998; Pelliccioli and Wirz, 2002).

As mentioned in Section 1.3.2, two-photon imaging is rapidly becoming the most important technique to measure neuronal activity. For this reason, it is also desirable that the caged compounds absorb two (NIR) photons, as well as one, with a high absorption cross section⁹, as this permits the implementation of two-photon microscopes for uncaging.

Among the commercially available caged compounds (Tocris Bioscience), two of them are the most commonly used: 4-methoxy-7-nitroindolinyl-X (MNI) and RuBi-X, with X being a molecule of biological interest. Table 1.1 shows a comparison between the two of them.

Table 1.1: **Comparison of RuBi and MNI compounds.** Among the commercially available caged compounds, these are the two most widely used. The most important characteristics of the two are shown in the table. It can be observed that RuBi compounds have several advantages over the MNI, especially the two-photon absorption and cross-section, and the concentration at which the GABA receptor antagonist effect becomes significant.

	RuBi	MNI	Source
Solubility in water	20 mM	50 mM	Tocris Bioscience (https://www.tocris.com/)
One-Photon Excitation (nm)	473-532	300-380	Salierno et al. (2010)
Two-Photon Excitation (nm)	800	720	Salierno et al. (2010) and Matsuzaki et al. (2004)
Quantum Yield	0.13	0.085	Fino et al. (2009) and Tocris Bioscience (https://www.tocris.com/)
Cross section	0.14	0.02-0.06	Salierno et al. (2010), Matsuzaki et al. (2001), and Tocris Bioscience (https://www.tocris.com/)
Concentration needed for 2P uncaging	300 uM	>2.5 mM	Fino et al. (2009)
Antagonism	300 uM	<300 uM	Fino et al. (2009)

MNI compounds are based on an organic structure. RuBi compounds, instead, are based on an inorganic structure, with a centre of Ruthenium (Ru(II)) forming six coordinating bonds with the ligands. These ligands donate 1 or 2 pairs of electrons (mono and bidentate ligands, respectively) for the bond to take place, and so they must be good electron donors (Cotton et al., 1999). In the case of RuBi, the ligands are two bipyridines, a trimethyl-phosphine,

⁹The absorption cross section is a measure for the probability of a photon (or two, as in this case) absorption process. The higher the cross section, the higher the probability of two photons to be absorbed, and hence the more suitable the compound for two-photon uncaging.

and the molecule with biological activity.

Upon light absorption, which for some protective groups can be either in the form of one or two photons, there is an electronic transfer from the metal (Ruthenium) to the ligand, going from the basal state to an excited singlet state $^1\text{MLCT}$ (Metal-to-Ligand charge transfer). From here, the electron can populate the triplet $^3\text{MLCT}$ band which, in turn, can be deactivated in three ways: emitting light (radiative), through non-radiative processes or, if the energy is enough, population of the non-bonding state (d-d) (Figure 1.6). The population of the d-d state will lead to the release of the ligand (Zayat et al., 2013). The probability of dissociation will be subject to the energy difference (ΔE) between the states $^3\text{MLCT}$ and d-d: the smaller the difference, the higher the probability of photo-release and, thus, the quantum yield. This difference is given by the properties of the bond between the ligands and the Ruthenium, and therefore the combination of the optimal ligands defines the characteristics of the caged compound. To complete the energy transfer, the RuBi complex absorbs light with maximum efficiency at 400-500 nm.

As previously stated, solubility in polar solvents is a very important requirement, since the compound has to be soluble in solvents that are compatible with living tissue. Both types of compounds, RuBi and MNI, are soluble up to a concentration in the order of tens mM. Previous evidence has shown that, in order to observe a biological effect, it is necessary to use them at concentrations of a few hundred μM for RuBi and less than 10 mM in the case of MNI (Fino et al., 2009; Matsuzaki et al., 2004).

A common problem to all protective groups is that in reality they are not completely inert, and they do have some effect on the cells when applied: they act as a GABA receptor antagonist, blocking GABAergic transmission when they are applied in high concentrations (Molnar and Nadler, 2000; Maier et al., 2005; Rial Verde et al., 2008). For this reason, a high two-photon absorption cross section is crucial, given that this would allow the use of lower concentrations without diminishing the probability of absorption and would avoid the antagonist effect on the GABA receptors. It was previously shown that the RuBi's antagonist effect starts becoming relevant when used at concentrations greater than 300 μM , while in the case of MNI, 300 μM already has a very strong effect over the inhibitory currents (Fino et al., 2009).

The quantum yield is also higher for RuBi than for MNI (~ 0.13 vs ~ 0.085 , respectively) (Fino et al., 2009), meaning that less power of light is required to photo-release the same amount of Glutamate (or any other ligand) molecules. This is always an advantage when experimenting with living tissue, since very energetic irradiation is not good for the cells.

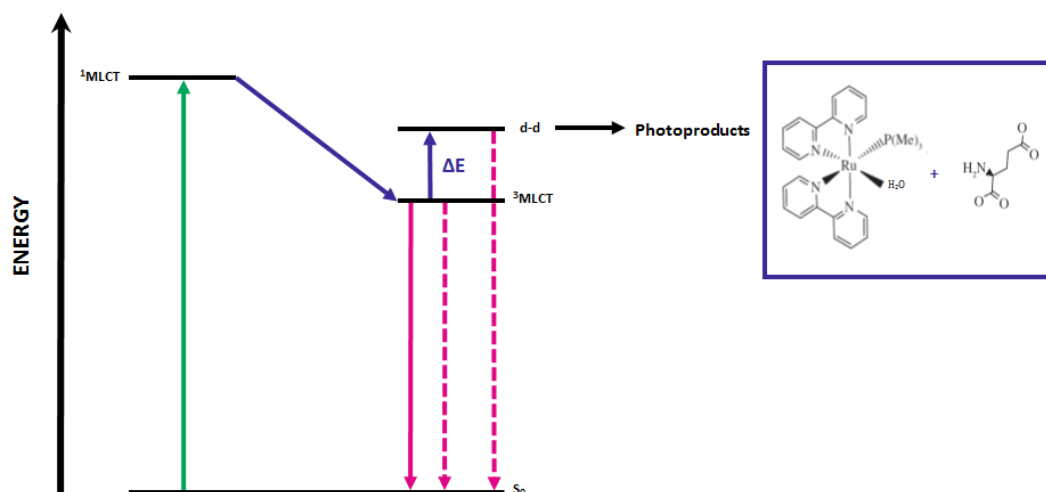


Figure 1.6: **Jablonski diagram for a typical inorganic caged compound photorelease.** When the protective group absorbs a photon, there is a charge transference from the metal to the ligand, to a singlet state called $^1\text{MLCT}$. From there, it relaxes to a triplet state of lower energy, $^3\text{MLCT}$. The final relaxation from here can be in radiative and non-radiative ways, but, if there is enough energy, a third energy level can be populated, called d-d, which leads to the release of the ligand.

Another advantage of the RuBi compounds over the MNI is that the photo-cleavage can occur with light of longer wavelength (473-532 nm vs. 300-380) (Salierno et al., 2010). Using longer wavelengths implies less scattering, which at the same time means higher spatial resolution and tissue penetration (Svaasand and Ellingsen, 1983). Also, UV light sources are much more expensive than visible light lasers, which drastically reduces the cost when using RuBi compared to MNI.

As previously mentioned, another important property of caged compounds is its absorption of energy in the form of two-photons. Not all the caged compounds can be released using NIR light, through the simultaneous absorption of two photons. As with imaging, two-photon absorption provides better spatial

resolution which makes it a useful tool for exciting or inhibiting dendritic spines, or deep tissue (e.g *in vivo*). Regarding two-photon absorption, RuBi absorbs light of 800 nm (Salierno et al., 2010) while the optimal wavelength for MNI is 720 nm (Matsuzaki et al., 2001). This is of particular importance, since a longer wavelength not only has deeper penetration but it is also closer to the range of wavelengths suitable for most of the GECIs (~ 900 nm).

Taking into account the various advantages the RuBi compounds have over the MNI compounds when applied for two-photon uncaging, they were chosen to perform the experiments that will be described in this thesis.

1.5 Aims and organisation of the thesis

This thesis is divided in three parts, each describing a different project. The first two projects, both *in vitro*, were carried out by myself, and the third one, *in vivo*, was a collaboration with two other members of the Centre for Systems Neuroscience.

The scientific aim of the first part, which consisted of doing *in vitro* electrophysiology, was to replicate a classic finding that Kainic acid (Kainate) induces gamma oscillations in hippocampal slices. The motivation of this project was to empirically assess and gain confidence on a particular slicing technique. These experiments are described in Chapter 2.

The second project, involved doing *in vitro* two-photon imaging, as described in Chapter 3. For this project, a whole imaging set-up was mounted, including the necessary tools for electrical stimulation. It was also necessary to perform weekly surgeries in order to have mice expressing the calcium indicator protein GCaMP6s. The optimal wavelength to excite GCaMP6s is around 920 nm, while the optimal wavelength for uncaging is around 800 nm. This project aimed to find an optimal excitation wavelength to do calcium imaging with proteins from the GCaMP family and Glutamate uncaging at the same time, without the necessity of changing the wavelength between one process and the other or using two light sources. This new approach would easily allow the simultaneous excitation (or inhibition) of several neurons using a diffractive material. One limitation of the current approach, which uses two different beams of light of two different wavelengths, is that it is impossible to photorelease caged compounds

and do 2P imaging in several positions at the same time. This is because, for doing this, it is necessary to split the beam of light using a diffractive material and these materials affect differently light of different wavelengths. To overcome this issue, we developed a method to uncage and do 2P imaging with a single laser beam using the same wavelength, which could potentially be applied to manipulate the activity of a network of neurons *in vitro* and *in vivo*.

For achieving this objective, it was necessary to first characterise the protein in order to understand its behaviour at excitation wavelengths different than the optimal ones.

Once this technique is optimised it will be applied to the third project described in this thesis, in Chapter 4. This project started as a collaboration among Dr. Molano-Mazón, Dr. Boyraz-Jentsch and myself. The long-term objective is to study the existence of analogue neurons to the concept cells described for humans in mice. This would allow the development of an animal model for a more thorough study of these neurons that are believed to be the base for memory formation. In order to study this, we built a virtual reality set-up in which mice perform a two-alternative forced choice between two objects with different shapes (two holes on a wall that look like a tight space where the animal can enter). One of them is rewarded, the other one is not. Once the animals achieve a high performance on this task and significantly choose the rewarded object more than the non-rewarded one, the next step is to test invariance, by changing low-level features of the objects. It is expected that, once the animals perform this task under the two-photon microscope, there will be neurons in the hippocampus that will respond to all the variations of the objects presented during the training. If this is the case, then the final objective will be to apply caged compounds with inhibitory and excitatory neurotransmitters (i.e. GABA and glutamate, respectively) in order to selectively inhibit or excite specific neurons and assess its effect on the animals' behaviour.

Chapter 2

In vitro electrophysiology

2.1 Introduction

In vitro experiments are ideal for studying some neuronal processes. While *in vivo* experiments are more realistic and allow a wider variety of studies, they are technically more difficult and sophisticated (and usually more expensive). In spite of the huge amount of *in vivo* experiments done in the last decades, some questions must be addressed through *in vitro* experiments, either because of technical limitations or to take care of the animals' welfare (e.g. drug testing, effect of toxins, etc.).

Brain slices are a widely used model for *in vitro* experiments, since they contain a large number of neurons, connected among each other and, if well cut, some of the connections of the intact brain are well preserved. Also, once cut, they can last for several hours, allowing a whole day of experiment.

The preservation of the connections among different neurons is essential for some kinds of experiments, and it makes the model more realistic. The preservation of the connections after cutting the slices depends on many factors, being probably the most important one the angle with which the slices are cut. The optimal angle is different for different areas of the brain and when learning the slicing technique it is one of the most challenging steps. Because of this reason, we ran a series of experiments to test the quality of the slices before moving to more complex experiments.

2.2 Methods

All procedures were approved by the University of Leicester's Animal Welfare and Ethical Review Body (AWERB) committee and performed under license from the UK Home Office in accordance with the Animals (Scientific Procedures) Act 1986.

2.2.1 Animals

Mouse hippocampal slices were prepared from CBA mice aged between 10 and 20 post-natal days. Young mice are known to be better for the kind of experiments that were performed, as there is an age-dependent reduction of kainate-induced gamma oscillations (Vreugdenhil and Toescu, 2005).

2.2.2 Slices

For slices preparation, mice were decapitated and the brain was removed and rapidly cooled by being placed in iced low Na^+ artificial cerebro-spinal fluid (slicing aCSF) -see Table 2.1 for composition-. The solutions, were freshly prepared, at least every two days. Using a blade, two cuts were made: one posterior, to separate the cerebellum and another one anterior, to separate the olfactory bulb. A third cut was made to separate the two hemispheres and one of them was kept in ice-cold slicing aCSF in case it was needed. A last cut was made to the other hemisphere to remove some of the cortex, obtaining a flat dorsal surface. This surface was first dried with fine filter paper and then glued onto a tray that goes immersed in iced slicing aCSF being continuously gassed with carbogen (95% O_2 5% CO_2). Slices were cut using a vibrating microtome (Model Integraslice7550 PSDS; Campden Instruments Ltd.) at a frequency of 50 Hz, speed of 0.10 mm/s, and with an amplitude of 1.0 mm. Normally, six hippocampal slices (250 μm thick) were obtained from one half of the brain. If not needed, the other hemisphere was discarded. Once the slices were cut, they were kept in an incubation chamber filled with normal aCSF at 37°C for 30 minutes and then for 1 hour at room temperature for recovery. The normal aCSF was gassed with carbogen throughout the entire day of experiment.

After the incubation period, the hippocampus was separated from the rest of the slice under the microscope using two needles and finally transferred to the recording chamber. A platinum harp with strings made of unwaxed dental floss was placed on top of the slice to minimise movement.

Table 2.1: **Composition of the different artificial cerebro-spinal fluid used for *in vitro* experiments.** The low- Na^+ solution is only used during slicing and the normal solution is used throughout the entire experiment. Low- Ca^{2+} solution is used to impair neurotransmitters release. Concentrations are expressed in mM.

	Low Na^+ (slicing)	Normal	Low Ca^{2+}
NaCl	-	125	125
KCl	2.5	2.5	2.5
MgCl_2	4	1	3
CaCl_2	0.1	2	-
NaH_2PO_4	1.25	1.25	1.25
NaHCO_3	26	26	26
Na-Pyruvate	2	2	2
Myo-Inositol	3	3	3
Ascorbic Acid	0.5	0.5	0.5
Glucose	10	10	10
Sucrose	250	-	-

2.2.3 Extracellular recordings and stimulation

The electrophysiology recordings were taken using a multi-electrode array (MED) of 64 channels. The acquisition software used was Mobius 0.2.16 (Alpha MED Science, Japan). An Olympus CK40 microscope (OLYMPUS, Japan) was used for visual control while placing the slice in the multi-electrode dish. The solutions were perfused with a peristaltic pump (Gilson, Inc., USA). The temperature in the chamber was kept constant at 32C. The MED consisted of an 8-by-8 array with an electrode size of 50 μm , and the electrodes separated from each other by a distance of 150 μm (type: MED515A, Alpha MED Science, Japan).

Any of the 64 electrodes could be used for delivering electrical stimuli. The stimulus intensity could be easily changed from the amplifier. The stimulus consisted of a biphasic (-/+) paired-pulse and had a length of 0.5 msec.

One of the most important things to keep in mind when cutting brain slices is that the connections between cells can be easily damaged in the process.

Depending on the cutting angle, the fibres can be damaged or better preserved. It is not easy to determine if the angle is or is not the correct one when the brain is being cut. In order to assess the quality of the slices, two kinds of experiments were performed: Evoked responses by electrical stimulation and induction of Gamma oscillations through pharmacological stimulation. All the drugs used in this part of the project were bath applied. Kainate (Kainic Acid) and DNQX were purchased from Sigma-Aldrich.

-Evoked responses by electrical stimulation

In order to assess the quality of the slices, we first measured the response to electrical stimulation under different pharmacological conditions. The experiments consisted of 100 traces of 0.1 second of duration. Five sets of recordings were taken: one with constant perfusion of normal aCSF, another one with constant perfusion of low-Ca²⁺ aCSF, a third one with aCSF (recovery), a fourth one with DNQX, and finally a second recovery with aCSF. The stimuli were delivered at the beginning of every trace. The stimulus intensity was set according to previous Stimulus-response curves, done with the purpose of finding the range of intensities in which the amplitudes of the responses were detectable. This guaranteed that the stimulus intensity was enough for eliciting a response but not so strong that could damage the cells. For the stimulus-response curves, 100 traces were recorded, with a pulse at the beginning of each trace, going from stimuli of 0 μ A to stimuli of 27 μ A, with 10 repetitions of the same stimulus intensity (raising the intensity in steps of 3 μ A). This experiment was repeated in 4 slices from 4 different mice, and for each slice 4 electrodes recording from the 4 areas of interest were selected (dentate gyrus, CA3, CA2, and CA1). Because of the variability of the results for different slices, at the beginning of every experiment a narrower range of stimulus intensities was tested before starting the actual experiment.

- Gamma Oscillations induced by Kainate

Longer traces (i.e. 1 minute) were also recorded for studying the induction of oscillations by Kainate. We estimated that the Kainate, once started being perfused, will actually reach the chamber and the final concentration (after

replacing all the aCSF) about 3 minutes later. 10 animals (27 slices) were used for this experiment.

The experimental protocol was as follows: a 1 minute long trace was recorded as a baseline (the slice was perfused with normal aCSF) and then the same was done while perfusion of 50, 100, 200 or 400 nM of kainate. For each concentration, three traces were recorded, leaving 3 minutes between each other. The results show the last trace for each concentration. Because the last trace was recorded 8 minutes after starting the perfusion of Kainate, the concentration of Kainate during the recording of the last trace should be the same as the solution perfused.

2.2.4 Data Analysis

Data analysis was performed using MATLAB R2010a (MathWorks) and MED64 Mobius.

-Local field potential analysis

An elliptic filter was used to filter the data in order to obtain the local field potential (LFP) without the contamination from action potentials. The signal was filtered between 1 and 300 Hz, to obtain the LFP and between 300 and 3,000 Hz to obtain spikes.

To study gamma oscillations the signal was filtered between 20 and 60 Hz (low gamma) and between 60 and 80 Hz (high gamma). A Notch filter was also applied at 50 Hz to discard line noise.

The calculation of the power spectra was done as follows: the signal was windowed with a rectangular window and the power spectral density (PSD) estimate was obtained using a fast Fourier Transform (FFT).

-Spike detection and sorting

The algorithm for spike sorting used in the laboratory is called Wave_Clus. It was developed by Quian Quiroga (2004) and it is continuously under improvements. The algorithm makes use of the fact that the spikes from different neurons have different shapes, depending on the morphology of their dendritic trees and the distance to the recording electrode (Gold et al., 2006).

Wave_Clus performs four basic steps to sort the spikes: filtering, spike detection, feature extraction and clustering. First, the data is filtered as described above. After filtering, a threshold based on the median of the data is determined for spike detection. Once the spikes are detected, the algorithm extracts some features of the spikes that are useful to classify each spike. Finally, the spikes are assigned to the different clusters according to their features.

-Spike-triggered average

All the spikes from one neuron were aligned, and the moment at which each of them occurred was considered as $t = 0$. The average of the LFP was calculated 50 msec before and after each spike. Only single units were taken into account for this analysis, and in order to make the average more robust, the spike triggered average was only calculated for those units that fired at least 5 spikes in the 30 seconds recorded without Kainate, and at least 10 spikes after the Kainate was added. 128 single units were analysed to study the locking of the action potentials to a specific phase of the LFP.

2.3 Results

This section describes the results obtained from the different experiments described in section 2.2.

2.3.1 Extracellular recordings and stimulation

-Evoked responses by electrical stimulation

Stimulus-Response Curves were done in order to first find the range of stimulus intensities that could elicit an evoked response in the slice, without stressing the stimulation electrode and the slice too much. Figure 2.1 (left) shows the mean curves recorded from electrodes located in different positions, with intensities ranging between 0 and 27 μA . Each point is the mean of 4 slices, from 4 different mice, 4 channels each and ten repetitions of stimulation with the same stimulus intensity. The dashed curves represent the standard deviation.

Figure 2.1 (right) shows the location of the stimulation and recording electrodes. The stimulation electrode (represented with the arrow) was located

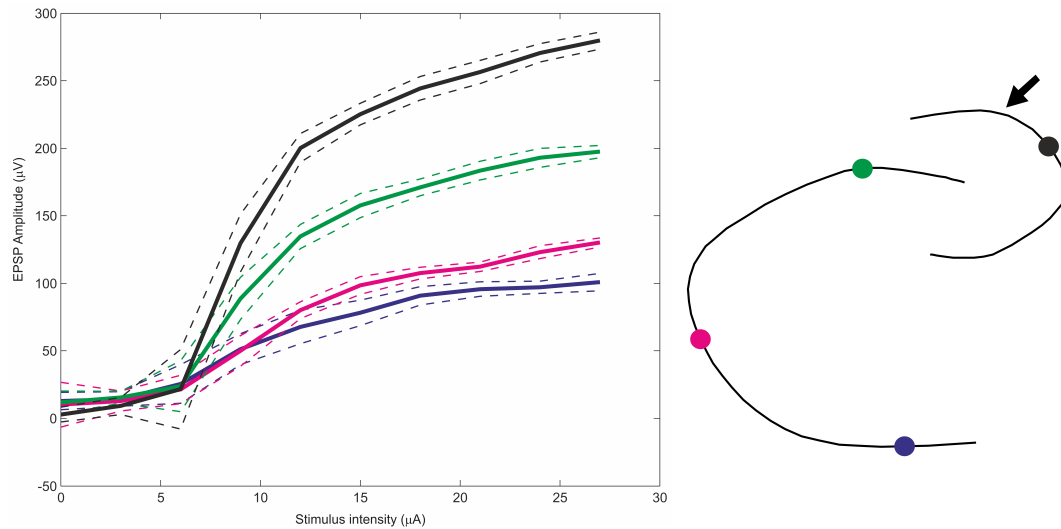


Figure 2.1: **Responses to electrical stimulation in hippocampal slices.** Left: Stimulus-response curve for four different locations. EPSPs were measured in response to electrical stimulation. The filled curves show the mean EPSP amplitude in response to different stimulus intensities. The dashed curves represent standard deviation. Right: scheme of a slice with the curved lines representing the dentate gyrus (upper right side) and the proper hippocampus (lower left side). The arrow indicates the estimated position of the stimulation electrode in each slice. The dots are an approximation of the four different recording areas: dentate gyrus, CA3, CA2, and CA1.

close to the dentate gyrus, as well as the recording electrode represented in black. The green curve shows the responses recorded with an electrode located close to CA3, the magenta CA2, and the blue was near CA1.

-Pharmacological modulation of excitatory postsynaptic potentials (EPSPs)

In order to test the quality of the slices, we measured the responses evoked by electrical stimulation in different pharmacological conditions: control (aCSF), low Ca^{2+} , recovery (aCSF), DNQX, and recovery (aCSF). Figure 2.2 shows that the EPSP elicited after stimulation in the control condition (sCSF), was inhibited after 10 minutes of perfusion of Low- Ca^{2+} aCSF solution (Low- Ca^{2+}). The response was recovered after washing out the low- Ca^{2+} solution for 10 minutes with normal aCSF (Recovery 1). Application of DNQX (10 μM), an AMPA and Kainate receptor antagonist, decreased the amplitude of the

response (DNQX), which was recovered after washing out the DNQX with normal aCSF (Recovery 2). This experiment was carried out with 5 animals, 1 slice from each animal. The data shown is the mean of 4 channels recording from each slice and 100 repetitions for each channel. The error bars represent the standard deviation of the mean. The inset shows a trace for each of the five conditions. The different conditions are represented with the same colours as in the bars.

- Gamma oscillations induced by Kainate

Figure 2.3 shows gamma oscillations induced by 200 nM of Kainate. The black trace shows the LFP (1-300 Hz) before the application of Kainate and the green trace after adding Kainate. The blue and magenta traces are both after the application of Kainate and show low gamma (20-60 Hz) and high gamma (60-80 Hz) oscillations, respectively.

The power spectra for different concentrations of Kainate were calculated, and the results for the different electrodes and slices were variable: some of the channels show no oscillations at all, independently of the concentration of Kainate used (not shown); some others show that 200 nM is not enough to induce oscillations in the gamma band but 400 nM is (not shown); others show no difference between 200 nM and 400 nM (not shown); and in others there is a peak in the spectrum with 200 nM in the so-called low-gamma band, and with 400 nM there is also a peak at higher frequencies, that could indicate the presence of high-gamma oscillations (Figure 2.4, top). For calculating the spike-triggered average, we first sorted the spikes in order to evaluate the synchrony of 128 single neurons to the oscillations. From the total number of single units analysed, 87% showed locking to a phase of the LFP after Kainate was applied (either with 200 or 400 nM, or both). Figure 2.4 (bottom) shows an example of phase locking of a single unit with gamma oscillations induced by 200 nM of Kainate. Before the Kainate is bath applied (Figure 2.4 (top), black trace), no oscillations in the gamma band can be detected and therefore the spikes are not locked to any particular phase of the oscillations. This is why the average of the LFP looks flat around the spikes (Figure 2.4 (bottom), left). However, after the Kainate application (200 nM) (Figure 2.4 (top), magenta trace), the AP are fired at a specific phase of the oscillations

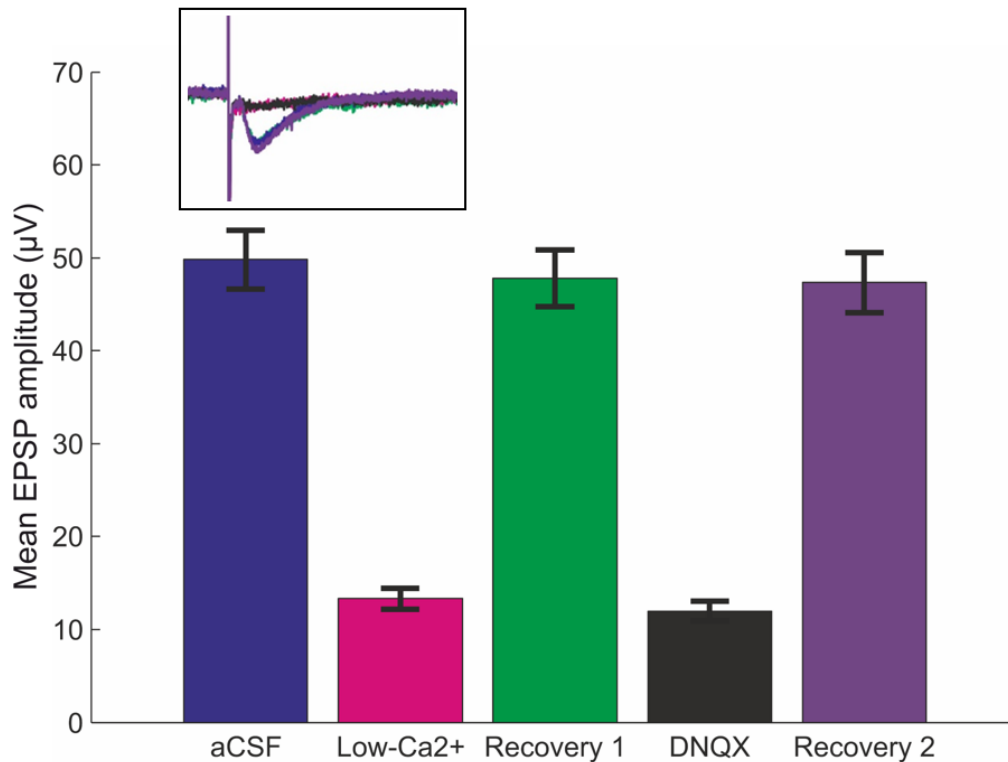


Figure 2.2: **Pharmacological modulation of electrically-evoked EPSPs.** The amplitude of the EPSPs decreases after perfusion of Low-Ca²⁺ aCSF for 10 minutes (Low-Ca²⁺ and magenta curve in inset), compared to control (aCSF and blue curve in inset). The activity is recovered when the Low-Ca²⁺ aCSF is washed out with normal aCSF (Recovery 1 and green curve in inset). Application of 10 μ M DNQX (black curve in inset), a Glutamate receptor antagonist, abolished the response, which recovers again after washing out the DNQX with normal aCSF (Recovery 2 and purple curve in inset). The error bars represent the standard deviation of the mean. Inset shows a typical response to a stimulation pulse under each pharmacological condition.

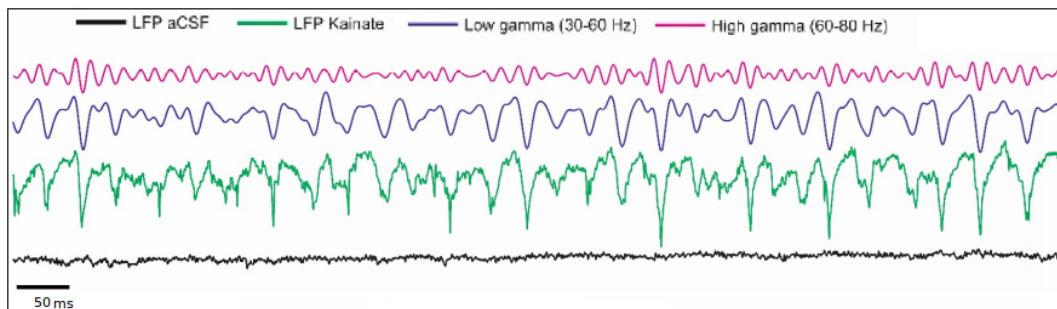


Figure 2.3: **Gamma Oscillations induced by Kainate.** The black trace shows the LFP (1-300 Hz) before the application of Kainate. The green trace shows the LFP (1-300 Hz) after the application of 200 nM of Kainate. The blue and magenta traces show the same signal but filtered in the low (30-60 Hz) and high (60-80 Hz) gamma band.

(Figure 2.4 (bottom), right).

2.4 Conclusions

As mentioned before, an EPSP can be evoked either by direct stimulation from the stimulation electrode or by synaptic stimulation in the cells that are too far away for the current to reach them. The latter case is only seen if the connections between cells are intact after the slicing process. Because of this, the best way of assessing if the different areas of the hippocampus are still connected among each other is by electrical stimulation. When an electrode is used to inject depolarizing current in the presynaptic neurons, an excitatory potential is elicited in the postsynaptic neurons (excitatory post-synaptic potential –EPSP–). The cells that are close to the stimulation electrode will be depolarized directly by the current injection, but the ones that are far away from the electrode will only receive an input from the presynaptic cells, but in order for this to happen the fibres must be well preserved. A good way of testing this is by comparing the amplitude of the responses elicited by stimulation when the slice is perfused with normal aCSF (control condition) to when it is perfused with low- Ca^{2+} aCSF. The calcium is needed for the release of neurotransmitters, so if there is no calcium in the environment the synaptic connections between cells will not be functional. The decrease in the response

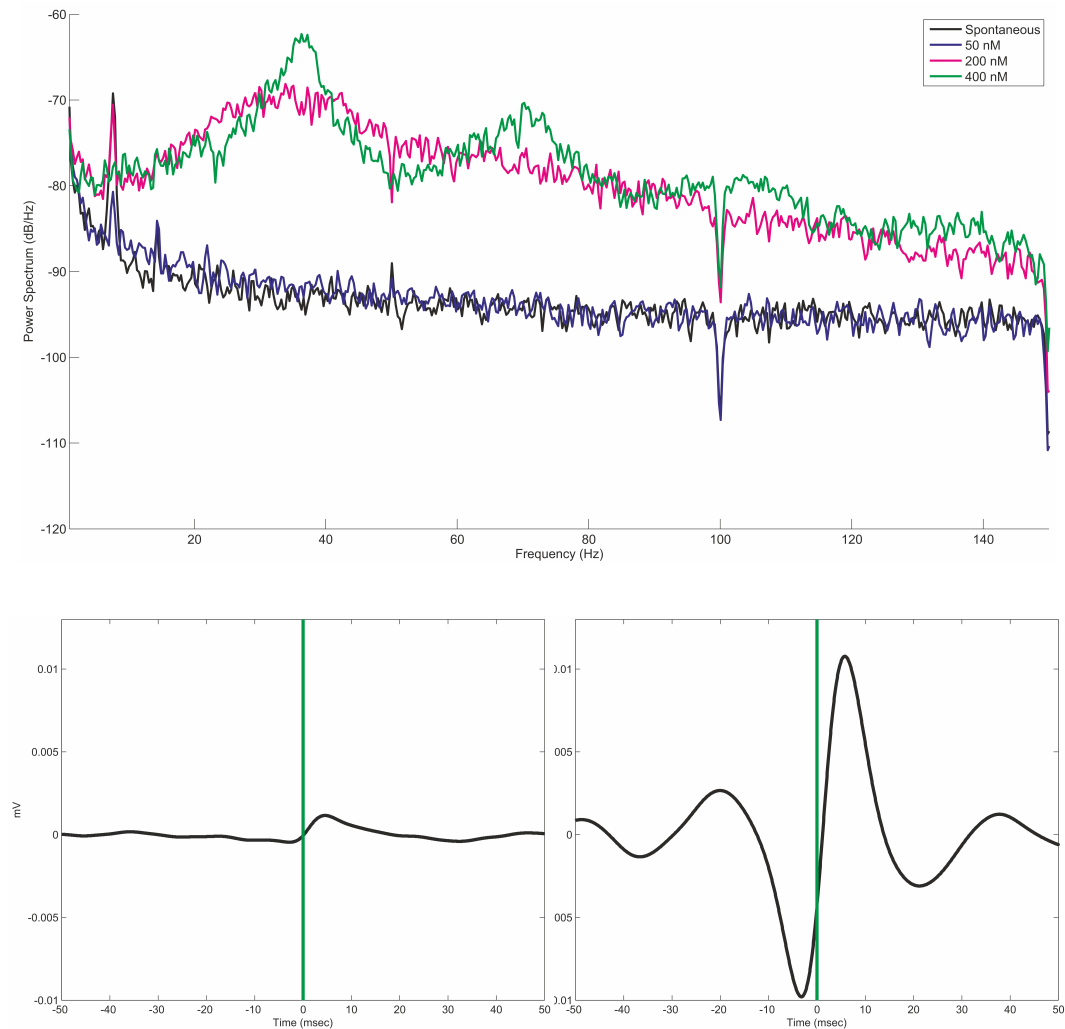


Figure 2.4: **Power spectrum and single cell phase-locking to the LFP.** Top: Power spectrum for four different concentrations of Kainate: Spontaneous (0 nM), 50 nM, 200 nM, and 400 nM. With the two lowest concentrations of Kainate (0 and 50 nM), the spectrum shows no oscillations in the LFP, but when the concentration of Kainate was increased to 200 nM, it can be observed that there is an increase of the power in the range of 20 to 50 Hz. With the highest concentration of Kainate, the power increased not only between 30 and 50 Hz, but also between 60 and 80 Hz. The peaks seen at 50 Hz (and the harmonics) correspond to an artefact of the Notch filter. Bottom: Left: spike-triggered average before the application of Kainate (0 nM). Right: spike-triggered average after perfusion of 200 nM of Kainate.

amplitude in the low- Ca^{2+} condition indicates that the stimulation was being synaptic, rather than electrical. This was further confirmed using a Glutamate receptor antagonist, such as DNQX. With normal aCSF, and the Glutamate receptors blocked, Glutamate-mediated presynaptic stimulation did not have any effect in the post-synaptic cells. The facts that the lack of Calcium and the presence of a Glutamate receptor antagonist abolish the response, and that the response recovers after going back to normal aCSF, are indicators that the recorded response to the stimulus is triggered synaptically (chemically) and not through the direct injection of current, and therefore that at least some of the connections are intact.

Gamma oscillations are not spontaneously originated in a brain slice, since the connections of the hippocampus and the dentate gyrus with the areas in the brain that normally generate the oscillations are not preserved (Colgin et al., 2009). Thus, it is necessary to induce the oscillations, either pharmacologically or through electrical stimulation (Traub, 2004). By the use of Kainate, we successfully generated oscillations within the range of frequencies that represent gamma oscillations.

The use of Kainate also allowed us to observe another common phenomenon present in several areas of the brain: phase-locking. We could observe a considerable phase-locking of the spikes to the a phase of the oscillations induced by Kainate, which is another indicator of the good quality of the slices.

Both electrical and pharmacological stimulation were successful at triggering activity in a system that has little or non basal activity. From an experimental point of view, electrical stimulation is easier to perform than pharmacological stimulation. This is due especially to the long periods of time that some drugs need to be completely washed out. However, depending on the drug used, pharmacological stimulation can be more realistic when triggering its effect on the slice, since many processes in the brain are mediated by neurotransmitters or molecules with biological activity that are mimicked by a great variety of drugs commercially available.

This set of experiments was a great training on the slicing methodology and a reassurance of the quality of the slices. The fact that we could replicate some results from an important paper in oscillations as the one by Fishan et al. (2004) indicates that the slicing technique is good enough to give the next step:

in vitro 2P imaging.

Chapter 3

In vitro two-photon imaging and Glutamate uncaging

3.1 Introduction

Two-photon imaging is becoming one of the most widely used technique, for both *in vitro* and *in vivo* experiments. This fact is not surprising when the many advantages and few disadvantages of this technique are considered.

As mentioned before, 2P imaging allows the measurement of a large population of neurons and visual identification of all the neurons being recorded, without the necessity of sophisticated data analysis. It also offers the possibility of measuring the activity of one cell, or even studying processes that take place in subcellular compartments, such as dendritic spines.

The combination of this recording technique with others has a huge potential in Neuroscience. One example is the 2P uncaging combined with 2P imaging. Uncaging provides the opportunity of exciting or inhibiting in a very fast fashion only one neuron or a part of a neuron, without affecting the rest of the cells. When working with small cellular parts, such as dendritic spines, it is of extreme importance to have high spatial resolution, and this is exactly what the 2P uncaging technique offers. These two techniques combined can also be used for manipulating the activity of a whole network, allowing the study of connectivity of cells or spatial organisation.

There are several examples of the combined use of the two techniques, but so far all of them used one laser to uncage and another one for imaging, both tuned at different wavelengths. This is because most of the GECIs are optimally excited by light at around 900 nm, while the uncaging occurs with the highest efficiency when produced by absorption of two photons at around 800 nm (or at even shorter wavelengths). Because tuning the same laser to two different wavelengths takes some time, if the wavelength is changed after the uncaging

for imaging, part of the response will be missed. It is also difficult to target several cells at the same time, since this is normally done by splitting the beam of light using diffractive materials. Since these materials affect differently light of different wavelengths, then if two beams of light are used, one for exciting GCaMP and another one for uncaging, splitting both beams together would not be possible, and so we are restricted to only one area.

The project described in this chapter sought to combine the two techniques using the same laser, for which it was necessary to determine the best wavelength to carry out both processes together.

3.2 Methods

All procedures were approved by the University of Leicesters Animal Welfare and Ethical Review Body (AWERB) committee and performed under license from the UK Home Office in accordance with the Animals (Scientific Procedures) Act 1986.

3.2.1 Animals

CBA mice aged 10-45 post-natal days (P10-45) were used for this part of the project. If younger than P21, after surgery and until weaning, mice were housed with their mother and litter mates. Same sex mice older than P21 were housed together, separately from their litter mates.

3.2.2 Intracranial virus injection

The animals were first injected with a virus to induce brain expression of a calcium indicator protein (GCaMP6s) and after 2-3 weeks they were culled and the brains were sliced.

The virus used was an Adeno-Associated virus carrying the genetic sequence for GCaMP6s (Chen et al., 2013), under the human promoter Synapsin 1, to ensure that only neurons express the protein (Kügler et al., 2003). Two different serotypes of the virus were used: AAV5.Syn.GCaMP6s.WPRE.SV40 and AAV9.Syn.GCaMP6s.WPRE.SV40, both obtained from Penn Vector Core.

Before surgery, anaesthesia was induced by inhalation of 5% isoflurane in pure oxygen until the animal stopped moving, after which the anaesthesia level was reduced to 2-2.5% and maintained at that level for the rest of the procedure. The depth of the anaesthesia was frequently assessed by the rate and depth of the respiration and the response to a mild painful stimulus (pedal withdrawal reflex). Mice were then injected with three different drugs to avoid pain and inflammation: Carprofen (10 mg/Kg), Buprenorphine (0.1 mg/Kg), and Marcaine (0.05-0.0625 mg/Kg). The body temperature of the animal was controlled by placing the animal onto a warming plate (37°C).

An eye lubricant (Lacri-Lube) was applied on the eyes to prevent them from drying.

To minimise the risk of infection, the head was first shaved with a trimmer and then hair removal cream was applied over the shaved area to remove any traces of hair. The ear was marked to allow posterior identification.

After preparation in the pre-op area, the animal was moved into a sterile environment and the rest of the surgery was carried out under strict aseptic conditions to minimise the risk of infection.

The virus was kept at -80°C. Before the injections, 250 nL aliquots were diluted in 250 nL of pure water and kept in dry ice until it was loaded into the syringe. For the injections, a Neuros Syringe (Model 7001, 1 μ L; Hamilton) was used to minimise tissue damage. The syringe was controlled by a syringe pump (Model 11 Elite Nanomite; Harvard Apparatus) which was programmed to inject at a rate of 35 nL/min and with a force level of 30%.

The mouse was placed in the stereotaxic apparatus using ear bars and a nose clamp. Xylocaine in cream was previously applied to the tip of the ear bars to prevent discomfort and pain after surgery. A small incision was made with a sterile blade to expose the skull, following the sagittal suture on the surface of the skull.

Hydrogen peroxide (10 vol.) was applied to the surface of the skull to make the sutures more visible and to remove all the soft tissue (periosteum) covering the skull.

A small craniotomy was made with a drill (model K.1020, Chuck Type; Freedom) using a 0.9 mm drill bit (Fine Science Tools) leaving the dura intact. The syringe was then lowered into the brain. A total volume of 500 nL of

the diluted virus (1:1) was injected to each animal. Figure 3.1 shows the coordinates used for all the animals injected (taken into account for analysis). The open circles represent one animal each, with expression in the hippocampus (blue), the cortex (green), or other areas (magenta). Black open circles show the coordinates used for injecting animals that did not show any expression. Closed circles are the mean coordinates for each category. The size of the circles represent the age of the animals.

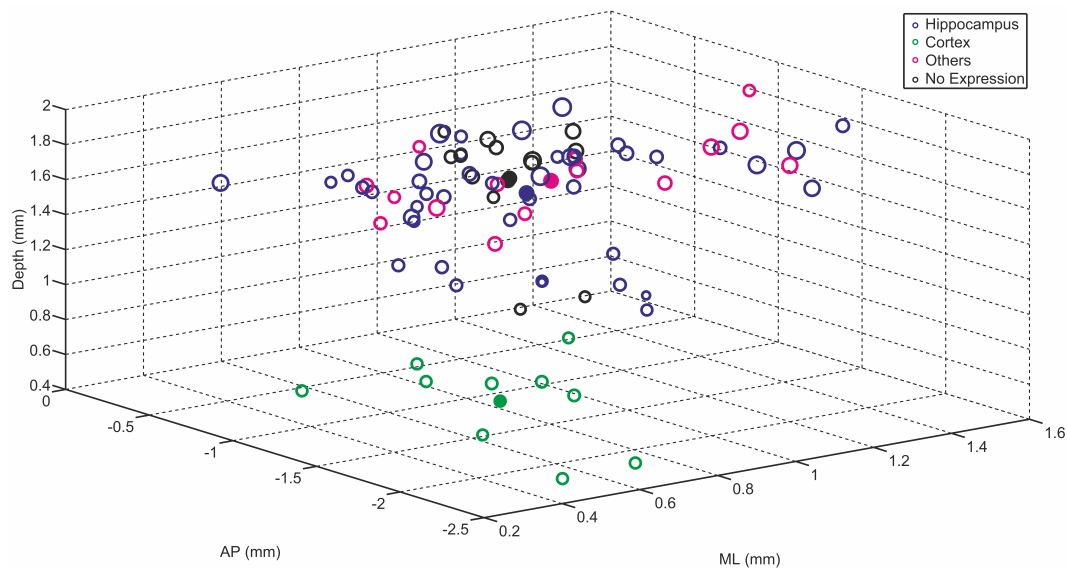


Figure 3.1: **Coordinates for intracranial injections.** Medio-lateral (ML) and antero-posterior (AP) coordinates and depth used for all the animals that showed expression in the hippocampus (blue), cortex (green), and other areas (magenta). The black circles represent the coordinates of injection for the animals that showed no expression. The size of the circles represent the age of the injected animals. The filled circles indicate the mean coordinates for all the injected animals that showed expression within each area (blue, green, and magenta), or no expression at all (black). The size of the filled circles indicates the mean age of the injected animals.

Around 15 minutes after the injection, the needle was slowly retrieved. To increase the probability of expression, sometimes the pump was programmed to keep injecting while the needle was being retrieved (which means that the final injected volume of virus was slightly over 500 nL).

After the injection the wound was closed with cyanoacrylate glue (Gluture) and the animal was injected with Saline with Glucose (0.9% Sodium, 5% Glucose) to prevent dehydration. Finally, the animal was placed in its cage

and left overnight in the post-op room for recovery.

3.2.3 Slices

Two-three weeks after the injection, mice were decapitated and the brain was removed and rapidly cooled in iced slicing aCSF. Using a blade, two cuts were made: one posterior, to separate the cerebellum and another one anterior, to separate the olfactory bulb. Following the cuts, the anterior part of the brain was dried with filter paper and glued with cyanoacrylate adhesive to a metallic tray for posterior cutting. A third cut was then made with a blade to separate both hemispheres.

The tray was then immersed in iced slicing aCSF being continuously gassed with carbogen (95% O₂ - 5% CO₂). 350 μm thick slices were cut using a vibrating microtome (Model Integraslice7550 PSDS; Campden Instruments Ltd.) at a frequency of 50 Hz, speed of 0.10 mm/s, and with an amplitude of 1.0 mm. Once the slices were cut, they were kept in an incubation chamber filled with normal aCSF at 37°C for 30 minutes and then for 1 hour at room temperature for recovery. The normal aCSF was gassed with carbogen all the time. Once recovered, slices were transferred to the recording chamber, and were continuously perfused with gassed normal aCSF (except when scanning, to avoid movement of the slice). A harp was placed on top of the slice to minimise movement.

3.2.4 Microscope

In vitro calcium recordings were taken using a microscope (Model Acerra II, Thorlabs) based on a Ti:Sapphire laser Chameleon Ultra II 80 MHz, 140 fs (Coherent) with a galvo-resonant mirror system (8 KHz). The intensity of the laser was controlled by a Pockels cell and the fluorescence was detected with two Photomultiplier tubes (GaAsP PMTs, positioned directly behind the objective; Thorlabs). A 4x objective (Model RMS4X, Olympus) was used to position the stimulation electrode, and a 20X objective (1.0 NA; Olympus) was used for two-photon imaging. Data was acquired using ThorImage 2.1 (ThorLabs). The microscope was covered with a black-out fabric to prevent light coming from the computer monitor to be detected. Also, the entire room

was isolated from ambient light with a curtain. Figure 3.2 shows a schematic representation of the laser beam path and the most important components of the microscope. Figure 3.3 shows a picture of the actual set-up, where the *in vitro* microscope and the laser can be seen.

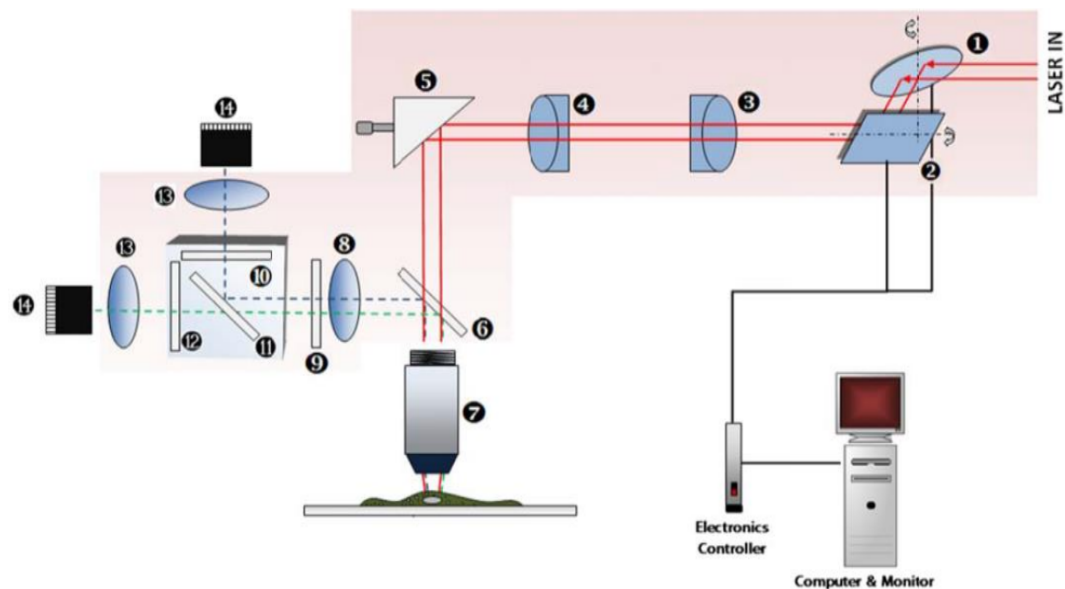


Figure 3.2: **Schematic representation of the beam path for two-photon excitation.** 1) Resonant Scanner 2) Galvo Scanner 3) NIR Scan lens 4) NIR tube lens 5) Turning mirror 6) Primary dichroic mirror 7) Objective lens 8) Collector lens 9) NIR blocking filter 10) Emission filter Ch1 11) Secondary dichroic mirror 12) Emission filter Ch2 13) Focusing lens 14) Photomultiplier tube
Figure used with permission from ThorLabs.

3.2.5 Electrical stimulation

In order to deliver electrical stimuli to the slices, a custom-made glass electrode was used (Figure 3.3 (10)), connected to a stimulator and placed close to the area with more expression of GCaMP6s. The stimulation electrode was held and positioned with a micromanipulator (LBM-7, Scientifica) (Figure 3.3 (4)). The amplitude of the pulses was adjusted for each slice and delivered always at 10 Hz.

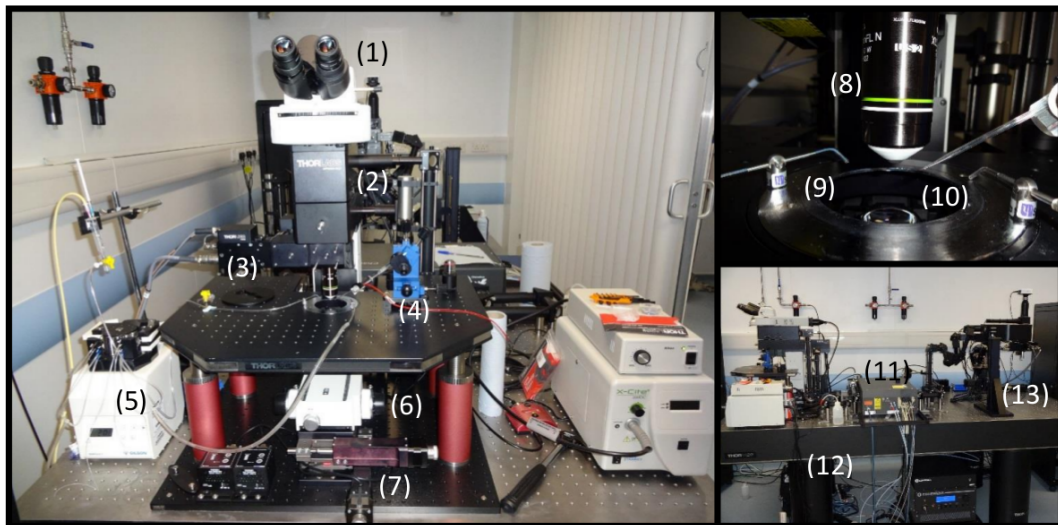


Figure 3.3: **Two-photon imaging set-up.** Left: front-view of the *in vitro* set-up. (1) Eye-piece. (2) Primary galvo-resonant scan path. (3) GaAsP Photomultiplier (1 of 2). (4) Micro-manipulator for stimulation electrode and puff pipette positioning. (5) Micropump for aCSF perfusion. (6) Focus. (7) X-Y stage motion controller. Right: Top: (8) 20x objective. (9) Perfusion system. (10) Stimulation electrode. Bottom: (11) Laser. (12) Optical table. (13) *In vivo* microscope.

3.2.6 Drug delivery

Two different compounds were used for this part of the project: Na^+ -Glutamate (Sigma-Aldrich) and RuBi Glutamate -Caged Glutamate- (Salierno et al., 2010). Both of them were diluted in normal aCSF and delivered with the use of a patch clamp glass pipette. The pipette was connected through a modified patch clamp pipette holder to a syringe that contained the drug to be delivered, and the flow could be controlled by applying either positive or negative pressure. To be able to know the exact moment when the solution reached the field of view, Sulforhodamine 101 (Sigma-Aldrich) was added to the solution. Because the position of the pipette varies from one slice to the other, the Sulforhodamine is a good indicator of when the solution diffuses from the pipette tip and reaches the visual field. This way, it is expected that the onset of the red signal (Sulforhodamine signal) coincides with the onset of the response to Glutamate. Ideally, the pipette is positioned to allow the solution to reach the visual field as soon as possible, without producing the movement of the slice while injecting the solution. This would cause a change in the focus or a change in the x-y

position, which would mean the loss of the imaged cells during baseline.

3.2.7 GCaMP6s characterisation

The characterisation of the Calcium indicator protein GCaMP6s was done in two ways: 1) measuring fluorescence from pictures and 2) measuring changes in fluorescence after electrical stimulation.

1. Fluorescence vs. Wavelength curve with pictures: In order to characterise the absorption spectrum for GCaMP6s, the laser was tuned at 23 different wavelengths, from 780 nm to 1000 nm, with an interval of 10 nm, and a picture was taken at each wavelength. The final pictures were averages of 4 pictures, to increase the quality of the image. The intensity of the laser was constant across all the wavelengths, and it was set so as not to saturate at any wavelength.
2. Fluorescence vs. Wavelength curve with activity: Next, we wanted to study how accurately we could measure activity in a cell exciting the fluorophore with light at different wavelengths. For a first analysis, we picked 800, 810, and 820 nm as the excitation wavelength.

For stimulation-driven activity, we used the following protocol:

- Frames 1-29: baseline
- Frames 30-60: stimulation (5V, 10 Hz)
- Frames 61-99: stimulation off
- Frames 100-130: stimulation (5V, 10 Hz)
- Frames 131-150: stimulation off

-Comparison among different wavelengths

Different wavelengths were compared using the same intensity. Three different excitation wavelengths were tested (830, 840, and 850 nm), and the amplitudes of the responses to stimulation were compared to the ones obtained with light at 920 nm. The stimulation protocol was the same as before. The wavelengths

tested were chosen because they allowed us to measure activity, and were reasonably bright and close to 800 nm, the optimal wavelength for uncaging.

3.2.8 Glutamate Stimulation

The Glutamate was added to the bath while scanning at 850 nm. A solution of 1 mM Glutamate in aCSF, containing also Sulforhodamine, was puffed into the bath after frame 30. Both the red and the green PMTs recorded 250 frames (30 for baseline + 220 for response).

3.2.9 RuBi-Glutamate uncaging with light at 850 nm

Figure 3.4 shows a schematic representation of the experimental design. Two baselines were taken: the first one was a real baseline, without any kind of manipulation (Bsl1), and the second was to assess if the pulse of high energy light had any effect on the slice (Bsl2). Bsl1 was taken as the baseline for the analysis.

After the second baseline, we delivered a puff with RuBiGlu and the Sulforhodamine (Puff), and allowed some time for diffusion (RuBi+SrH). After that period of time, the first pulse of high energy light (~ 270 mW for 300 ms) was delivered and the response was measured for 250 frames (Response 1). These last two steps (pulse of light and response) were repeated once more (Response 2).

3.2.10 Data Analysis

Virus Expression

-Serotype

In order to study if the levels of expression with the two different serotypes differed significantly, a non-parametric random permutation test was run. The main reason for choosing this test is the disparity in the sizes of the two samples, given that only 9 animals were injected with AAV5 serotype, while the serotype AAV9 was used in 84 animals. Out of the 84 animals injected with the serotype 9, 74 were injected in the hippocampus and 10 in the cortex, while the ones

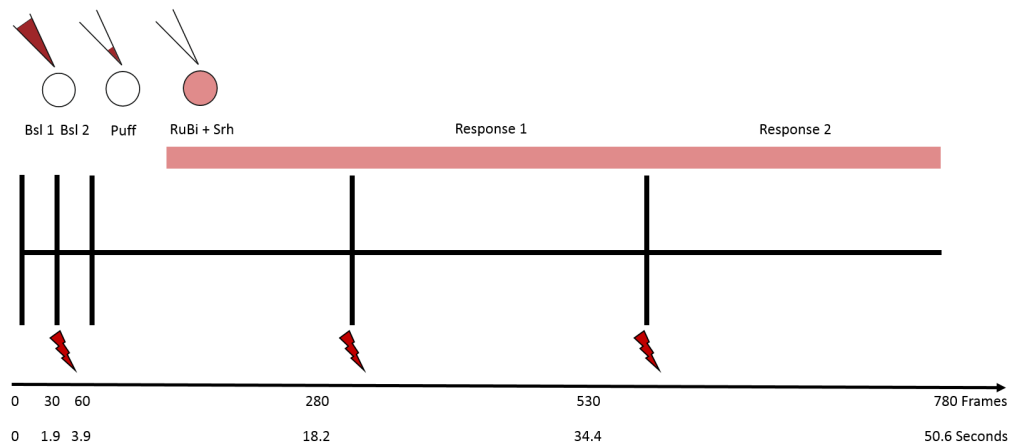


Figure 3.4: **Experimental design for uncaging.** A first baseline was taken just scanning (Bsl 1). After that baseline we delivered a pulse of light with the same characteristics as for uncaging as a control. Next, the RuBiGlu was delivered together with the Sulforhodamine (Puff) and some time was left to allow diffusion (RuBi + Srh). Following the diffusion time, there was a pulse of light (high energy) to uncage the Glutamate and the response was measured immediately after (Response 1). These last two steps (pulse of light and response) were repeated once more (Response 2).

injected with the serotype 5 were all injected in the hippocampus. Because the level of expression across different areas for the different serotypes is not the same (Aschauer et al., 2013), only the animals injected in the hippocampus with both serotypes were used to make the comparison.

A label was assigned to each of the animals injected with the serotype AAV9: 1 if it showed expression and 0 if the expression was unsuccessful. A vector was generated with all the 74 numbers and it was randomly permuted 1,000 times. Each of those times, the first 9 elements of the new vectors were selected, and it was calculated how many times, out of 1,000, the summation of the 9 first elements was equal to 1. The result was finally divided by 1,000, giving as a result the probability of obtaining 1 mouse out of 9 showing expression, when injected with the AAV9 serotype.

Following this analysis, none of the 9 animals injected with the serotype 5 of the virus were taken into account for further analysis.

-Hippocampus vs. Cortex

The same test was used to study if there was any difference in the probability of expression in the hippocampus and in the cortex, using the same serotype (AAV9). In this case, from the randomly permuted 1,000 vectors with the labels from the animals injected in the hippocampus, the first 10 elements of each were used to calculate the probability of having 10 animals with successful expression out of 10 animals injected in the hippocampus.

-Age effect on the probability of expression

To study if there is any effect of the age of the animal in the probability of expression, a logistic regression was performed. This test was chosen because of the logistic nature of the variable (expression or no expression). The model used to fit the results was:

$$\ln\left(\frac{P_{exp}}{1 - P_{exp}}\right) = \alpha + \beta x \quad (3.1)$$

where P_{exp} is the probability of expression and x is the age of the animal (in post-natal days) at the moment of the injection.

GCaMP6s characterisation

The acquisition of the data was done through ThorImageLS 2.2, a software developed by ThorLabs.

The analysis of the data was performed off-line using ImageJ (<http://imagej.nih.gov/ij/>) or Fiji (<http://fiji.sc/Fiji>) and Matlab. Regions of interest (ROIs) were defined around individual somata and dendrites.

-Fluorescence vs. Wavelength curve with pictures

The 23 pictures taken at different wavelengths were stacked using Fiji and several regions of interest were defined around cells (always the same ones across all the wavelengths).

To make it suitable for comparison, the fluorescence of each ROI was normalised to the fluorescence at 920 nm, which is within the range of optimal

excitation wavelengths for this protein (900-940 nm). The normalisation was done as follows:

$$\frac{Fx}{F920} \quad (3.2)$$

where Fx is the fluorescence measured at each wavelength and $F920$ is the fluorescence measured at 920 nm.

-Fluorescence vs. Wavelength curve with activity

Relative fluorescence changes ($\Delta F/F$) were calculated for each individual ROI as follows:

$$\frac{\Delta F}{F} = \frac{F - F_0}{F_0} \quad (3.3)$$

where F_0 is the mean of the baseline.

After calculating the $\Delta F/F$ for each wavelength, we selected the highest 42 data points (21 from the response to the first stimulation period -frames 55 to 75- and another 21 from the response to the second stimulation period -frames 120 to 140-) and calculated the mean and the standard deviation.

Glutamate Stimulation

-Sulforhodamine onset

To measure the onset of the Sulforhodamine signal, we selected a ROI from an area far away from the location of the pipette and calculated the $\Delta F/F$. We defined the onset of the signal as the moment from which the $ZScore$ became larger than 3. This condition was maintained for the rest of the experiment. The $ZScore$ was calculated as follows:

$$ZScore = \frac{F - \mu(bsl)}{\sigma(bsl)} \quad (3.4)$$

where F is the raw signal, $\mu(bsl)$ is the mean of the baseline (or F_0) and $\sigma(bsl)$ is the standard deviation of the baseline.

-Activity onset

15 ROIs were defined for this analysis. The baseline was defined as the time before the Glutamate puff was delivered.

For each ROI, the $\Delta F/F$ and the $ZScore$ were calculated as before. The onset of the response was calculated as the moment from which the $ZScore$ becomes larger than 10.

RuBi-Glutamate uncaging with light at 850 nm

-Sulforhodamine onset

To measure the onset of the Sulforhodamine signal, we selected a ROI from an area far away from the location of the pipette and calculated the $\Delta F/F$. We calculated the $ZScore$ as before using equation (3.4).

We defined the onset of the signal as the moment from which the $ZScore$ became larger than 3. This condition was maintained for the rest of the experiment.

-Activity onset

8 ROIs were defined for this analysis.

For each ROI, the $\Delta F/F$ and the $ZScore$ were calculated as before. Taking into account that the amplitude of the response is smaller than for the free Glutamate, the onset of the response was calculated as the moment from which the $ZScore$ becomes larger than 5 (or 10 for one of the responses that is bigger than the others –green curve in Figure 3.14 (top)–).

3.3 Results

This section will describe the results obtained from the imaging experiments performed for this thesis.

First, we will describe the results for the virus injection to express an exogenous calcium indicator protein in the Hippocampus and the Cortex.

Secondly, it will be described how the excitation wavelength affects the emission of GCaMP6s, both in a static image (picture) and following stimulation (activity).

In the third place, we will show a typical response to Glutamate stimulation.

Finally, the results of Glutamate uncaging experiments will be shown.

3.3.1 Virus injection

We performed intracranial injections of an Adeno-Associated Virus to deliver the gene encoding the protein GCaMP6s, under the human Synapsin 1 promoter (AAV.Syn.GCaMP6s.SV40) into 93 CBA mice, with ages ranging from 10 post-natal days (P10) to 45 post-natal days (P45). From the total number of animals injected, 71 showed expression (76.34%).

The expression was not quantified, because it was not of our interest to know how many cells were expressing the protein, but rather in how many animals out of the total number that were injected, the virus injection and expression were successful.

-Serotype

Two different serotypes of the same virus were used: AAV5 and AAV9. The injection of the serotype 9 showed a level of expression above 80%, while the expression with serotype 5 was only successful in 11% of the animals injected. Only 9 animals were injected with the virus of serotype 5, all of them targeting the hippocampus, where it is supposed to show higher levels of expression compared to other areas of the brain, such as the cortex (Aschauer et al., 2013).

Statistical analysis was performed in a way that the difference in the sample size was not taken into account, to make a fair comparison. The animals injected with the serotype 9 in the cortex were not included in the analysis.

The injection of the serotype AAV5 showed a significantly lower rate of success, compared to the serotype 9 ($p \sim 0$) (Figure 3.5). Because of the low level of expression with the serotype 5 in the hippocampus, the serotype 9 was used exclusively for the rest of the project.

This is consistent with the results obtained by Aschauer et al. (2013), which show that the level of expression using the serotype AAV5 is lower than when using the serotype AAV9. The animals injected with the serotype AAV5 were excluded for all further analysis.

-Age of the animals

The spread of viral particles in the brain parenchyma is very limited. Because of this reason, the success of the infection is dependent on the age of the animal:

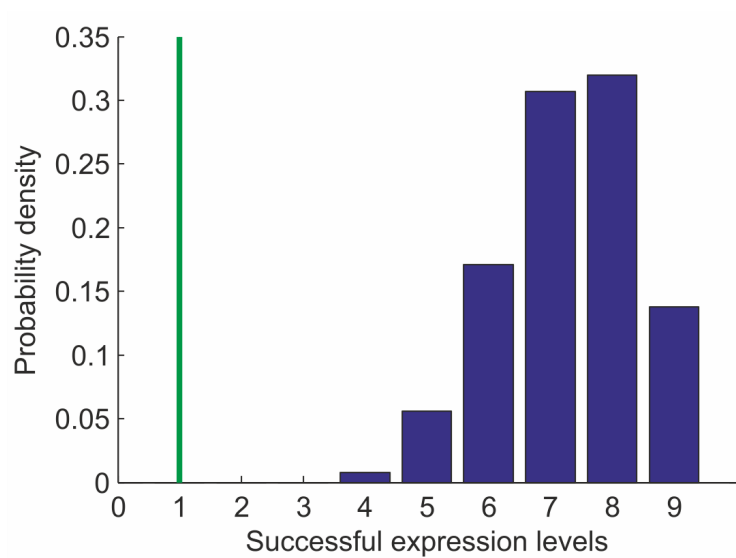


Figure 3.5: **Differences in Expression with serotypes AAV5 and 9.** Normalised histogram of successful expression levels. Blue bars: distributions of random permutations. Green vertical line: observed expression levels with serotype AAV9. The serotype AAV9 seems to be more successful than the serotype AAV5 for gene delivery in the hippocampus. From the animals injected with the serotype AAV9, above 81% showed expression of GCaMP6s. The serotype AAV5 was only successful in 11% (1 out of 9) of the injected animals. Expression was significantly higher with AAV9 than with AAV5 ($p=0.009$).

adult animals have smaller extracellular space and this provides resistance to the virus spread, as opposed to young animals, whose neurons are less tightly packed (Cetin et al., 2006). Even though the animals injected for this thesis were all young, the ages varied from P10 to P45, so we wanted to study if there were differences in the number of animals of different ages that expressed the protein.

We performed a logistic regression to test the success of infection within this range of ages, which showed that the age of the animals at the moment of the injection had no effect on the probability of expression ($p=0.6979$).

-Area of expression

Two areas of the brain were targeted for expression of GCaMP6s: Hippocampus and motor and posterior parietal association Cortex (which are above the Hippocampus and the dentate gyrus) (Figure 3.6).

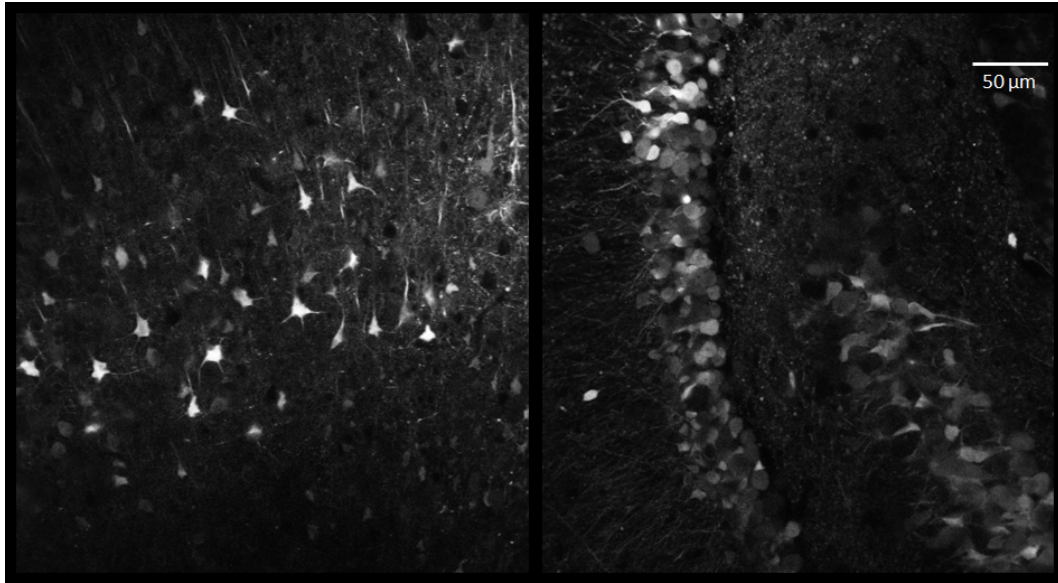


Figure 3.6: **Cortical and hippocampal cells expressing GCaMP6s.** Two examples of images from the Cortex (left) and the Hippocampus (right), showing part of the Dentate Gyrus and CA4.

74 animals were injected targeting the Hippocampus. (Figure 3.7). Out of those 74, 60 showed expression of GCaMP6s (81,08%). From those 60 that showed expression, 44 expressed in the target area (59.46%) while the remaining 16 animals (21.62%) showed expression of GCaMP6s in other areas (mainly striatum). From the 10 animals injected in the cortex, 100% showed expression in the target area (Figure 3.7). A non-parametric permutation test was run in order to study if the expression in the cortex through the serotype AAV9 was more successful than in the hippocampus (see: Section 3.2.10, Hippocampus vs. Cortex). The probability of having an expression of 100% in the hippocampus was 0.11

3.3.2 GCaMP6s characterisation

-Fluorescence vs. Wavelength curve with pictures

In order to evaluate the excitability of the calcium indicator protein GCaMP6s, we measured the intensity of the emission when it is excited at different wavelengths, within a range from 780 to 1000 nm and every 10 nm.

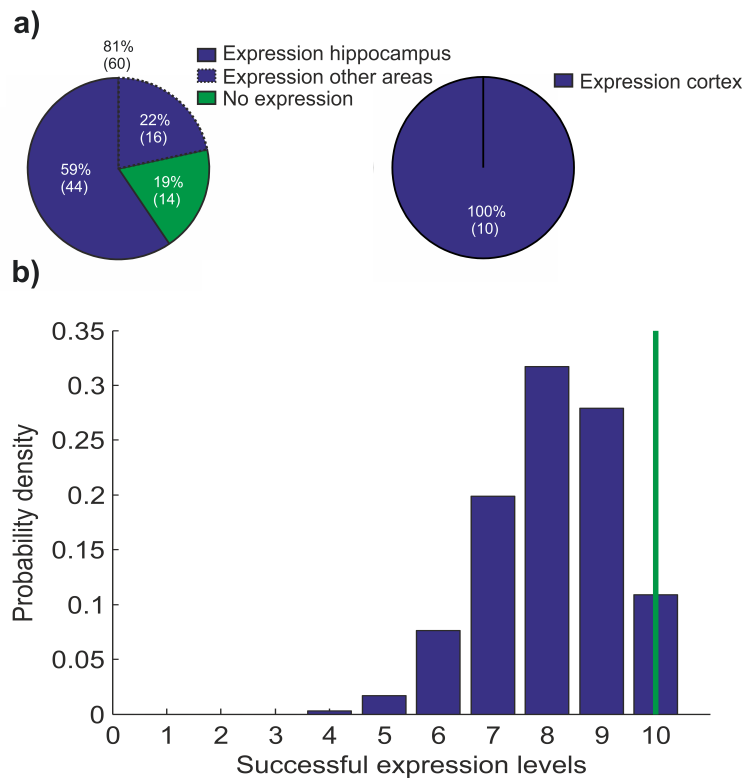


Figure 3.7: **Target area and area of expression.** a) 60 animals out of 74 (81%) injected in the hippocampus expressed GCaMP6s (left). 44 animals showed expression in the hippocampus (59%) and 16 (22%) in other areas (e.g. striatum). 10 animals were injected in the cortex (right), and all of them showed expression of GCaMP6s in the target area. b) Normalised histogram of successful expression levels. Blue bars: distributions of random permutations. Green vertical line: observed expression levels in the cortex.

4 ROIs were defined for 1 slice and other 6 for another slice (10 ROIs in total), and fluorescence was measured across all the wavelengths (Figure 3.8 a). It was found that when excited at 800, 810, and 820 nm the intensity of the signal was the highest, being the average normalised fluorescence for all the ROIs 4.8460 ± 1.2265 , 4.9926 ± 1.2065 , and 4.7116 ± 1.1251 , respectively (mean \pm SEM) (Figure 3.8 b and c).

Up to this point, light with a wavelength within the range of 800-820 nm seemed suitable for uncaging and imaging. Actually, the fact that the fluorescence measured with excitation light of 800, 810, and 820 is more than 4 times higher than for 920 nm, seemed to indicate that it would be better to

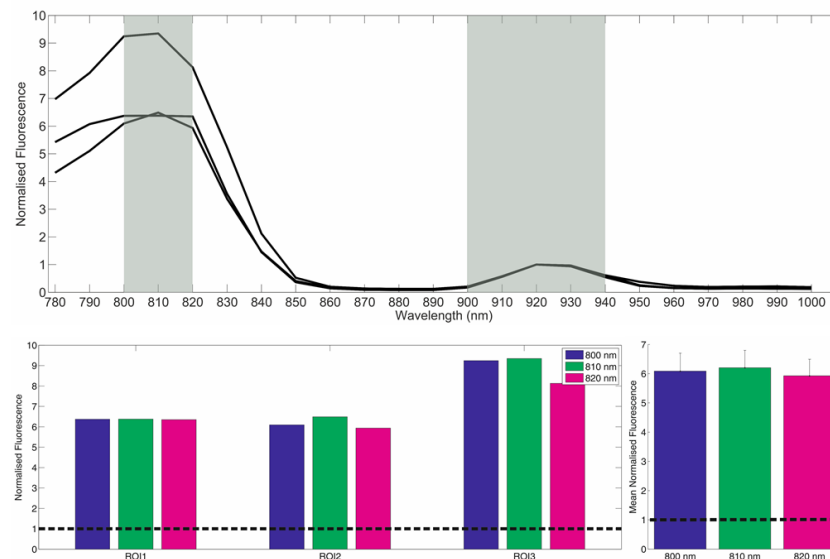


Figure 3.8: **Normalised Fluorescence for different wavelengths.** a) Fluorescence normalised (to 920 nm) for each wavelength. 3 ROIs are shown. The shaded areas indicate two wavelengths ranges of interest: 800-820 nm (for suitability for uncaging and level of brightness) and 900-940 nm (for suitability for exciting GCaMP6s). b) Level of normalised fluorescence at 800, 810, and 820 nm for the three ROIs shown in a). The dashed line marks the level of fluorescence at 920 nm. c) Mean normalised fluorescence for the 10 ROIs, at 800, 810, and 820 nm. The dashed line marks the level of fluorescence at 920 nm. Error bars represent SEM.

use wavelengths shorter than the normally used.

- Fluorescence vs. Wavelength curve with activity

In this section we show that:

1. At different wavelengths, the amount of fluorescence measured is different, both in absolute (raw data) and relative ($\Delta F/F$) terms. It will be shown that some wavelengths are more suitable to measure changes in fluorescence than others.
2. There is a range of excitation wavelengths, going from 830 to 850 nm, that allows activity-driven changes in fluorescence to be measured (detected) and are closer to the optimal wavelength for 2P RuBi uncaging.

After measuring brightness at different wavelengths and observing that the highest levels of brightness were obtained with excitation light at 800, 810, and 820 nm, we tested how well we could measure activity with these three excitation wavelengths to choose the best one for imaging. However, we saw that with none of the three excitation wavelengths mentioned before we were able to see any fluorescence change, meaning that, even though we could see fluorescence, we could not see the increase in fluorescence compared to baseline in response to stimulation (Figure 3.9). Controls at 920 showed that the slice was healthy and responding to electrical stimulation.

Because of this reason, we measured activity using excitation light at different wavelengths, longer than 820.

We compared three wavelengths within the range of interest, using the same intensity of light (Figure 3.10). Comparing the amplitude of the peaks of the responses when exciting at 920, 850, 840, and 830 nm, we saw that even though the amplitude decreases drastically at 850 nm (compared to 920 nm) it still allows the detection of the difference in fluorescence after stimulation, compared to baseline. The amplitude of the peaks measured when using excitation light at 850 nm, was larger than with light at 840 nm ($p < 0.05$).

From these results, it was decided that it would be worth trying 850 nm as the excitation wavelength to reach our goal of imaging and uncaging using a single laser.

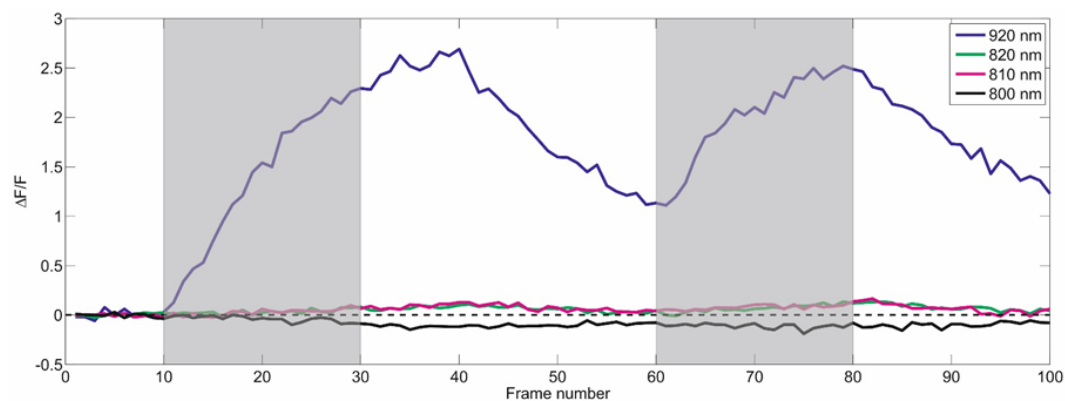


Figure 3.9: **Activity measured after stimulation.** Three different excitation wavelengths are compared to 920 nm: 800 (in black), 810 (in magenta), and 820 nm (in green). The $\Delta F/F$ is close to zero (dashed line) for the three wavelengths after stimulation (shaded areas). The response at 920 is shown for comparison.

3.3.3 Glutamate stimulation

In order to study the response to glutamate, we delivered a solution containing sulforhodamine 101 and Na^+ -glutamate (1mM), using a glass pipette and controlling the flux of the solution from the pipette to the bath by pressure control (Figure 3.11).

The recordings were made with excitation light at 850 nm. Figure 3.12 shows the response of 4 ROIs as an example.

The shaded area represents the time interval in which the puff of glutamate was delivered, and the dashed line shows the onset of the red signal (sulforhodamine). The average response was a 1.05 ± 0.09 -fold increase (mean \pm SEM) with respect to baseline (15 ROIs) and the average time of the onset of the response was 9.08 ± 0.09 seconds (mean \pm SEM), 0.88 seconds after the onset of the sulforhodamine 101 signal (Figure 3.13).

3.3.4 Glutamate uncaging with light at 850 nm

We next wanted to assess the feasibility of uncaging RuBi-Glutamate using light at 850 nm.

Out of the total number of responsive cells taken into account for the analysis, 5 of them responded after the first pulse of high power light (group 1),

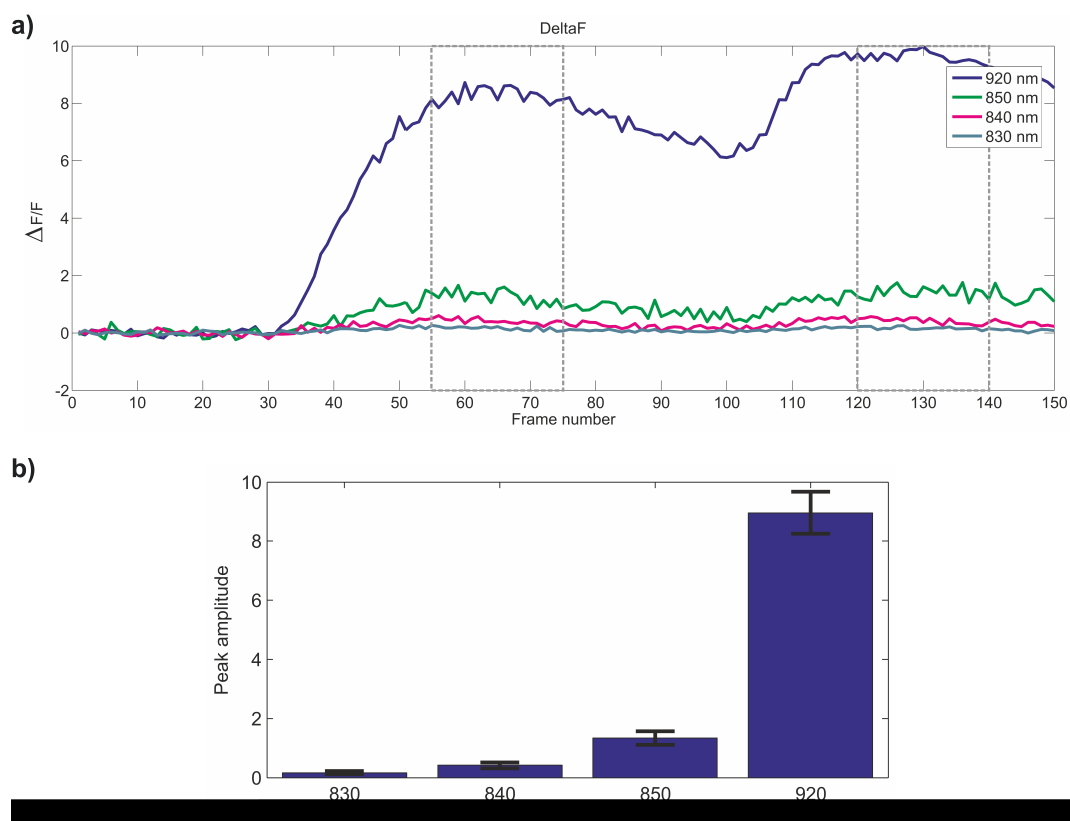


Figure 3.10: **Comparison of three different excitation wavelengths against 920 nm.** a) When $\Delta F/F$ is calculated, it can be seen that for detecting changes in fluorescence, apart from 920 nm, 850 nm is the best of the wavelengths among the three wavelengths tested. The grey rectangles indicate the frames that were used to calculate the peak amplitudes. b) The amplitude of the peaks was calculated and the average of the two peaks for each wavelength is shown. The difference between the mean peak amplitudes at 850 and 840 is significant (paired t-test, $p < 0.05$). Error bars represent standard deviation.

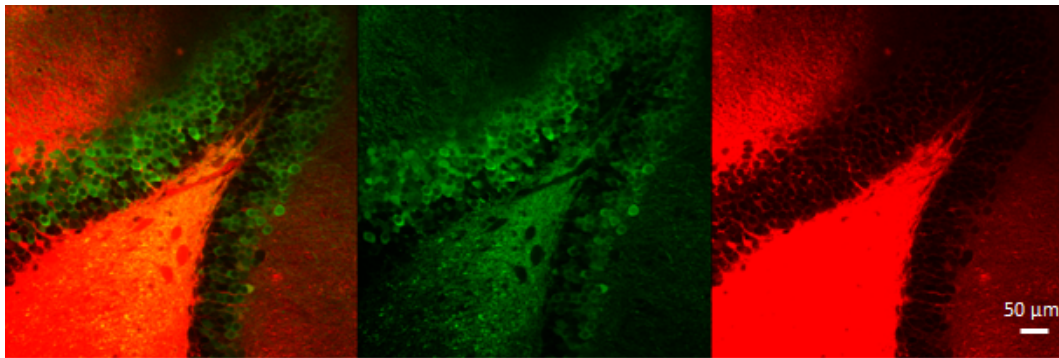


Figure 3.11: **Effect of glutamate (+sulforhodamine 101) in granule cells.** A puff of a solution containing glutamate (1mM) with sulforhodamine 101, was delivered to excite granule cells from the dentate gyrus. In green, granule cells expressing GCaMP6s are showing a great level of activity in response to glutamate (centre). Connective tissue and glial cells are seen in red, dyed by the sulforhodamine 101 (right). Importantly, the merged image shows that the neurons are not dyed by the sulforhodamine 101 (left).

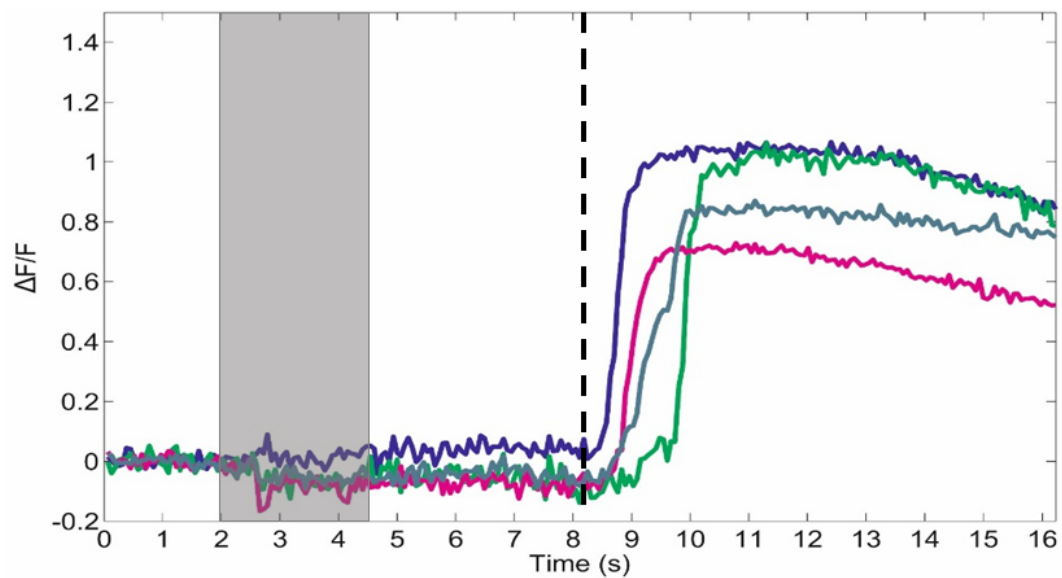


Figure 3.12: **Response to glutamate.** Response of four different cells from the same slice to a puff of glutamate (1 mM) + sulforhodamine 101. The shaded area represents the time when the puff was delivered. The dashed line depicts the onset of the Sulforhodamine signal.

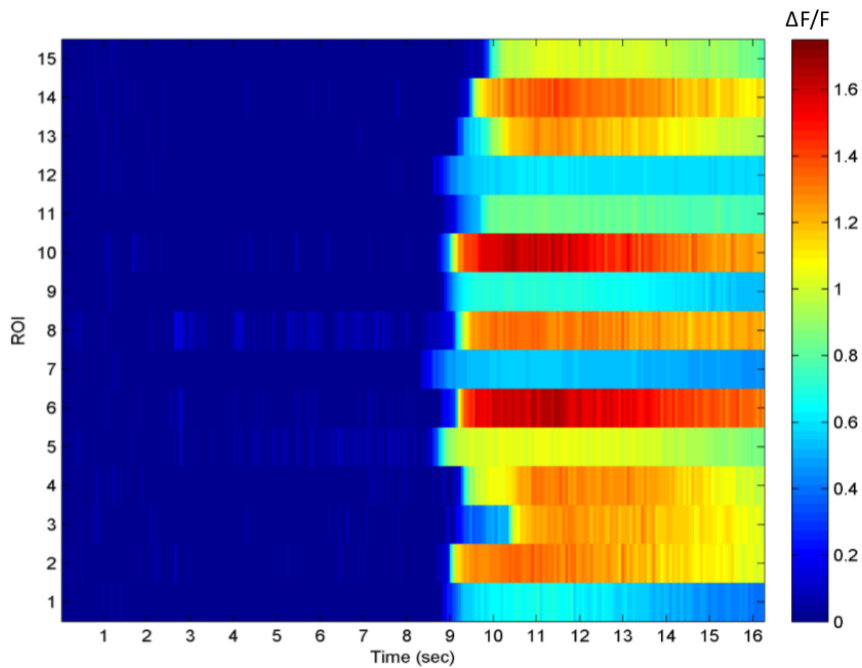


Figure 3.13: **Onset time and amplitude of response to glutamate.** Response to glutamate stimulation of 15 different ROIs. The onset of the response was, on average, at 9.08 ± 0.09 seconds, 4.5 seconds after the end of the puff, and 0.88 seconds after the onset of the sulforhodamine signal. The mean amplitude of the response was 1.05 ± 0.09 . The order of the ROIs is aleatory

while the 3 remaining did it after the second pulse (group 2). In some cases, the activity decreased over time, and in some others the cells remained active for, at least, several seconds.

The mean onset of the response for group 1 was 0.485 ± 0.58 seconds (mean \pm sd) after the pulse, and for group 2, the response started 4.55 ± 2.60 seconds (mean \pm sd) after the second pulse.

Figure 3.14 shows a total of 8 responsive ROIs, 6 of them (Figure 3.14 top and centre) from the same slice, and the other 2 (Figure 3.14 bottom) from a different slice from a different animal. In the first case, the experiment was repeated twice: after the caged compound was applied and the stimulation pulses were delivered, the compound was washed out (until no Sulforhodamine was observed) and applied again to repeat the experiment.

The ROI represented in blue in Figure 3.14 (centre) shows two interesting characteristics: 1) it responded to both repetitions of the experiment and 2) it can be seen how the signal increases and decreases every 2-5 seconds. According to Chen et al., 2013, this is approximately the time it takes to GCaMP6s to decrease the level of fluorescence when the $[Ca^{2+}]_i$ decreases. It could be the case that this neuron is not constantly firing action potentials in response to Glutamate, but instead is firing trains of action potentials with a frequency between trains low enough to allow the detection of the decay in the fluorescence.

When repeated in a different slice (Figure 3.14, bottom) we only observed a response after the second pulse of high intensity light. One of the ROIs (green curve) maintained a high level of activity (~ 1.5 -fold increase in fluorescence with respect to baseline), and the other one (blue curve) decreased its level of activity (~ 1.7 -fold increase) after a few seconds.

Figure 3.15 shows all the 8 ROIs analysed together. The dashed lines indicate the moment when the stimulation occurred. It shows how some responses come after the first pulse of high energy light and some others come after the second pulse. It also shows how the onset of the response of the cells that responded after the first pulse comes sooner after the pulse than in the case of the cells that responded after the second pulse.

This experiment was performed in six different slices, from three different animals. In three of the slices, the experiment was run only once, and in the

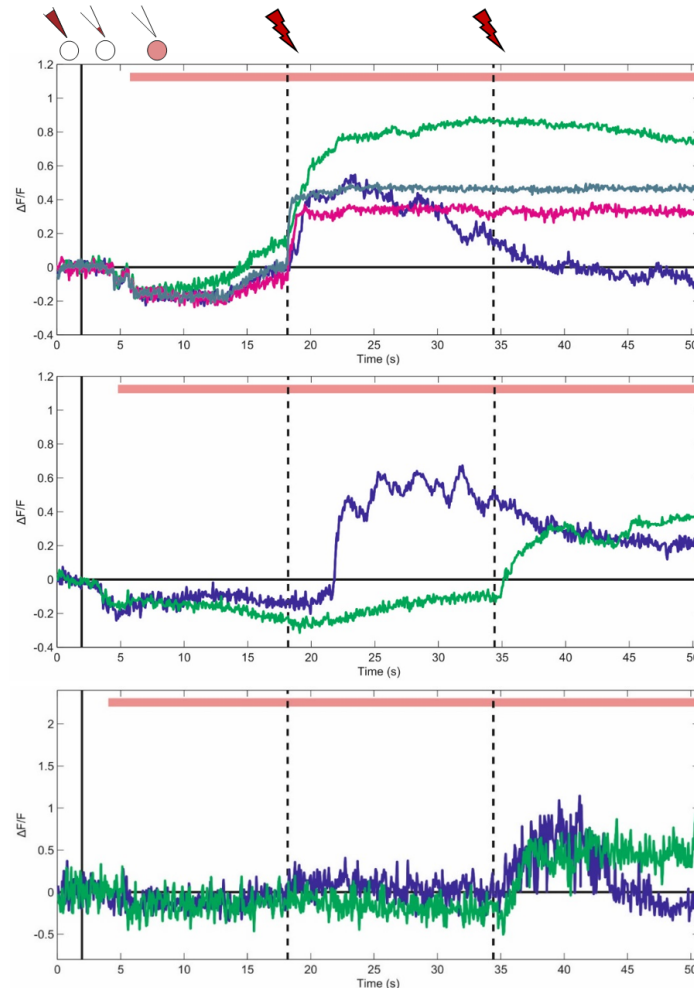


Figure 3.14: **Response to stimulation with RuBiGlutamate.** Response from different ROIs from different repetitions of the experiment to Glutamate uncaging using light at 850 nm. The filled vertical line indicates the end of the baseline (no caged compound) and the two dashed lines indicate the moments of stimulation (300 ms at ~ 270 mW). The bar on top depicts the onset of the Sulforhodamine signal. After baseline, the caged compound was delivered together with Sulforhodamine, during ~ 2.5 seconds. Top: after delivering the compound for the first time. Centre: after washing out the compound and applying it for the second time. Bottom: same experiment on a different slice from a different mouse. The ROIs measured in top and bottom are different from each other, except for the one represented in blue that is the same for both experiments.

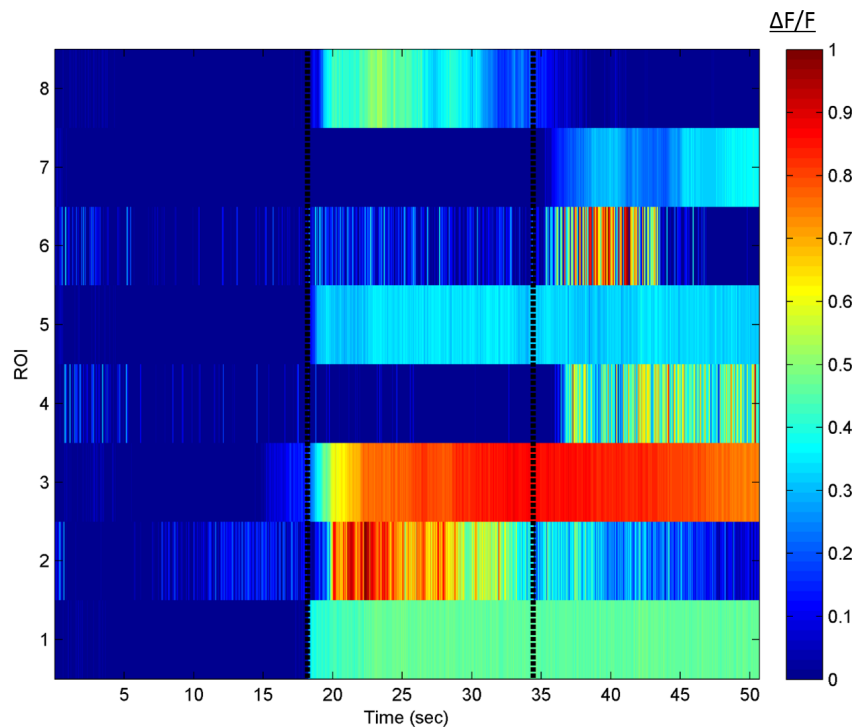


Figure 3.15: **Onset time and amplitude of response to RuBiGlutamate uncaging.** Response to Glutamate uncaging for the 8 ROIs analysed. The mean onset of the response after pulse 1 (first dashed line) was 0.485 ± 0.58 seconds (mean \pm sd) and the cells that responded after the second pulse (second dashed line) did it, on average 4.55 ± 2.60 seconds after the pulse (mean \pm sd).

other three, the uncaging was tested twice (washing out the caged compound between the two repetitions). From these six slices, the uncaging was successful in two (see: Section 5.2 for discussion).

3.4 Conclusions

The experiments aimed to characterise GCaMP6s were important to get to know more about its functionality and absorption and emission spectrum. They showed that at short wavelengths, within the range of 800-820 nm, it is not possible to see a difference in fluorescence. This means that the level of fluorescence does not change in response to a change in Ca^{2+} intracellular concentrations, rendering the protein useless to report neuronal activity. A

possible explanation for this is that the absorption of light at these wavelengths is equal for low and high Ca^{2+} intracellular concentrations (see: Chapter 5). Even though the emission with excitation light at 920 was around 4 times less bright than with excitation light at 800-820 nm, it was shown that it is the best excitation wavelength to measure activity (i.e. changes in fluorescence).

Moving to longer wavelengths, there is a range of wavelengths (from 830 to 850 nm) in which activity can be measured and the intensity of the emitted light is not as low as for longer wavelengths (860-890 nm). Among these wavelengths, 850 nm seems to be the best option for detecting changes in fluorescence, and therefore, to report changes in the level of activity of the cells.

Because of these reasons, 850 nm was the chosen wavelength to try the uncaging. But since all the experiments up to this point had been done with electrical stimulation, and we wanted to measure a response to Glutamate uncaging, we first ran some experiments with Glutamate, always with an excitation wavelength of 850 nm.

The use of Sulforhodamine as a reporter in the experiments with free Glutamate was a crucial control for having the precise time in which the solution with the drug reached the visual field. This allowed us to calculate the time it takes for the Glutamate to activate the cells to a level we can detect with GCaMP6s excited with light at 850 nm. This way, the onset of the response to Glutamate could be compared to the time when the red signal (given by the Sulforhodamine) became detectable.

Even more important was the use of Sulforhodamine for the uncaging experiments. Having the security that the caged compound was already over the cells being imaged at the time of the high intensity light pulse was essential. Without this control, in the case of not observing a response to the uncaging, we would have not been sure if it was because the time left for diffusion was not enough and the compound was not yet over the cells within the visual field or because the uncaging was not working.

The uncaging at 850 nm was successful in two slices, and three repetitions of the experiment. A significant increase of the $\Delta F/F$ can be observed for a total of 8 ROIs between the two slices. Some ROIs had to be discarded for analysis because the amplitude of the response was not high enough. There are two types of response: one that comes after the first pulse of high intensity

light (Response1) and another that happens after the second pulse of light (Response2). One possible explanation for this is that there are cells that are less sensitive than others, and the first pulse of light does not uncage enough Glutamate to excite them. The second pulse, however, might be releasing extra Glutamate that, summed up to the already free Glutamate from the first pulse, rises the concentration of free Glutamate to a level that is enough to excite them.

The results for this set of experiments were conclusive about the possibility of exciting GCaMP6s with light of a wavelength outside the range. This allowed us to move from 920 nm towards the 800 nm, necessary for the RuBi uncaging. The reason why 850 nm was finally chosen to try the uncaging was because it was the closest wavelength to 800 nm that we could get without compromising the fluorescence signal.

The experiments with uncaging and 2P imaging confirmed that 850 nm is a good wavelength to combine both techniques, without the necessity of a second laser.

Chapter 4

Development of an animal model for concept representation in the hippocampus

4.1 Introduction

The main objective of the *in vivo* project is to develop an animal model to study concept representation in the hippocampus. There are several advantages of developing an animal model for studying the analogous to concept cells that, so far, have only been described in human beings. An animal model would i) allow implanting large number of electrodes in single or multiple areas involved in concept formation; ii) provide the possibility of studying concept representations at different stages to understand the mechanisms involved in their formation and plasticity; iii) make it possible to use 2P imaging recordings, assessing the activity of large neural populations and studying their spatial organisation and iv) allow the manipulation of the firing of selected groups of neurons involved in representing specific concepts, which would permit us to study their connectivity and influence in behaviour.

The original plan for this project includes five steps: 1) Building a virtual reality (VR) set-up; 2) programming the virtual environment; 3) training the animals in the virtual environment; 4) doing 2P imaging during training; and 5) doing *in vivo* uncaging. So far, the first 3 steps have been successfully achieved and number 4 is currently being carried out by Dr. Schiavon.

During training, the animals navigate in a virtual reality environment and perform a two-alternative forced choice task, in which they need to choose between 2 “holes” on a wall that is presented in front of them on each trial. The

two holes have different shapes (e.g. one triangular and one semi-circular) and only one of them is rewarded (see: Figure ??). When the animal approaches the correct hole, it receives a reward (water or water + sugar).

Once the animals have a high and stable performance, the objective is to study invariance (i.e. if they can still recognise the shapes as the correct and incorrect ones, even if some low-level features have been changed, such as pattern, size, etc.).

The VR setup allows flexible control of the environment and task difficulty, as well as the precise timing and location of stimulus presentations. Also, it is a great advantage that the animals are head-fixed but still performing a complex task, since this offers the possibility of doing 2P imaging while they are doing the task. There are several reasons that led us to look for concept representation in the hippocampus: i) concept cells in humans were found in the MTL (including the hippocampus); ii) it was found that some cells in the mouse hippocampus fire in response to different nests (Lin et al., 2007) irrespective of their position or shape and, according to the authors, they represent the concept of “nest”; iii) it is known that information from different sensory areas converges to the hippocampus, both in humans and rodents (Jeffery, 2007); iv) the rodent hippocampus plays an important role in memory functions (Quiñero, 2012); and v) place cells were found in the hippocampus, with spatial locations being such relevant concepts for rodents.

Based on the studies about the human hippocampus carried out by members of the Centre for Systems Neuroscience, we hypothesised that the function of the rodent hippocampus is not limited to spatial navigation and is indeed a potential system to study concept representation in an animal model.

4.2 Methods

This project was a result of a collaboration among Dr. Molano-Mazón, Dr. Boyraz-Jentsch and myself. I collaborated with the virtual reality set-up building, the surgeries and the training of the animals. Currently, the project is being carried out by Dr. Schiavon, with whom I also collaborated providing assistance with the 2P microscope and the virus injection.

All procedures were approved by the University of Leicesters Animal Welfare

and Ethical Review Body (AWERB) committee and performed under license from the UK Home Office in accordance with the Animals (Scientific Procedures) Act 1986.

4.2.1 Animals

C57BL/6J mice were obtained from Charles River at 3-weeks age. After arriving at the unit they were maintained in a reversed light cycle so that the training sessions would be during their active period.

After a week of acclimatisation, the animals started to be handled every day in the laboratory to get them familiarized with the researchers and the environment. They were allowed to spend some time of the day in a new environment (i.e. big box with toys/tunnels and polystyrene materials) and their home environments were enriched. After 6-8 weeks the animals were implanted with head-plates for head-fixation in the Virtual Reality set-up.

4.2.2 Head-plate implantation

In order to head-fix the animals in the set-up, they had to be implanted with a head-plate. This head-plate was made of titanium because the hardness and the lightness of this material made it ideal for this purpose. The final design of the head-plate weighed less than 1g and was 0.8 mm thick and had a size of 7x30 mm. The head-plate was designed in order to minimise the discomfort that it could mean for the animal but at the same time to be useful for head-fixing the animals without generating high levels of stress to them. Surgical procedures were performed under general anaesthesia with Isoflurane (2-2.5 % for induction and 1-1.5 % for the rest of the procedure). Pre-operative procedures were the same as for the animals injected with the virus (Section 3.2.2).

After preparation in the pre-op area, the animal was moved into a sterile environment and the rest of the surgery was carried out under strict aseptic conditions to minimise the risk of infection.

The animals were fixed for surgery using a stereotaxic frame, just like we did for virus injections.

After removal of the skin, the skull was thoroughly cleaned by scraping

it with a blade to completely remove the periosteum. This step was crucial for a long duration of the implant. Using a drill with a drill bit of 0.9 mm (FineScienceTools), we performed 3 to 4 craniotomies to then insert self-tapping bone screws onto the skull. These screws functioned as an anchor to bone cement.

Before inserting the screws, the skull was completely dried and if there was any bleeding generated by the craniotomies the screws were not inserted until the bleeding stopped.

A first layer of bone cement (Henry Schein) was first applied covering the screws. Before it got dried the head-plate was positioned, and covered with a new layer of cement. The cement used had to be cured with UV light.

The animals were single-housed for a few hours after surgery (until they were fully awake and moving in the cage). After recovery, they were returned to their cage-mates whenever possible, always monitoring the cage-mates' behaviour during the first few hours.

4.2.3 Virtual Reality Set-up

The VR Set-up consists of: a) three plasma screen monitors; b) a treadmill; c) a pump for reward delivery; d) one camera to monitor the animal from behind and e) a second one close to its mouth; an air puff system (not shown) and two speakers (not shown) (Figure 4.1).

The design of the set-up was adjusted from the one described by Dombek et al. (2007). The three monitors (a) are positioned in a way that cover the whole visual field of the animal. The treadmill (b) consists of a Styrofoam ball (20 cm outer diameter), floating on a custom-designed 3D printed base, with a compressed-air inlet at a constant pressure (~ 50 psi) that can be adjusted for each animal.

An optical mouse placed in front of the ball (between the ball and the monitors), detects the movements of the ball and provides the information to the software to update the image on the screens.

The reward system (c) consists of a pump (NE-500 Programmable OEM Syringe Pump, New Era pump systems) connected to the computer and controlled by the software. The pump is connected to a rat feeding needle (Fine Science Tools) that is positioned in front of the animal's mouth.

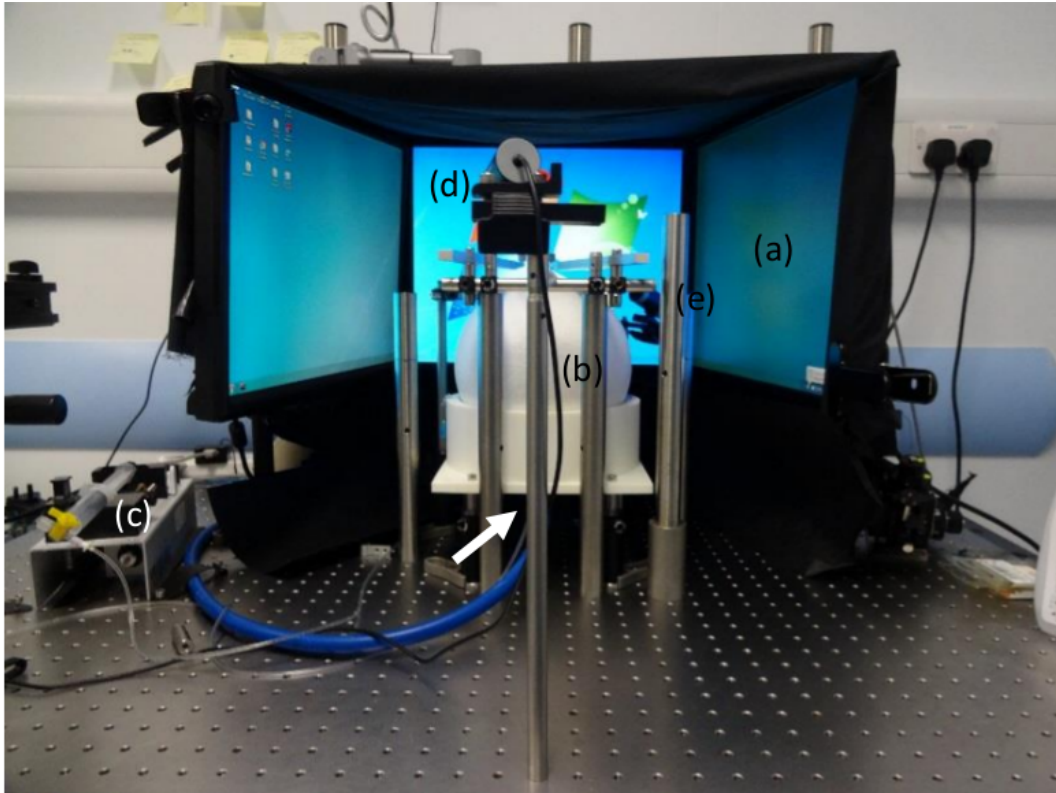


Figure 4.1: **Virtual Reality Set-Up.** The set-up consists of three computer plasma screens (20"), that cover the entire mouse visual field (a). The treadmill is formed by a polystyrene ball (20 cm outer diameter) and a 3D printed base (b), which has a compressed-air inlet that allows the ball to float (arrow). A pump controls the delivery of water as a reward (c). Two cameras are used to monitor the mouse throughout the training session (d and e). The whole set-up is mounted on an optical table.

To encourage the animals to walk, we mounted an air puff system which delivers a puff of air pointing to the back of the animal every time a wrong trial is completed (which can either mean that the animal chose the wrong door or that it did not compete the trial and instead it stayed still).

Two speakers are located at each side of the mouse, and a sound is played at the end of each trial. The sound is different for successful and incorrect trials, to enhance learning.

The head-plate has two holes and a screw is passed through each of them and fixed to two holding arms located on top of the ball.

There are also two webcams, one to record the animal from behind during

the training and the other one placed close to the animal's mouth to confirm that it effectively drinks water after completion of successful trials. The cameras were connected to a second computer (different to the one that controls the virtual environment). The cameras were installed to be able to monitor the animal during training, since the whole set-up is covered with blackout fabric to isolate the animal from external visual stimuli (e.g. movements from the experimenters, light coming from computer monitors, etc.).

The software used to generate and control the virtual environment was Blender, which is a Python-based software.

The virtual environment was programmed by Dr. M. Molano-Mazón.

4.2.4 Training paradigm

The protocol used to train the animals was based on a two-alternative forced choice paradigm: at the beginning of the trial the mouse was presented with 2 objects and had to approach one of them. Only one of those two objects gave the animal a reward. Whenever the animal went to the correct object, it received a reward (water), a bell sounded and then the next trial started. Whenever the mouse went to the other object, ran towards the walls, or took more than 60 seconds to approach the object, the trial ended with a sound and the mouse received an air puff on the back and time out (3 sec).

The objects the mouse had to discriminate were holes on a wall with different shapes (Figure 4.2). By using this kind of objects we were taking advantage of the natural behaviour that mice have to explore the environment. With previous paradigms we observed that mice tried to go towards the walls, to the corners, and even go through tight holes between walls. Thus, we thought that a task in which the mice had to actually go to a hole to get the reward would help the training without diminishing its scientific value.

The walls had patterns to give a more realistic feeling of movement.

The animals were under a water restriction regime while the training lasted. This restriction was used to enhance the motivation of the animals to learn the task.

The restriction scheme consisted of 5 days a week with no more water than the amount received during training, as long as the body weight did not drop further than 15% of the initial weight, and 2 days a week with free water. At

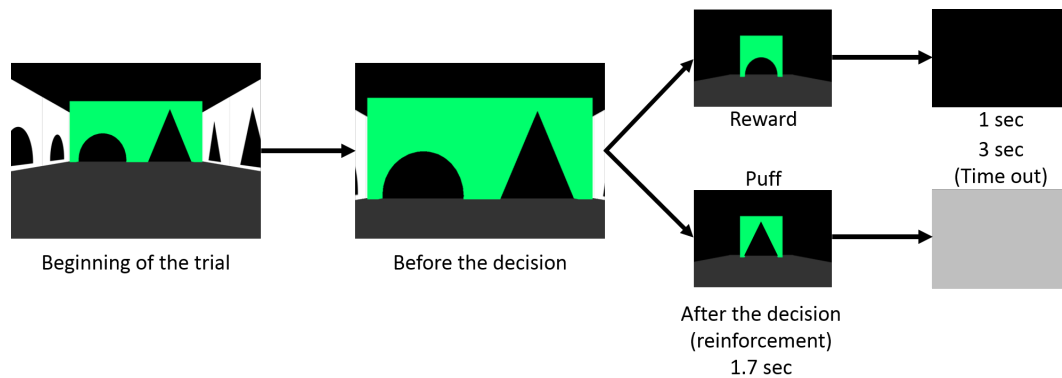


Figure 4.2: **Decision process from the beginning to the end of the trial.** At the beginning of the trial the mice have to walk towards the front wall that contains the two holes. Once in front of the wall, they have to choose between the two shapes. After the decision is made, the chosen shape is shown to reinforce the chosen option. During the reinforcement (1.7 sec), the animals receive either a reward (when they choose the correct hole) or a puff of air (when they choose the wrong option). Finally, a black screen is shown for 1 second, after choosing the correct option, or a light grey screen was shown during 3 seconds (time out) after choosing the wrong hole.

the beginning of the training, free water was delivered in the set-up to avoid dehydration, because the performance was too low. If the water intake during training was below 1 ml, additional water was given to the animals, at least 1 hour, after finishing the training session.

The training consisted of three phases: 1) high contrast (black and white), 2) medium contrast (black and grey), and 3) no contrast (black).

During the first training sessions, the correct choice was in black and the incorrect one in white (phase 1). This way, we were also making use of another natural tendency of mice to get away from bright light. When the animal increased the performance, we decreased the contrast to phase 2, in which the correct object was still black but the incorrect one was now grey. Finally, as the performance kept improving, the training got to the final phase (phase 3) in which both objects were black. For data analysis, only the trials of phase 3 were taken into account.

4.2.5 Data Analysis

The data analysis was performed by Dr. Molano-Mazón and based on his analysis I have done some modifications to show some of the results in this thesis.

-Daily mean performance and probability of random behaviour

To score the performance of an animal in a specific day, a number was assigned to each completed trial (1 if it was successful and 0 if the animal chose the wrong object) and a running average was calculated across trials. Trials that were not completed (because the animal did not move or could not make a decision in time) were not considered for calculating performance. These trials never exceeded 30% of the total number of trials. Since the training session had always the same length (30 minutes), the number of trials completed in each session varied from day to day and from animal to animal.

-p-value calculation

In order to establish if the performance was significantly higher than chance, we simulated training sessions in which the animal was performing randomly (choosing one object or the other with the same probability in every trial). For the simulations, the Matlab function “rand” was used, which creates random values uniformly distributed between 0 and 1. We defined as correct, the trials in which the random value was larger than 0.5 and incorrect the ones for which the assigned random value was smaller than 0.5. As with the real data, correct trials were labeled with a number 1 and incorrect trials with a 0. To evaluate if after n trials the mouse was performing significantly above chance, we simulated 10,000 training session with n trials and calculated the performance for each of those sessions. We then estimated the p-value as the proportion of times in which the simulated performance was larger than the real one for the session.

4.3 Results

4.3.1 VR set-up and animals' habituation to the set-up

The virtual reality set-up was built by Dr. Molano-Mazón in collaboration with Dr. Boyraz-Jentsch and myself. Dr. Molano-Mazón programmed the virtual environment.

The mice were first adapted to the set-up and the head-fixation. Normally, after three days of training they seemed habituated to the set-up and were able to drink water and explore the virtual environment.

Because we were trying different paradigms and constantly improving them, it is not easy to estimate how much time it took to the animals to learn the task (i.e. have a performance significantly different from chance). This is a question that needs to be answered with naïve mice.

After 2 weeks of training from Monday to Friday with the 5-days water restriction scheme, we decided to reduce the training regime to 4-days a week because the lack of motivation on Mondays (after spending the weekend with *ad-libitum* water) made the animals freeze on the ball and after some time they became really stressed. To avoid dehydration on Mondays, we gave them 1 ml of water.

4.3.2 Performance

Three mice were trained using the protocol described in Section 4.2.4. All of them were trained with different versions of the paradigm, which makes it difficult to estimate how long it took for them to reach a performance higher than chance. Figure 4.3 (top) shows the cumulative moving average performance for one day of training (Friday) of one animal across trials. From trial 28, the p-value stays below 0.05 until the end of the training session (bottom). This suggests that a few tens of trials in one training session are enough to reach a plateau of nearly constant performance.

Figure 4.4 (top) shows that the level of performance was above chance (dashed line) for the entire training week. The mean performance for the week

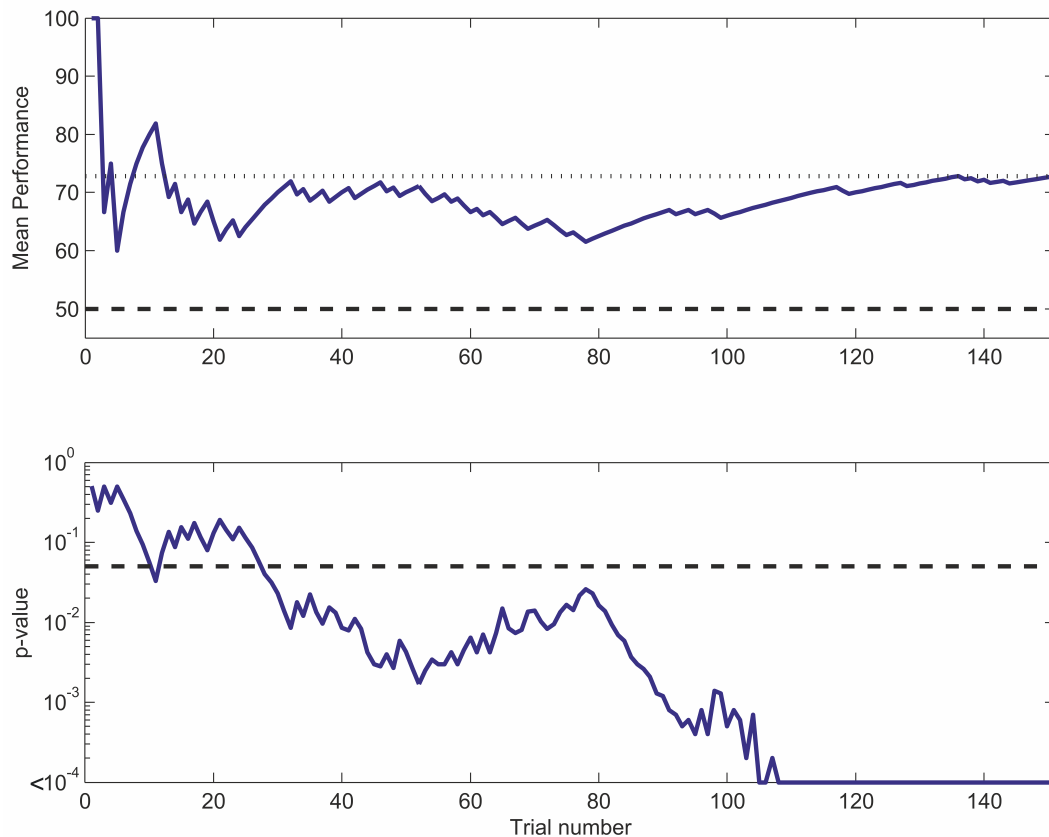


Figure 4.3: **Daily mean performance and p-value.** 151 trials were completed by the mouse this day. Top: cumulative moving average of performance. Dashed line: chance level (50%). Bottom: cumulative probability of random behaviour across trials (in logarithmic scale). Dashed line: chance level (0.05).

was 68.19 ± 1.94 (mean \pm SEM). It is also possible to appreciate that the mouse did not seem to significantly improve or decrease its performance throughout the week. Figure 4.4 (bottom left) shows that, for the same week, the mean performance was $68.19\% \pm 1.94$ (mean \pm SEM). The amount of failed trials (i.e. trials in which the mouse did not make a choice) varied throughout the days, within a range of 3 and 28% of the total trials (Figure 4.4, bottom right). The mean percentage of failed trials for the week was $12.6\% \pm 0.19$ (mean \pm SEM).

4.4 Conclusions

During 2013 and 2014 I collaborated with the building of the virtual reality set-up, implanted most of the animals for training, and helped with the training, apart from contributing to the project with ideas to improve the training and the paradigm. Before using the current protocol, we tried several others that did not seem to work for mice (some of them were more stressing for the animals, some others were too complex, etc.). Even the current protocol was modified several times in order to improve it.

Because the mice were trained with the different protocols, it is hard to estimate how long it took for them to learn the task (i.e. to have a high and stable performance). This is a question that will need to be answered with naïve mice. Even though we cannot estimate how long it took for them to learn the task, we can conclude from these behavioural results that they did learn and reached a performance that had some stability throughout the week. This last result is very important taking into account that the water restriction scheme was not constant. This could have had a huge impact on the performance on different days of the week. Although it did impact the performance on Mondays, this was sorted out by shortening the training week to four days instead of five.

For the future building of a new set-up, the use of an automatic way of detecting licks should be considered, since knowing if the animals are licking (and when) could provide information on how well motivated they are and if there is any expectation of reward delivery when they choose the correct option but not when they choose the incorrect option.

The next steps for this project are, first, to train naïve animals, and second to monitor neuronal activity with a 2P microscope while the animal is performing the task to look for neurons responding to the presented objects.

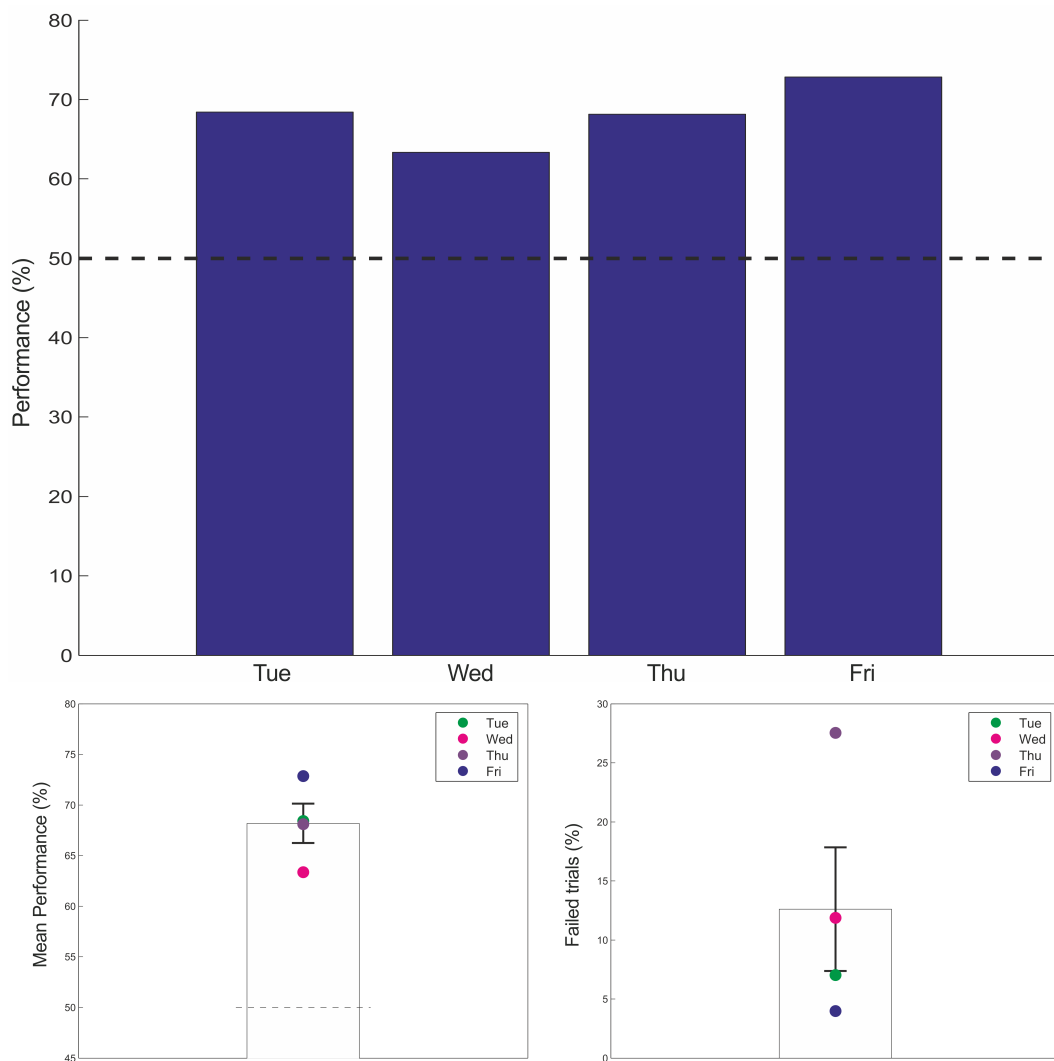


Figure 4.4: **Weekly performance of an animal.** Top: Performance for a typical training week (Tuesday to Friday). The performance throughout the week varied between 63 and 73%. The mean performance for that week was $68.19\% \pm 1.94$ (mean \pm SEM)(bottom left). The mean number of failed trials for the same week was $12.6\% \pm 0.19$ (mean \pm SEM).

Chapter 5

General Discussion, Conclusions and Future Directions

In this PhD thesis we advanced towards the combination of two techniques widely used in Neuroscience: two-photon imaging and two-photon uncaging. Even though this is not a completely new approach, the contribution of this thesis resides in the fact that we used only one NIR light source to carry out the two processes at the same time. Once this technique is optimised, it will be applied *in vivo*, aiming to overcome some of the current experimental limitations.

We also started a project to develop an animal model for studying concept representation in the hippocampus.

This thesis consisted of three parts: *in vitro* electrophysiology, *in vitro* two-photon imaging and uncaging, and *in vivo* behavioural testing in a learning paradigm.

The objective of the first *in vitro* part of the thesis was to replicate an important result in the field of oscillations induced by kainate. This was a reassurance of the quality of the slices we were going to use for the project described in Chapter 3. Because the uncaging method was going to be developed and tested *in vitro*, we needed to make sure that the slicing technique was implemented correctly and the slices were healthy. The experiments carried out with this purpose were conclusive about the quality of the slices, since the connectivity among cells was tested by electrical and pharmacological stimulation, showing the expected results.

The main goal of the second part of the *in vitro* project was to find a wavelength that allows simultaneous uncaging (at high laser power) and imaging Calcium with a protein from the GCaMP family (at low laser power). This way, the same laser can be used for the two techniques at the same time, without the necessity of a second laser, which saves not only a lot of money, but also physical space. It also permits the implementation of diffractive materials

in order to split the beam of light to image (and manipulate, as in this case) several neurons at the same time.

Finally, the ongoing *in vivo* project aims to find out how mice represent concepts and develop an animal model for studying this representation in parallel to the recordings in humans. Three of the five steps originally proposed have been achieved: we built the virtual reality set-up, Dr. Molano-Mazón programmed the virtual environment, and we started training the animals in the virtual environment with successful behavioural results. Dr. Schiavon is now starting to do 2P imaging during training, after having significantly improved the behaviour with changes to the paradigm, to the water restriction scheme, and to the training protocol.

5.1 *In vitro* electrophysiology

The experiments carried out during the first year of my PhD were of invaluable help to get to know more about the hippocampus, learn about its areas, its connections, its physiology and pharmacology, etc. I also developed data analysis tools that were useful for subsequent analyses focused on 2P imaging and uncaging.

These experiments were also useful to ensure that the slicing technique was appropriate for measuring neuronal activity. This part was extremely important for the following project, because as a new method was going to be developed, we needed to make sure that the system on which we were going to try it was appropriate. This was done in two ways: 1) measuring responses to electrical stimulation under different pharmacological conditions and 2) replicating results from a classical study on gamma oscillations (Fisahn et al., 2004), for which I performed my first experiments with pharmacological stimulation of hippocampal slices.

5.2 *In vitro* two-photon imaging and uncaging

As discussed before, two-photon imaging has been, for the last few years, gaining importance among laboratories studying the brain. Apart from being expensive, it has very few limitations and these are highly compensated by its advantages. It is no surprising then that many scientists around the world are implementing this technique to try to shed some light on the many different processes carried out by the brain.

Another technique discussed here is the one to stimulate a single neuron, or part of a neuron, with very high spatial and time control. Caged compounds have been developed independently by many laboratories, and each of them have advantages and disadvantages. However, there is no doubt that there has been great improvement since the first ones were reported. This, together with great results using them, is a clear sign of the usefulness of these compounds and their possible combination with other techniques has a lot of potential in Neuroscience.

With the use of a two-photon microscope it is possible to uncage a molecule of interest, and measure the response to the uncaging either with electrophysiology or with Calcium imaging. However, when the response is measured with two-photon imaging, two lasers might be needed, one for uncaging, tuned at the correct wavelength for this process (between 720 and 800 nm), and a separate one to excite the Calcium indicator, also set at the right wavelength to excite the fluorophore (which is normally around 900 nm, in the case of the GECIs). If the same laser was used, the wavelength would need to be changed and part of the response to the uncaging would be missed, because tuning the laser to a different wavelength takes some time.

There are currently several examples of caged compounds applications (Matsuzaki, 2004; Branco, 2010; Kwon, 2011; Buchanan, 2012; Araya, 2013), all of them showing exciting results.

In these examples, one laser is used to excite the calcium indicator and a separate one is used for uncaging. Even though this technique works perfectly, most of the laboratories do not have two Ti-Sapphire lasers available. Also, as mentioned before, it is difficult to target several cells at the same time,

since normally this is achieved by splitting the beam of light using a diffractive material. If light of different wavelengths is used for uncaging and for imaging, it would be difficult (if not impossible) to make the two beams coincide on the same spots, given that diffractive materials affect differently light of different wavelengths. If we only use one laser at the same wavelength for uncaging and doing imaging, it is possible to split the beam of light in order to manipulate neuronal activity of many cells simultaneously. This kind of experiment would allow the study of networks or the manipulation of the behaviour of an intact animal.

In order to find the optimal wavelength for simultaneous imaging and uncaging we started by characterising the GCaMP6s protein, to get to know more about its physicochemical properties and define a range of wavelengths in which the protein is functional. We first found that activity (changes in fluorescence with respect to baseline) could not be detected when the protein was excited with light at 800-820 nm. A possible explanation for this is that when excited with light within this range of wavelengths, the emission of the protein is independent of the intracellular concentration of Calcium.

However, wavelengths ranging from 830 to 850 seemed to be more suitable for measuring activity. Given that 850 nm was significantly better at detecting changes in fluorescence than 840 and 830, we decided to test if it was good enough for uncaging as well.

Because the activity we had measured up to this point was driven by electrical stimulation we decided to first measure responses to Glutamate, using excitation light at 850 nm. These results confirmed that responses to Glutamate stimulation can also be detected when exciting GCaMP6s with light at 850 nm. We observed that after some time of the response onset, the signal decreases, as if the $[Ca^{2+}]_i$ was decaying. Because the Glutamate was not washed out until the end of the recording, and because we were using a high concentration of the neurotransmitter, we think that this decay in the activity might be due to desensitisation.

We finally tried the uncaging at 850 nm and we observed a variety of responses after increasing the power of the laser to induce the photorelease of the Glutamate. Some of the responsive cells showed activity right after the first pulse of high intensity light, while some others responded only after the second

pulse. One possible explanation for this difference is that the cells responding after the second pulse might be less sensitive to Glutamate and so need a higher concentration of the neurotransmitter to respond to it. Because we were not washing out the compound, the amount of free Glutamate accumulated with the two pulses, increasing its concentration and therefore activating the less sensitive neurons. Also, we repeated the experiment with the same slice to evaluate if the caged compound (and the effect of the photoreleasing) could be washed out but also to test if the light intensity during stimulation was too high so as to produce photodamage. Only one of the responsive cells from the first repetition responded again in the second one, and there was a new responsive cell that had not responded before. The fact that most of the cells that responded with the first repetition did not respond again during the second repetition of the experiment, might also be related with the phenomenon of desensitisation. The fact that there are cells responding after 2 and even 4 pulses of high intensity light is an indicative that, at least with this protocol, the light intensity is not damaging the cells. However, more experiments are needed to confirm this assumption.

The uncaging at 850 nm was not successful on every slice. We have thought of different possibilities to improve the efficiency of the method. 1) The high energy pulse could be delivered in the form of short pulses instead of one long pulse. 2) The optimal pulse length should be studied, since too long pulses might damage the cells, and too short pulses might not be enough to uncage. 3) Also the intensity of the pulse should be studied. We tried with the maximum power that our Ti-Sapphire laser allows, but maybe more power is needed to increase the efficiency of the uncaging, or it might be the case that less power is enough to produce the photoreleasing of the neurotransmitter and would avoid photodamage of the cells. 4) The uncaging was tried in an area of $296.11 \mu\text{m} \times 296.11 \mu\text{m}$. Taking a smaller area to uncage might also improve the technique. 5) Finally, it would also be a good idea to try to uncage and measure the amount of free Glutamate as a result of the 2P excitation with a Glutamate sensor, such as iGluSnFR (Marvin et al., 2013). This would give us a direct estimation of the amount of Glutamate being released without the cells' response as an intermediary.

Until recently, optogenetics was exclusively performed with visible light,

since the opsins used absorbed within that range of wavelengths. However, as mentioned before, visible light is much more highly scattered than NIR light, which decreases the spatial resolution of the activation/inhibition. Since the discovery of the red-shifted opsin C1V1_T, optogenetics can be applied with 2P excitation, which provides a much higher spatial resolution than before. Even though optogenetics is a great technique for selective inhibition and stimulation, there are two disadvantages that are worth mentioning. 1) Because it is based on an exogenous protein that has to be artificially expressed in the brain, when combined with GECIs, it is necessary to either inject two viruses, or have transgenic animals, which are very expensive. 2) Because the protein is an ion channel (Na⁺ or Cl⁻) the activation or inhibition of the postsynaptic neuron is not mediated by neurotransmitter release. The application of caged compounds is a more realistic way of mimicking what actually happens when the postsynaptic cell is excited or inhibited by the presynaptic.

In conclusion, we have achieved the main goal of this thesis that was to find a suitable wavelength for both 2P uncaging and imaging with a GECI. Even though there are many aspects that need to be improved, we demonstrated that we can uncage RuBi-Glutamate with light at 850 nm and measure the response to the uncaging using a protein from the GCaMP family, without changing the wavelength.

This method can be applied *in vitro* and, potentially, *in vivo*. There are several possible applications for this method, ranging from studying circuits, long and short-term potentiation, and spine dynamics, to altering behaviour through the selective inhibition or excitation of a network.

5.3 In search of an animal model for studying concept representation

This project was, from the beginning, a very ambitious one, with great questions to answer and methodological challenges, even without taking into account that the lab is new to animal experimentation. However, when we started carrying it out, we realised it was going to be even more challenging than originally thought.

First, we had to plan and learn how to perform a surgery to implant the

animals with a head-plate. Three different protocols were followed in order to assess which one was the best in terms of side effects for the animals and stability and duration of the implant. We finally chose one of the protocols that involved the use of bone screws that act as an anchor for the dental cement. This protocol was successful for some animals, but unfortunately some other lost the implant after 1-2 months.

Since the beginning of the training, the paradigm has suffered several modifications, as we learnt from the animals which aspects needed to be changed and improved. Also, the training protocol suffered from changes. Just to mention a few of them: the wall with the two holes was turned into a green wall, instead of grey, to induce the use of cones for the discrimination of the two shapes, instead of rods (Wang et al., 2011); the side walls were replaced by walls containing repetitions of the shape on each side; and the chosen hole was presented on its own in the end of the trial to reinforce the association with the chosen object and the reward or the puff of air. Because the animals to which I contributed to train went through all those changes, we cannot estimate from them how long they need to be trained to learn the task. Naïve mice are currently being trained with a fixed paradigm and it should be possible to get an estimation from them.

Some of the mentioned improvements were proposed and implemented by Dr. Schiavon during the last year. Now that the improvements made are proving to have a positive effect on the health of the animals and on their performance, Dr. Schiavon is putting efforts in starting the training under the two-photon microscope, to be able to record from neurons while the animals are performing the task. He has learnt how to perform a surgery for doing a cranial window, removing part of the cortex¹ and injecting a virus to induce the expression of GCaMP6s in the hippocampus (see: Section 5.3.1).

The next steps to be taken for this project are: doing 2P imaging while the animals are performing a two-alternative forced choice task and manipulating neuronal activity patterns of specific neurons to study their impact on behaviour through the use of caged compounds. For this last step, the technique described in Chapter 3 will be applied. Because the uncaging technique was tested

¹In order to be able to do imaging from the Hippocampus, part of the cortex on top of it has to be removed. For doing this, Dr. Schiavon is following the surgical procedures described in Dombeck et al., 2010.

only *in vitro*, future experiments will be necessary to decide if it is a suitable technique for application *in vivo*. However, given all the evidence showing that 2P imaging and 2P optogenetics work perfectly *in vivo*, we are confident that our technique will be suitable for stimulation or inhibition of single neurons in an intact animal.

5.3.1 Current state of the project

As mentioned before, I collaborated with some parts of this project until 2014. Since then, several improvements have been implemented, especially by Dr. Schiavon, providing better and more stable behavioural results.

The modifications ranged from changes in the water restriction scheme to changes in the protocol for implanting the head-plates. Also, a new virtual reality set-up has been built in order to perform 2P imaging while the animals are performing the task. Naïve animals are currently being trained with all the changes implemented and the results are promising.

Stability of the implants has been increased by using a method that does not involve screws. It consists of thoroughly cleaning the scalp to remove all the connective tissue and then apply a layer of cement, in which the head-plate is embedded. Dr. Schiavon is additionally injecting the same virus used for the experiments described in Chapter 3, in order to express GCaMP6s in the hippocampus and doing a cranial window to perform 2P imaging, for which he needs to remove part of the cortex. The surgeries have been successful so far, with no adverse effects from the cranial window nor the removal of cortex.

The animals are currently water deprived 7-days a week, and the water reward has been replaced by water + sugar, which seems to be more motivating for the animals than water. With this water deprivation scheme, not only the training week can be longer, but also the animals' weight seems to be more stable, which is good for their health.

Figure 5.1 (top, left) shows a week of training for an animal after 6 weeks after starting the training. This animal maintained a performance above 75% of correct trials throughout the week. Interestingly, the number of trials in which the animal did not move was zero for the five days of the week (not shown). This might be due to a higher motivation from the animal to get reward given by the new water deprivation protocol. The mean performance for the week

was $90.04\% \pm 4.17$ (mean \pm SEM) (Figure 5.1, top, right).

The virus injection is proving to be also successful *in vivo*. Figure 5.1, bottom, shows an image of a group of neurons from the hippocampus at three different times, while the animal is running on the ball on the virtual reality set-up (not performing the task). The activation of a big number of neurons can be seen, especially, at the bottom of the image.

Now that the performance is high and stable, Dr. Schiavon is planning to test invariance, by changing low level features of the doors (e.g. pattern or height/width ratio). At the same time, he will start looking for neurons responding specifically to one of the two shapes to test if they encode the concept of the object.

In the last two years, this project has progressed from one behavioural set-up with a constantly changing paradigm and unstable performance -mainly given by an interrupted water deprivation protocol- to a new set-up for doing *in vivo* 2P imaging while the animal is performing the task, with a high and stable performance. The paradigm used during this last year seems to be suitable for achieving the main goal of this project: creating an animal model for studying concept representation in the hippocampus.

This project combines cutting-edge behavioural and recording techniques to develop an animal model for concept representation. Human studies have shown concept representations in the hippocampus but there are still several questions that need to be addressed: How are concepts formed? How are the different areas of the MTL involved in the formation and representation of concepts? How far can these concept representations be modified by time and learning? Do neurons representing different concepts interact with each other? How are they connected among each other? Can we control the behaviour of an animal by manipulating the firing of these neurons? These questions cannot be addressed with human beings and we hope an animal model will give us some of the answers we are looking for.

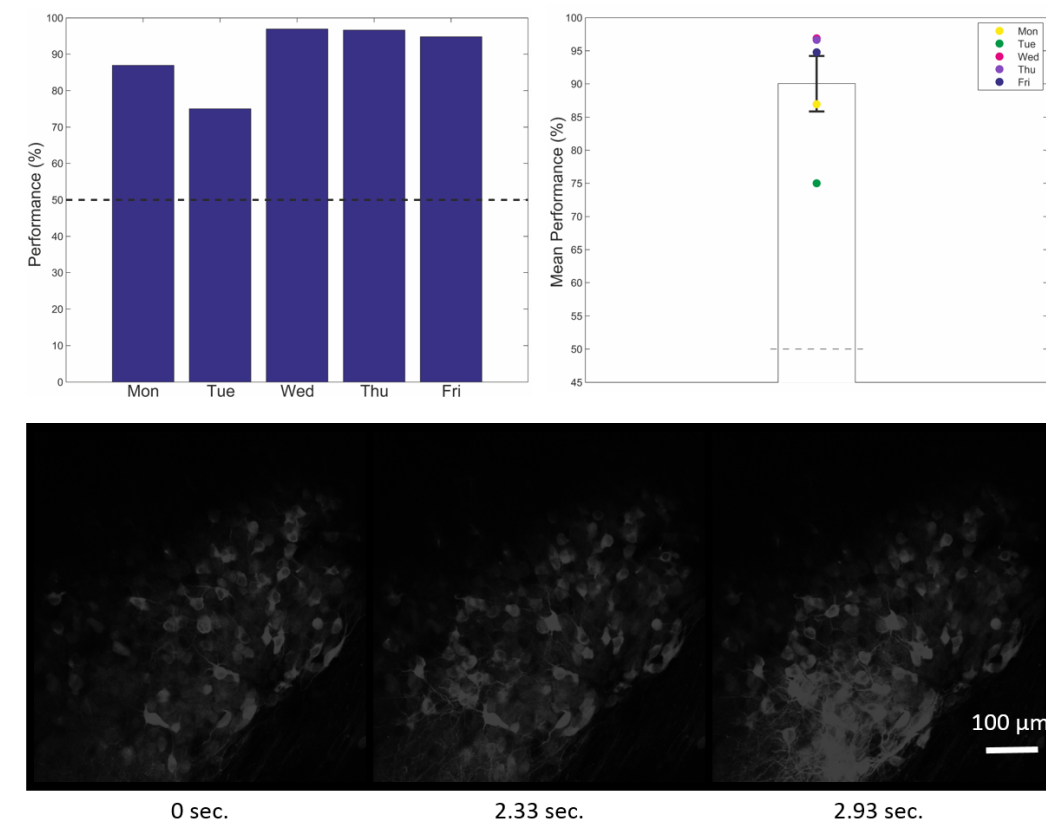


Figure 5.1: **Weekly performance of an animal and *in vivo* 2P imaging.** Top left: Performance for a typical training week (Monday to Friday). Top right: The performance throughout the week varied between 75 and 97%. The mean performance for that week was $90.04\% \pm 4.17$ (mean \pm SEM). Bottom: *In vivo* 2P imaging of the hippocampus from a mouse on the virtual reality set-up (not performing the task). Pictures at different moments are shown and activation of several neurons can be observed.

List of Abbreviations

1P	One photon
2P	Two photons
AAV	Adeno-Associated Virus
aCSF	Artificial cerebro-spinal fluid
AP	Action Potential
ChR2	Channelrhodopsin-2
d-d	Non-bonding state
EGFP	Enhanced Green Fluorescent Protein
EPSP	Excitatory post-synaptic potential
GECIs	Genetically Encoded Calcium Indicators
GFP	Green Fluorescence Protein
LFP	Local Field Potential
MED	Multi-electrode array
MLCT	Metal-to-Ligand Charge Transfer
MTL	Medial Temporal Lobe
MNI	7-nitroindoliny- and 4-methoxy-7-nitroindoliny-amino
MPM	Multiphoton microscopy
NIR	Near-Infrared
ROI	Region of interest
RuBiGlu	Ruthenium-Bipyridine-Trimethyl-phosphine-Glutamate
SNR	Signal-to-Noise Ratio
Srh	Sulforhodamine 101
Ti-Sapphire	Titanium-Sapphire
VR	Virtual Reality

Bibliography

- Akerboom, J., Chen, T.-W., Wardill, T. J., Tian, L., Marvin, J. S., Mutlu, S., Calderón, N. C., Esposti, F., Borghuis, B. G., Sun, X. R., et al. (2012). Optimization of a gcamp calcium indicator for neural activity imaging. *The Journal of neuroscience*, 32(40):13819–13840.
- Amaral, D. G., Scharfman, H. E., and Lavenex, P. (2007). The dentate gyrus: fundamental neuroanatomical organization (dentate gyrus for dummies). *Progress in brain research*, 163:3–790.
- Andersen, P., Morris, R., Amaral, D., Bliss, T., and O’Keefe, J. (2007). *The Hippocampus Book*. Oxford University Press, New York.
- Aschauer, D. F., Kreuz, S., and Rumpel, S. (2013). Analysis of transduction efficiency, tropism and axonal transport of aav serotypes 1, 2, 5, 6, 8 and 9 in the mouse brain. *PloS one*, 8(9):e76310.
- Bayley, P. J., Hopkins, R. O., and Squire, L. R. (2006). The fate of old memories after medial temporal lobe damage. *The Journal of Neuroscience*, 26(51):13311–13317.
- Bean, B. P. (2007). The action potential in mammalian central neurons. *Nature Reviews Neuroscience*, 8(6):451–465.
- Bechara, A., Damasio, H., and Damasio, A. R. (2000). Emotion, decision making and the orbitofrontal cortex. *Cerebral cortex*, 10(3):295–307.
- Berridge, M. J., Lipp, P., and Bootman, M. D. (2000). The versatility and universality of calcium signalling. *Nature reviews Molecular cell biology*, 1(1):11–21.
- Bliss, T. V. and Lømo, T. (1973). Long-lasting potentiation of synaptic transmission in the dentate area of the anaesthetized rabbit following stimulation of the perforant path. *The Journal of physiology*, 232(2):331–356.
- Buzsáki, G., Anastassiou, C. A., and Koch, C. (2012). The origin of extracellular fields and currentseeg, ecog, lfp and spikes. *Nature reviews neuroscience*, 13(6):407–420.
- Canepari, M., Nelson, L., Papageorgiou, G., Corrie, J., and Ogden, D. (2001). Photochemical and pharmacological evaluation of 7-nitroindolinyland 4-methoxy-7-nitroindoliny-amino acids as novel, fast caged neurotransmitters. *Journal of neuroscience methods*, 112(1):29–42.
- Cardin, J. A., Carlén, M., Meletis, K., Knoblich, U., Zhang, F., Deisseroth, K., Tsai, L.-H., and Moore, C. I. (2009). Driving fast-spiking cells induces gamma rhythm and controls sensory responses. *Nature*, 459(7247):663–667.

- Cardin, J. A., Carlén, M., Meletis, K., Knoblich, U., Zhang, F., Deisseroth, K., Tsai, L.-H., and Moore, C. I. (2010). Targeted optogenetic stimulation and recording of neurons in vivo using cell-type-specific expression of channelrhodopsin-2. *Nature protocols*, 5(2):247–254.
- Caruana, D. A., Alexander, G. M., and Dudek, S. M. (2012). New insights into the regulation of synaptic plasticity from an unexpected place: hippocampal area ca2. *Learning & memory*, 19(9):391–400.
- Cetin, A., Komai, S., Eliava, M., Seeburg, P. H., and Osten, P. (2006). Stereotaxic gene delivery in the rodent brain. *Nature protocols*, 1(6):3166–3173.
- Chen, T.-W., Wardill, T. J., Sun, Y., Pulver, S. R., Renninger, S. L., Baohan, A., Schreiter, E. R., Kerr, R. A., Orger, M. B., Jayaraman, V., et al. (2013). Ultrasensitive fluorescent proteins for imaging neuronal activity. *Nature*, 499(7458):295–300.
- Chen, X., Leischner, U., Rochefort, N. L., Nelken, I., and Konnerth, A. (2011). Functional mapping of single spines in cortical neurons in vivo. *Nature*, 475(7357):501–505.
- Collingridge, G., Herron, C., and Lester, R. (1988). Synaptic activation of n-methyl-d-aspartate receptors in the schaffer collateral-commissural pathway of rat hippocampus. *The Journal of physiology*, 399:283.
- Corkin, S. (2002). What’s new with the amnesic patient hm? *Nature Reviews Neuroscience*, 3(2):153–160.
- Cotton, F. A., Wilkinson, G., Murillo, C. A., Bochmann, M., and Grimes, R. (1999). *Advanced inorganic chemistry*, volume 1355. Wiley New York.
- Cunningham, M. O., Davies, C. H., Buhl, E. H., Kopell, N., and Whittington, M. A. (2003). Gamma oscillations induced by kainate receptor activation in the entorhinal cortex in vitro. *The Journal of Neuroscience*, 23(30):9761–9769.
- Damasio, H., Grabowski, T., Frank, R., Galaburda, A. M., Damasio, A. R., et al. (1994). The return of phineas gage: clues about the brain from the skull of a famous patient. *Science*, 264(5162):1102–1105.
- de Lavilléon, G., Lacroix, M. M., Rondi-Reig, L., and Benchenane, K. (2015). Explicit memory creation during sleep demonstrates a causal role of place cells in navigation. *Nature neuroscience*.
- Deisseroth, K. (2011). Optogenetics. *Nature methods*, 8(1):26–29.
- Deller, T., Adelmann, G., Nitsch, R., and Frotscher, M. (1996). The alvear pathway of the rat hippocampus. *Cell and tissue research*, 286(3):293–303.
- Deng, W., Aimone, J. B., and Gage, F. H. (2010). New neurons and new memories: how does adult hippocampal neurogenesis affect learning and memory? *Nature Reviews Neuroscience*, 11(5):339–350.

- Denk, W. (1994). Two-photon scanning photochemical microscopy: mapping ligand-gated ion channel distributions. *Proceedings of the National Academy of Sciences*, 91(14):6629–6633.
- Denk, W., Strickler, J. H., and Webb, W. W. (1990). Two-photon laser scanning fluorescence microscopy. *Science*, 248(4951):73–76.
- DeYoung, C. G., Hirsh, J. B., Shane, M. S., Papademetris, X., Rajeevan, N., and Gray, J. R. (2010). Testing predictions from personality neuroscience brain structure and the big five. *Psychological science*.
- Di Virgilio, F., Steinberg, T., Swanson, J., and Silverstein, S. (1988). Fura-2 secretion and sequestration in macrophages. a blocker of organic anion transport reveals that these processes occur via a membrane transport system for organic anions. *The Journal of Immunology*, 140(3):915–920.
- Dingledine, R., Borges, K., Bowie, D., and Traynelis, S. F. (1999). The glutamate receptor ion channels. *Pharmacological reviews*, 51(1):7–62.
- Dombeck, D. A., Harvey, C. D., Tian, L., Looger, L. L., and Tank, D. W. (2010). Functional imaging of hippocampal place cells at cellular resolution during virtual navigation. *Nature neuroscience*, 13(11):1433–1440.
- Dombeck, D. A., Khabbaz, A. N., Collman, F., Adelman, T. L., and Tank, D. W. (2007). Imaging large-scale neural activity with cellular resolution in awake, mobile mice. *Neuron*, 56(1):43–57.
- Fino, E., Araya, R., Peterka, D., Salierno, M., Etchenique, R., and Yuste, R. (2009). Rubi-glutamate: two-photon and visible-light photoactivation of neurons and dendritic spines. *Frontiers in neural circuits*, 3(2).
- Fisahn, A., Contractor, A., Traub, R. D., Buhl, E. H., Heinemann, S. F., and McBain, C. J. (2004). Distinct roles for the kainate receptor subunits glur5 and glur6 in kainate-induced hippocampal gamma oscillations. *The Journal of Neuroscience*, 24(43):9658–9668.
- Freund, T. F. and Buzsáki, G. (1996). Interneurons of the hippocampus. *Hippocampus*, 6(4):347–470.
- Gipson, K. E. and Yeckel, M. F. (2007). Coincident glutamatergic and cholinergic inputs transiently depress glutamate release at rat schaffer collateral synapses. *Journal of neurophysiology*, 97(6):4108–4119.
- Givens, R. S., Weber, J. F., Jung, A. H., and Park, C.-H. (1998). [1] new photoprotecting groups: Desyl and p-hydroxyphenacyl phosphate and carboxylate esters. *Methods in enzymology*, 291:1–29.
- Gold, C., Henze, D. A., Koch, C., and Buzsáki, G. (2006). On the origin of the extracellular action potential waveform: a modeling study. *Journal of neurophysiology*, 95(5):3113–3128.

- Grienberger, C. and Konnerth, A. (2012). Imaging calcium in neurons. *Neuron*, 73(5):862–885.
- Gulyas, A., Toth, K., McBain, C., and Freund, T. (1998). Stratum radiatum giant cells: a type of principal cell in the rat hippocampus. *European Journal of Neuroscience*, 10(12):3813–3822.
- Harvey, C. D., Collman, F., Dombeck, D. A., and Tank, D. W. (2009). Intracellular dynamics of hippocampal place cells during virtual navigation. *Nature*, 461(7266):941–946.
- Hasan, M. T., Friedrich, R. W., Euler, T., Larkum, M. E., Giese, G., Both, M., Duebel, J., Waters, J., Bujard, H., Griesbeck, O., et al. (2004). Functional fluorescent Ca^{2+} indicator proteins in transgenic mice under tet control. *PLoS Biol*, 2(6):e163.
- Heffner, H. E. and Heffner, R. S. (1986). Hearing loss in japanese macaques following bilateral auditory cortex lesions. *Journal of Neurophysiology*, 55(2):256–271.
- Heim, R., Cubitt, A. B., and Tsien, R. Y. (1995). Improved green fluorescence. *Nature*, 373(6516):663–664.
- Helmchen, F. and Denk, W. (2005). Deep tissue two-photon microscopy. *Nature methods*, 2(12):932–940.
- Hernandez, G., Hamdani, S., Rajabi, H., Conover, K., Stewart, J., Arvanitogiannis, A., and Shizgal, P. (2006). Prolonged rewarding stimulation of the rat medial forebrain bundle: neurochemical and behavioral consequences. *Behavioral neuroscience*, 120(4):888.
- Hitti, F. L. and Siegelbaum, S. A. (2014). The hippocampal Ca^{2+} region is essential for social memory. *Nature*, 508(7494):88–92.
- Honore, T., Davies, S. N., Drejer, J., Fletcher, E. J., Jacobsen, P., Lodge, D., and Nielsen, F. E. (1988). Quinoxalinediones: potent competitive non-nmda glutamate receptor antagonists. *Science*, 241(4866):701–703.
- Howard, M. W., Fotedar, M. S., Datey, A. V., and Hasselmo, M. E. (2005). The temporal context model in spatial navigation and relational learning: toward a common explanation of medial temporal lobe function across domains. *Psychological review*, 112(1):75.
- Hubel, D. and Wiesel, T. (1963). Shape and arrangement of columns in cat's striate cortex. *The Journal of physiology*, 165(3):559.
- Hubel, D. H. and Wiesel, T. N. (1962). Receptive fields, binocular interaction and functional architecture in the cat's visual cortex. *The Journal of physiology*, 160(1):106–154.

- Huber, D., Gutnisky, D., Peron, S., Oconnor, D., Wiegert, J., Tian, L., Oertner, T., Looger, L., and Svoboda, K. (2012). Multiple dynamic representations in the motor cortex during sensorimotor learning. *Nature*, 484(7395):473–478.
- Huxley, A. (1996). Kenneth Stewart Cole. 10 July 1900–18 April 1984. *Biographical Memoirs of Fellows of the Royal Society*, 38:99–110.
- Ison, M. J., Mormann, F., Cerf, M., Koch, C., Fried, I., and Quiroga, R. Q. (2011). Selectivity of pyramidal cells and interneurons in the human medial temporal lobe. *Journal of neurophysiology*, 106(4):1713–1721.
- Ison, M. J., Quiroga, R. Q., and Fried, I. (2015). Rapid encoding of new memories by individual neurons in the human brain. *Neuron*, 87(1):220–230.
- Jeffery, K. J. (2007). Integration of the sensory inputs to place cells: what, where, why, and how? *Hippocampus*, 17(9):775–785.
- Jin, J., Gong, K., Zou, X., Wang, R., Lin, Q., and Chen, J. (2013). The blockade of nmda receptor ion channels by ketamine is enhanced in developing rat cortical neurons. *Neuroscience letters*, 539:11–15.
- Johnston, G. A. (1994). Gaba receptors: as complex as abc? *Clinical and experimental pharmacology and physiology*, 21(7):521–526.
- Jones, M. W. and McHugh, T. J. (2011). Updating hippocampal representations: Ca²⁺ joins the circuit. *Trends in neurosciences*, 34(10):526–535.
- Kaplan, J. H., Forbush III, B., and Hoffman, J. F. (1978). Rapid photolytic release of adenosine 5'-triphosphate from a protected analog: utilization by the sodium: potassium pump of human red blood cell ghosts. *Biochemistry*, 17(10):1929–1935.
- Kim, D. H., Kim, J. M., Park, S. J., Cai, M., Liu, X., Lee, S., Shin, C. Y., and Ryu, J. H. (2012). Gabaa receptor blockade enhances memory consolidation by increasing hippocampal bdnf levels. *Neuropsychopharmacology*, 37(2):422–433.
- Kohara, K., Pignatelli, M., Rivest, A. J., Jung, H.-Y., Kitamura, T., Suh, J., Frank, D., Kajikawa, K., Mise, N., Obata, Y., et al. (2014). Cell type-specific genetic and optogenetic tools reveal hippocampal ca²⁺ circuits. *Nature neuroscience*, 17(2):269–279.
- Kohl, M. M., Shipton, O. A., Deacon, R. M., Rawlins, J. N. P., Deisseroth, K., and Paulsen, O. (2011). Hemisphere-specific optogenetic stimulation reveals left-right asymmetry of hippocampal plasticity. *Nature neuroscience*, 14(11):1413–1415.
- Kügler, S., Kilic, E., and Bähr, M. (2003). Human synapsin 1 gene promoter confers highly neuron-specific long-term transgene expression from an adenoviral vector in the adult rat brain depending on the transduced area. *Gene therapy*, 10(4):337–347.

- Kwon, H.-B. and Sabatini, B. L. (2011). Glutamate induces de novo growth of functional spines in developing cortex. *Nature*, 474(7349):100–104.
- Lacaille, J.-C. and Schwartzkroin, P. (1988). Stratum lacunosum-moleculare interneurons of hippocampal ca1 region. ii. intrasomatic and intradendritic recordings of local circuit synaptic interactions. *The Journal of neuroscience*, 8(4):1411–1424.
- Lakowicz, J. R. (2013). *Principles of fluorescence spectroscopy*. Springer Science & Business Media.
- Lima, S. Q. and Miesenböck, G. (2005). Remote control of behavior through genetically targeted photostimulation of neurons. *Cell*, 121(1):141–152.
- Lin, L., Chen, G., Kuang, H., Wang, D., and Tsien, J. Z. (2007). Neural encoding of the concept of nest in the mouse brain. *Proceedings of the National Academy of Sciences*, 104(14):6066–6071.
- Liu, X., Ramirez, S., Pang, P. T., Puryear, C. B., Govindarajan, A., Deisseroth, K., and Tonegawa, S. (2012). Optogenetic stimulation of a hippocampal engram activates fear memory recall. *Nature*, 484(7394):381–385.
- Liu, X., Ramirez, S., and Tonegawa, S. (2013). Inception of a false memory by optogenetic manipulation of a hippocampal memory engram. *Philosophical Transactions of the Royal Society of London B: Biological Sciences*, 369(1633):20130142.
- Long, M. A. and Lee, A. K. (2012). Intracellular recording in behaving animals. *Current opinion in neurobiology*, 22(1):34–44.
- Looger, L. L. and Griesbeck, O. (2012). Genetically encoded neural activity indicators. *Current opinion in neurobiology*, 22(1):18–23.
- Lorente de Nó, R. (1922). The cerebral cortex of the mouse (a first contribution -the "acoustic" cortex). *Somatosensory and Motor Research*, 9(1):3–36.
- Maier, W., Corrie, J. E., Papageorgiou, G., Laube, B., and Grever, C. (2005). Comparative analysis of inhibitory effects of caged ligands for the nmda receptor. *Journal of neuroscience methods*, 142(1):1–9.
- Mank, M. and Griesbeck, O. (2008). Genetically encoded calcium indicators. *Chemical reviews*, 108(5):1550–1564.
- Manns, J. R., Hopkins, R. O., and Squire, L. R. (2003). Semantic memory and the human hippocampus. *Neuron*, 38(1):127–133.
- Mao, T., O'Connor, D. H., Scheuss, V., Nakai, J., and Svoboda, K. (2008). Characterization and subcellular targeting of gcamp-type genetically-encoded calcium indicators. *PloS one*, 3(3):e1796.

- Marosi, M., Nagy, D., Farkas, T., Kis, Z., Rózsa, É., Robotka, H., Fülöp, F., Vécsei, L., and Toldi, J. (2010). A novel kynurenic acid analogue: a comparison with kynurenic acid. an in vitro electrophysiological study. *Journal of neural transmission*, 117(2):183–188.
- Marvin, J. S., Borghuis, B. G., Tian, L., Cichon, J., Harnett, M. T., Akerboom, J., Gordus, A., Renninger, S. L., Chen, T.-W., Bargmann, C. I., et al. (2013). An optimized fluorescent probe for visualizing glutamate neurotransmission. *Nature methods*, 10(2):162–170.
- Matsuzaki, M., Ellis-Davies, G. C., Nemoto, T., Miyashita, Y., Iino, M., and Kasai, H. (2001). Dendritic spine geometry is critical for ampa receptor expression in hippocampal ca1 pyramidal neurons. *Nature neuroscience*, 4(11):1086–1092.
- Matsuzaki, M., Honkura, N., Ellis-Davies, G. C., and Kasai, H. (2004). Structural basis of long-term potentiation in single dendritic spines. *Nature*, 429(6993):761–766.
- McCormick, D. and Shepherd, G. (2004). The synaptic organization of the brain.
- Miyawaki, A., Llopis, J., Heim, R., McCaffery, J. M., Adams, J. A., Ikura, M., and Tsien, R. Y. (1997). Fluorescent indicators for ca^{2+} ; based on green fluorescent proteins and calmodulin. *Nature*, 388(6645):882–887.
- Molnar, P. and Nadler, J. V. (2000). γ -aminobutyrate, α -carboxy-2-nitrobenzyl ester selectively blocks inhibitory synaptic transmission in rat dentate gyrus. *European journal of pharmacology*, 391(3):255–262.
- Mountcastle, V. B. (1997). The columnar organization of the neocortex. *Brain*, 120(4):701–722.
- Mountcastle, V. B. et al. (1957). Modality and topographic properties of single neurons of cats somatic sensory cortex. *J neurophysiol*, 20(4):408–434.
- Nagel, G., Ollig, D., Fuhrmann, M., Kateriya, S., Musti, A. M., Bamberg, E., and Hegemann, P. (2002). Channelrhodopsin-1: a light-gated proton channel in green algae. *Science*, 296(5577):2395–2398.
- Nakai, J., Ohkura, M., and Imoto, K. (2001). A high signal-to-noise ca^{2+} probe composed of a single green fluorescent protein. *Nature biotechnology*, 19(2):137–141.
- Neher, E. and Sakaba, T. (2008). Multiple roles of calcium ions in the regulation of neurotransmitter release. *Neuron*, 59(6):861–872.
- ODoherty, J. P. (2004). Reward representations and reward-related learning in the human brain: insights from neuroimaging. *Current opinion in neurobiology*, 14(6):769–776.

- Ohki, K., Chung, S., Ch'ng, Y. H., Kara, P., and Reid, R. C. (2005). Functional imaging with cellular resolution reveals precise micro-architecture in visual cortex. *Nature*, 433(7026):597–603.
- O'Keefe, J. (1979). A review of the hippocampal place cells. *Progress in neurobiology*, 13(4):419–439.
- O'keefe, J. and Conway, D. (1978). Hippocampal place units in the freely moving rat: why they fire where they fire. *Experimental Brain Research*, 31(4):573–590.
- O'Keefe, J. and Dostrovsky, J. (1971). The hippocampus as a spatial map. preliminary evidence from unit activity in the freely-moving rat. *Brain research*, 34(1):171–175.
- O'keefe, J. and Nadel, L. (1978). *The hippocampus as a cognitive map*, volume 3. Clarendon Press Oxford.
- Paredes, R. M., Etzler, J. C., Watts, L. T., Zheng, W., and Lechleiter, J. D. (2008). Chemical calcium indicators. *Methods*, 46(3):143–151.
- Pelliccioli, A. P. and Wirz, J. (2002). Photoremovable protecting groups: reaction mechanisms and applications. *Photochemical & photobiological sciences*, 1(7):441–458.
- Penfield, W. and Milner, B. (1958). Memory deficit produced by bilateral lesions in the hippocampal zone. *AMA Archives of Neurology & Psychiatry*, 79(5):475–497.
- Peterka, D. S., Nikolenko, V., Fino, E., Araya, R., Etchenique, R., and Yuste, R. (2010). Fast two-photon neuronal imaging and control using a spatial light modulator and ruthenium compounds. In *BiOS*, pages 75484P–75484P. International Society for Optics and Photonics.
- Petersen, C. C. (2007). The functional organization of the barrel cortex. *Neuron*, 56(2):339–355.
- Popovic, M. A., Carnevale, N., Rozsa, B., and Zecevic, D. (2015). Electrical behaviour of dendritic spines as revealed by voltage imaging. *Nature communications*, 6.
- Powell, T. P. and Mountcastle, V. B. (1959). Some aspects of the functional organization of the cortex of the postcentral gyrus of the monkey: a correlation of findings obtained in a single unit analysis with cytoarchitecture. *Bull Johns Hopkins Hosp*, 105(133-62).
- Purves, D., Augustine, G., Fitzpatrick, D., Hall, W., Anthony, L., McNamara, J., and Williams, S. M. (2004). *Neuroscience*. Sinauer Associates, Inc, Massachusetts.
- Quian Quiroga, R. and Kreiman, G. (2010). Measuring sparseness in the brain: comment on bowers (2009). *American Psychological Association*, 117(1).

- Quirk, G. J., Muller, R. U., and Kubie, J. L. (1990). The firing of hippocampal place cells in the dark depends on the rat's recent experience. *The Journal of Neuroscience*, 10(6):2008–2017.
- Quiroga, R. Q. (2012). Concept cells: the building blocks of declarative memory functions. *Nature Reviews Neuroscience*, 13(8):587–597.
- Quiroga, R. Q., Kraskov, A., Koch, C., and Fried, I. (2009). Explicit encoding of multimodal percepts by single neurons in the human brain. *Current Biology*, 19(15):1308–1313.
- Quiroga, R. Q., Nadasdy, Z., and Ben-Shaul, Y. (2004). Unsupervised spike detection and sorting with wavelets and superparamagnetic clustering. *Neural computation*, 16(8):1661–1687.
- Quiroga, R. Q., Reddy, L., Kreiman, G., Koch, C., and Fried, I. (2005). Invariant visual representation by single neurons in the human brain. *Nature*, 435(7045):1102–1107.
- Ramirez, S., Liu, X., Lin, P.-A., Suh, J., Pignatelli, M., Redondo, R. L., Ryan, T. J., and Tonegawa, S. (2013). Creating a false memory in the hippocampus. *Science*, 341(6144):387–391.
- Redish, A. D., Battaglia, F. P., Chawla, M. K., Ekstrom, A. D., Gerrard, J. L., Lipa, P., Rosenzweig, E. S., Worley, P. F., Guzowski, J. F., McNaughton, B. L., et al. (2001). Independence of firing correlates of anatomically proximate hippocampal pyramidal cells. *J Neurosci*, 21(5):RC134.
- Redondo, R. L., Kim, J., Arons, A. L., Ramirez, S., Liu, X., and Tonegawa, S. (2014). Bidirectional switch of the valence associated with a hippocampal contextual memory engram. *Nature*, 513(7518):426–430.
- Reed, J. M. and Squire, L. R. (1998). Retrograde amnesia for facts and events: findings from four new cases. *The Journal of Neuroscience*, 18(10):3943–3954.
- Rempel-Clower, N. L., Zola, S. M., Squire, L. R., and Amaral, D. G. (1996). Three cases of enduring memory impairment after bilateral damage limited to the hippocampal formation. *The Journal of Neuroscience*, 16(16):5233–5255.
- Rial Verde, E., Zayat, L., Etchenique, R., and Yuste, R. (2008). Photorelease of gaba with visible light using an inorganic caging group. *Frontiers in neural circuits*, 2:2.
- Salierno, M., Marceca, E., Peterka, D. S., Yuste, R., and Etchenique, R. (2010). A fast ruthenium polypyridine cage complex photoreleases glutamate with visible or ir light in one and two photon regimes. *Journal of inorganic biochemistry*, 104(4):418–422.
- Sato, T. K., Häusser, M., and Carandini, M. (2014). Distal connectivity causes summation and division across mouse visual cortex. *Nature neuroscience*, 17(1):30–32.

- Save, E., Cressant, A., Thinus-Blanc, C., and Poucet, B. (1998). Spatial firing of hippocampal place cells in blind rats. *The Journal of Neuroscience*, 18(5):1818–1826.
- Scanziani, M. and Häusser, M. (2009). Electrophysiology in the age of light. *Nature*, 461(7266):930–939.
- Scoville, W. B. and Milner, B. (1957). Loss of recent memory after bilateral hippocampal lesions. *Journal of neurology, neurosurgery, and psychiatry*, 20(1):11.
- So, P. T., Dong, C. Y., Masters, B. R., and Berland, K. M. (2000). Two-photon excitation fluorescence microscopy. *Annual review of biomedical engineering*, 2(1):399–429.
- Squire, L., Berg, D., Bloom, F. E., Du Lac, S., Ghosh, A., and Spitzer, N. C. (2012). *Fundamental neuroscience*. Academic Press.
- Squire, L. R. (2004). Memory systems of the brain: a brief history and current perspective. *Neurobiology of learning and memory*, 82(3):171–177.
- Svaasand, L. O. and Ellingsen, R. (1983). Optical properties of human brain. *Photochemistry and photobiology*, 38(3):293–299.
- Svoboda, K. and Yasuda, R. (2006). Principles of two-photon excitation microscopy and its applications to neuroscience. *Neuron*, 50(6):823–839.
- Tian, L., Hires, S. A., Mao, T., Huber, D., Chiappe, M. E., Chalasani, S. H., Petreanu, L., Akerboom, J., McKinney, S. A., Schreiter, E. R., et al. (2009). Imaging neural activity in worms, flies and mice with improved gcamp calcium indicators. *Nature methods*, 6(12):875–881.
- Tolman, E. C. (1948). Cognitive maps in rats and men. *Psychological review*, 55(4):189.
- Trigo, F. F., Papageorgiou, G., Corrie, J. E., and Ogden, D. (2009). Laser photolysis of dpni-gaba, a tool for investigating the properties and distribution of gaba receptors and for silencing neurons in situ. *Journal of neuroscience methods*, 181(2):159–169.
- Viskontas, I. V., Quiroga, R. Q., and Fried, I. (2009). Human medial temporal lobe neurons respond preferentially to personally relevant images. *Proceedings of the National Academy of Sciences*, 106(50):21329–21334.
- Wang, Y. V., Weick, M., and Demb, J. B. (2011). Spectral and temporal sensitivity of cone-mediated responses in mouse retinal ganglion cells. *The Journal of Neuroscience*, 31(21):7670–7681.
- Wieboldt, R., Gee, K. R., Niu, L., Ramesh, D., Carpenter, B. K., and Hess, G. P. (1994). Photolabile precursors of glutamate: synthesis, photochemical properties, and activation of glutamate receptors on a microsecond time scale. *Proceedings of the National Academy of Sciences*, 91(19):8752–8756.

- Wilson, M. A. and McNaughton, B. L. (1993). Dynamics of the hippocampal ensemble code for space. *Science*, 261(5124):1055–1058.
- Yuste, R., MacLean, J., Vogelstein, J., and Paninski, L. (2011). Imaging action potentials with calcium indicators. *Cold Spring Harbor Protocols*, 2011(8):pdb-prot5650.
- Zayat, L., Filevich, O., Baraldo, L. M., and Etchenique, R. (2013). Ruthenium polypyridyl phototriggers: from beginnings to perspectives. *Philosophical Transactions of the Royal Society of London A: Mathematical, Physical and Engineering Sciences*, 371(1995):20120330.
- Zayat, L., Noval, M. G., Campi, J., Calero, C. I., Calvo, D. J., and Etchenique, R. (2007). A new inorganic photolabile protecting group for highly efficient visible light gaba uncaging. *ChemBioChem*, 8(17):2035–2038.
- Zola-Morgan, S., Squire, L. R., and Amaral, D. (1986). Human amnesia and the medial temporal region: enduring memory impairment following a bilateral lesion limited to field ca1 of the hippocampus. *The Journal of Neuroscience*, 6(10):2950–2967.